THEORETICAL AND EXPERIMENTAL STUDY OF ENERGETIC PROPERTIES OF CONFINED SOUND FIELDS

Doctoral thesis by:

Davide Bonsi

Supervisor: Prof. **Giuliano Schiffrer** (University of Ferrara: department of physics)

Co-supervisor: Dr. **Domenico Stanzial** (National Research Council: CEMOTER institute)

University of Ferrara: department of physics
Academic year: 1997/98

Acknowledgements

The research of this thesis has been supported by University of Ferrara and CIARM, an institution for promotion and coordination of acoustical research, with the partecipation of the University of Ferrara, of CNR (Cemoter Institute, Ferrara) and some other Universities and cultural or scientific institutions. The experimental work has been carried at the laboratory of acoustics of Cemoter.

UNIVERSITY OF FERRARA

CIARM

NATIONAL RESEARCH COUNCIL OF ITALY

Contents

Introduction

The contemporary history of room acoustics began at the end of the 19^{th} century, thanks to the pioneer works by Wallace Clement Sabine [1] , regarding the interpretation of reverberation processes in large halls. The study, for sure one of the most challenging in acoustics, was carried out inducing the global energetic behavior of the environment from a local analysis of the sound decay. In practice, Sabine performed several experiments about the decay velocity just by listening to the sound occurring after having shut a steady source (an organ pipe) off, then he devised the first formula describing the energy decay rate (Sabine formula). This was subsequently interpreted according to the whole energy balance

$$V\frac{\mathrm{d}w}{\mathrm{d}t} = \Pi - \Pi_a$$

linking the energy rate of increase to the difference of rates of energy production and absorption respectively (V is the volume of the environment). The essential point which made this available was the assumption that the quantity $\mathrm{d}w/\mathrm{d}t$ is independent of the position $\mathbf{x}$ where the decay is perceived and measured during the reverberation process. In short, the local energy density $w(\mathbf{x}, t)$ and the energy density flux $\mathbf{j}(\mathbf{x}, t)$, are supposed to be homogeneously and isotropically distributed over the volume V. On the other hand, this statistical assumption, which is referred to in the literature as the "diffuse field hypothesis", has never been carefully interpreted, so that nowadays a deep investigation of the relationship between local and global quantities is still lacking.

In the research area just mentioned the purpose of the present thesis is that of giving a contribution to the development of the analysis of confined fields, both from the theoretical and experimental viewpoint. First of all, the task will be approached by introducing a proper formal apparatus for expressing the energy transfer; after that, by the implementation of new intensimetric procedures, it will be shown how the local quantities previously defined are related to the overall structural properties of the acoustic field.

The entire work is subdivided in four chapters: below we summarize the main arguments treated in each of them.

(1) The most important quantities and physical laws of linear acoustics theory are introduced and discussed. A particular attention is devoted to the reformulation of energy fluxes in terms of the radiating and oscillating intensity.

(2) Here a short review of acoustics phenomena characterizing acoustic confined fields is given, by means of a wave and a statistical treatment. The main original subject which will be discussed is that of the impulse response technique, employed for obtaining the potential and the kinetic energy behavior during the sound decay (extension of Schroeder's method).

(3) The experimental techniques adopted for measuring the energetic quantities are here illustrated. These include the standard *p-p* (pressure-pressure) method for the intensity measurements as well as the cross-correlation procedure for determining pressure and velocity impulse responses and the convolution procedures (FFT, Hadamard transforms) for reconstructing stationary signals.

(4) The last part regards the discussion of the results obtained from a set of experiments performed in particular confined fields: an organ pipe, a plexiglass duct and an opera house ("Teatro Comunale" in Ferrara).

It follows a brief appendix, describing some important aspects of the signal processing algorithms used throughout the work.

The original contributions developed by the candidate are presented in Sections 2.5, 2.8, 3.4 and in Chapter 4.

CHAPTER 1

The equations of linear acoustics

The phenomenon of sound in fluids (liquids or gases) is due to positive and negative variations of the medium density with respect to their equilibrium values, which are generated by the action of the so-called *sound sources*: these may be either rapid compressions and dilatations caused by vibrating bodies or the intermittent introduction of matter into the medium. In the context we are about to study, that of *linear acoustics* in air, the above-mentioned variations are extremely small, that is not more than 10^{-5} times the equilibrium value. They are related to the behavior of other hydrodynamic quantities like pressure and velocity, in such a way that the entire process takes place on a space scale extremely larger than the dimension of a single oscillation: in other words, the so called *wave propagation* is established in the medium, so that the local perturbation is transmitted at large distances. The mechanism which makes this possible is founded on two basic physical properties: (i) the medium *elasticity*, which carries out a relationship between the fluid's normal stress (pressure) and its dilatations, (ii) the *inertia*, i.e. the property of opposing a dynamic reaction to an impulse variation.

The most important characteristic of sound propagation from our point of view is that acoustic pressure variations are associated with a local fluid velocity: this determines a wave energy transfer inside the medium, which in the linear approximation does not involve any long range matter movement, thanks to the oscillating behavior of the acoustic quantities.

In this chapter we will present the fundamental features of linear acoustics in fluids, in order to put the basis for a subsequent understanding of the processes related to the energetic quantities.

1.1 Fluid dynamics fundamentals

The first task to be treated regards the description of the laws of motion when dealing with small amplitude sound waves in a non viscous fluid [2] , [3] . A first requirement for this to be accomplished is the definition of the physical element taking part in the motion. In the

usual representation one speaks of a *fluid particle*: this has to be thought as a generic amount of matter contained in a volume element which is small compared with respect to the ordinary measurement precision, but sufficiently large to contain a huge number of molecules, in such a way that the physical quantities inside of it can be considered constant.

1.1.1 Kinematics

As known, the mathematical representation of fluid motion adopts these two alternative approaches:

- Lagrangian scheme
- Eulerian scheme

In the *Lagrangian scheme* the particles movement is described with respect to a fixed reference frame: one defines the position $\mathbf{x}_0$ of an element at $t = 0$ and follows the motion at subsequent instants, so tracing the path by means of the curve $\mathbf{x} = \mathbf{s}(\mathbf{x}_0; t)$. On the contrary, the *Eulerian scheme* is based upon the description of the fluid motion in each specified point. Some of the Eulerian quantities we shall encounter are: the sound pressure $p(\mathbf{x}, t)$, the particle velocity $\mathbf{v}(\mathbf{x}, t)$ and the mass density $\rho(\mathbf{x}, t)$.

It is useful to find out the kinematical relationships linking the two descriptions. For this we must introduce the Lagrangian velocity by calculating the time derivative of the trajectory vector: $\mathbf{v}_l(\mathbf{x}_0; t) = \partial \mathbf{s}(\mathbf{x}_0; t)/\partial t$. This expresses the velocity at the time t of the particle whose initial position is $\mathbf{x}_0$, therefore, with respect to the Eulerian velocity one finds: $\mathbf{v}_l(\mathbf{x}_0; t) = \mathbf{v}\left[\mathbf{s}(\mathbf{x}_0; t), t\right]$, so that $\mathbf{s}$ satisfies the following Cauchy problem

$$\frac{\mathrm{d}\,\mathbf{s}(t)}{\mathrm{d}t} = \mathbf{v}\left[\mathbf{s}(t), t\right] \qquad \mathbf{s}(0) = \mathbf{x}_0 \tag{1}$$

From the knowledge of the Eulerian velocity at any point and at any time, one can find the particles' trajectories corresponding to every initial point $\mathbf{x}_0$. Conversely, knowing the trajectories it is possible to obtain both the Eulerian and the Lagrangian velocity.

As far as the acceleration is concerned, we must take account of the different ways the time derivative has to be calculated in the two schemes. The Eulerian time derivative of a scalar function $g(\mathbf{x}, t)$ is performed in a fixed point, hence

$$g_t := \frac{\partial g(\mathbf{x}, t)}{\partial t} = \lim_{\tau \to 0} \frac{g(\mathbf{x}, t + \tau) - g(\mathbf{x}, t)}{\tau} \tag{2}$$

while the Lagrangian derivative is calculated following the particle trajectory:

$$\dot{g} := \frac{\mathrm{d}g[\mathbf{s}(t), t]}{\mathrm{d}t} = \frac{\partial g}{\partial t} + \sum_i \frac{\partial g}{\partial x_i}\frac{\mathrm{d}s_i}{\mathrm{d}t} = \frac{\partial g}{\partial t} + \sum_i v_i \frac{\partial g}{\partial x_i} = g_t + \mathbf{v} \cdot \boldsymbol{\nabla} g \tag{3}$$

Here the term $\mathbf{v} \cdot \boldsymbol{\nabla} g$ indicates the movement of $\mathbf{v}dt$ in the time dt. In particular, the quantity

$$\mathbf{a}_l(\mathbf{x}_0; t) = \frac{\partial \mathbf{v}_l(\mathbf{x}_0; t)}{\partial t} = \frac{\partial^2 \mathbf{s}(\mathbf{x}_0; t)}{\partial t^2} = \mathbf{v}_t + (\mathbf{v} \cdot \boldsymbol{\nabla})\mathbf{v} \tag{4}$$

is the acceleration of a particle which is in $\mathbf{x}_0$ at time t.

In the present work we shall make use of the Eulerian formulation: thus it will be possible to deal with acoustical quantities expressed as scalar or vectorial fields.

1.1.2 Mass conservation

We may now introduce the mass conservation equation, which gives a relationship between density and velocity in a fluid. Let's first take for simplicity the case of a one dimensional motion, for instance along the coordinate x, and indicate with $\rho(x,t)$ and $v(x,t)$ the mass for unit length and the fluid velocity, both in the Eulerian representation. The mass transfer is expressed by the *mass flux density* $m(x,t) := \rho(x,t)v(x,t)$: the amount of matter which crosses a surface of unit area normal to x in unit time. Let's now take a fluid portion inside a volume delimited by two parallel planes of unit area, placed normally to the motion axis, in the positions x and $x + \mathrm{d}x$ respectively: the corresponding fluxes $m(x,t)$ and $m(x + \mathrm{d}x, t)$ determine a gain and a loss of mass density between the two planes, so that their difference must be equal to the net variation of mass flux density inside the region. Indicating by $\rho(x,t)q(x,t)$ the source term (where q represents the rate of production or of absorption of mass) this variation is written as follows

$$\frac{\partial \rho(x,t)}{\partial t}\mathrm{d}x = \rho(x,t)q(x,t)\mathrm{d}x - m(x+\mathrm{d}x,t) + m(x,t)$$

therefore

$$\frac{\partial \rho}{\partial t} = \rho q - \frac{\partial m}{\partial x}$$

The last equality expresses the Eulerian *mass conservation law*: a mass increase (decrease) in a fixed space is caused by a net ingoing (outgoing) flux and/or by an introduction (absorption) of matter. For obtaining the same law with respect to a point moving with the fluid (Lagrangian formulation) the term $\partial\rho/\partial t$ is written as a function of the total derivative (see Eq. (3) in one dimension):

$$\dot{\rho} = \rho q - \rho\frac{\partial v}{\partial x} - v\frac{\partial \rho}{\partial x} + v\frac{\partial \rho}{\partial x} = \rho q - \rho\frac{\partial v}{\partial x} \tag{5}$$

The three dimensional generalization is straightforward in both cases: in this case the flux is given by the vector $\mathbf{m} := \rho\mathbf{v}$, therefore

$$\rho_t = \rho q - \boldsymbol{\nabla}\cdot\mathbf{m} \tag{6}$$

$$\dot{\rho} = \rho q - \rho\boldsymbol{\nabla}\cdot\mathbf{v} \tag{7}$$

We note that the mass velocity $\mathbf{v}$ can be interpreted as the ratio of the mass flux density to the mass density: $\mathbf{v} = \mathbf{m}/\rho$. Moreover, Eq. (7) for $q = 0$ can be written

$$\boldsymbol{\nabla}\cdot\mathbf{v} = -\frac{\dot{\rho}}{\rho} = -\frac{\mathrm{d}\log\rho}{\mathrm{d}t} \tag{8}$$

from which one realizes that if the trajectories do not diverge, i.e. $\boldsymbol{\nabla}\cdot\mathbf{v} = 0$, the fluid density remains constant, if on the contrary $\boldsymbol{\nabla}\cdot\mathbf{v} < 0$ (> 0), that is the trajectories are convergent (divergent), the density increases (decreases) along the path.

1.1.3 The Euler equation

The fundamental equation of fluid dynamics is directly derived from the Newton law. Since we are dealing with small acoustic perturbations in air, we can make the reasonable assumption that gravity and internal friction are negligible [4] , so that the only effective forces acting on a particle are the surface ones, due to the pressure exerted by the adjacent fluid portions. Therefore,

considering a volume V, delimited by a surface S, we have

$$\mathbf{F}_S = -\int_S \mathrm{d}^2\mathbf{x}\, p\mathbf{n} \tag{9}$$

where $\mathbf{n}$ is the external normal unit vector of the surface. Applying the divergence theorem to the three components we obtain the volume integral from the surface one:

$$\mathbf{e}_i \int_S \mathrm{d}^2\mathbf{x}\, p\mathbf{n} = \int_S \mathrm{d}^2\mathbf{x}\, p(\mathbf{e}_i \cdot \mathbf{n}) = \int_V \mathrm{d}^3\mathbf{x}\, \boldsymbol{\nabla} \cdot (\mathbf{e}_i p) = \mathbf{e}_i \cdot \int_V \mathrm{d}^3\mathbf{x}\, \boldsymbol{\nabla} p$$

Remembering Eq. (4) , we get the *Euler equation*

$$\int_V \mathrm{d}^3\mathbf{x}\, \rho \left[\frac{\partial \mathbf{v}}{\partial t} + (\mathbf{v} \cdot \boldsymbol{\nabla})\mathbf{v}\right] = \int_V \mathrm{d}^3\mathbf{x}\, \boldsymbol{\nabla} p \tag{10}$$

whose differential form is

$$\mathbf{v}_t + (\mathbf{v} \cdot \boldsymbol{\nabla})\mathbf{v} = \frac{\boldsymbol{\nabla} p}{\rho} \tag{11}$$

First of all we note that this is non linear, owing to the terms $(\mathbf{v} \cdot \boldsymbol{\nabla})\mathbf{v}$ and $\boldsymbol{\nabla} p/\rho$; moreover, the unknown functions are five ($\mathbf{v}$, p, ρ) so, even joining the scalar mass equation, we cannot find a unique set of solutions. Anyway, we'll see that in the case of perfect gases it is possible to derive a linear version of Eq. (11) — once some physical conditions are satisfied — as well as to establish a proportionality relationship among some of the variables: this will allow us to solve the problem.

Now we may spend some time in finding an alternative formulation of the general Euler equation, which will turn out to be useful later. For this we suppose the motion is *isentropic*, i.e. the effects due to the friction and thermal conductivity are negligible, so that the entropy content of a fluid particle may thought to remain constant along the path; note that this assumption is well justified in the audible frequency range [4] , which is just the situation we are going to study.

Let's introduce the thermodynamical functions: s, h, ε, representing the entropy, the enthalpy and the internal energy per unit mass. The entropy conservation is expressed by the vanishing Lagrangian derivative ($\dot{s} = 0$) while the first and second law of thermodynamics for an infinitesimal transformation are respectively given by

$$\mathrm{d}\varepsilon = \mathrm{d}Q - p\mathrm{d}V \qquad dQ = T\mathrm{d}s \tag{12}$$

where $\mathrm{d}Q$ is the heat absorbed per unit mass and T the absolute temperature. In our case $\mathrm{d}s = 0$, hence, expressing V in terms of the density ρ, one obtains

$$\mathrm{d}\varepsilon = \frac{p}{\rho^2}\mathrm{d}\rho \tag{13}$$

On the other hand, the variation of enthalpy ($h = \varepsilon + p/\rho$) is

$$\mathrm{d}h = \mathrm{d}\varepsilon - \frac{p}{\rho^2}\mathrm{d}\rho + \frac{\mathrm{d}p}{\rho}$$

Therefore, replacing $\mathrm{d}\varepsilon$ with the aid of Eq. (13) , we have $\mathrm{d}h = \mathrm{d}p/\rho$. It follows

$$\boldsymbol{\nabla} p = \rho \boldsymbol{\nabla} h \tag{14}$$

The Euler equation for an isentropic fluid motion is then

$$\mathbf{v}_t + (\mathbf{v}\cdot\boldsymbol{\nabla})\mathbf{v} = \boldsymbol{\nabla} h \tag{15}$$

1.1.4 Energy and momentum

The fluid energy per unit volume is

$$w = \rho\left(\frac{\mathbf{v}^2}{2} + \varepsilon\right) \tag{16}$$

where $\mathbf{v}^2/2$ and ε are the kinetic and the internal part. In order to obtain the expression describing the energy transfer, we must calculate the partial time derivative of w. The kinetic term gives (using Eqs. (6) and (15)):

$$\begin{aligned}\frac{1}{2}(\rho\mathbf{v}^2)_t &= \frac{1}{2}(\mathbf{v}^2\rho_t + 2\rho\mathbf{v}\cdot\mathbf{v}_t) = -\frac{\mathbf{v}^2}{2}\boldsymbol{\nabla}\cdot(\rho\mathbf{v}) - \rho\mathbf{v}\cdot(\mathbf{v}\cdot\boldsymbol{\nabla})\mathbf{v} - \rho\mathbf{v}\cdot\boldsymbol{\nabla} h \\ &= -\frac{\mathbf{v}^2}{2}\boldsymbol{\nabla}\cdot(\rho\mathbf{v}) - \rho\mathbf{v}\cdot\boldsymbol{\nabla}\left(\frac{\mathbf{v}^2}{2} + h\right)\end{aligned}$$

For the internal term we obtain

$$(\rho\varepsilon)_t = \rho\varepsilon_t + \rho_t\varepsilon = \frac{p}{\rho}\rho_t + \rho_t\varepsilon = \rho_t\left(\frac{p}{\rho} + \varepsilon\right) = -h\boldsymbol{\nabla}\cdot(\rho\mathbf{v})$$

where in the second equality we have made use of Eq. (13) , which implies $\varepsilon_t = p\rho^{-2}\rho_t$, while in the last one we have written the definition of enthalpy and used Eq. (6) once again. The sum of the two terms gives $-\boldsymbol{\nabla}\cdot[\rho\mathbf{v}\,(h + \mathbf{v}^2/2)]$, so, defining the vector $\mathbf{j} = \rho\mathbf{v}\,(h + \mathbf{v}^2/2)$,

$$w_t + \boldsymbol{\nabla}\cdot\mathbf{j} = 0 \tag{17}$$

This is exactly the fluids *energy conservation law*. Integrating Eq. (17) in a fixed volume V and then using the divergence theorem, it follows

$$\frac{\mathrm{d}}{\mathrm{d}t}\int_V \mathrm{d}^3\mathbf{x}\, w = -\int_S \mathrm{d}^2\mathbf{x}\,\mathbf{j}\cdot\mathbf{n} \tag{18}$$

The meaning of Eq. (18) can be simply stated as follows: when the source term is null, the energy variation in the unit time inside V is equal to the ingoing flux of $\mathbf{j}$ through S. Therefore, $\mathbf{j}$ plays the role of *energy flux density* but, unlike the case of the mass equation, where the flux was equal to the density times velocity, $\mathbf{j}$ is now not just equal to $w\mathbf{v}$; yet $\mathbf{j} = w\mathbf{v} + p\mathbf{v}$, from which:

$$w_t + \boldsymbol{\nabla}\cdot(w\mathbf{v} + p\mathbf{v}) = 0 \tag{19}$$

In short, $w\mathbf{v}$ is the analogous of $\rho\mathbf{v}$ in the law $\rho_t + \boldsymbol{\nabla}\cdot(\rho\mathbf{v}) = 0$ and may be interpreted as a convection term; on the other hand, $p\mathbf{v}$ is the work done by pressure.

The fluid motion produces also a transfer of momentum: its value per unit volume is equal to the mass density flux $\mathbf{m} = \rho\mathbf{v}$. With arguments similar to those illustrated above, one may get a vectorial relation expressing the *momentum conservation law*:

$$\mathbf{m}_t + \boldsymbol{\nabla}\cdot\mathfrak{T} = \mathbf{0} \tag{20}$$

The flux is now a second order symmetrical tensor which may be decomposed in two parts: $\mathfrak{T}$=$\mathfrak{J}$+$\mathfrak{P}$, where $\mathfrak{J}$ is the *convective momentum flux* and $\mathfrak{P}$ the *stress tensor*:

$$\mathfrak{J} = \rho \begin{pmatrix} v_x v_x & v_x v_y & v_x v_z \\ v_y v_x & v_y v_y & v_y v_z \\ v_z v_x & v_z v_y & v_z v_z \end{pmatrix} \qquad \mathfrak{P} = \begin{pmatrix} p & 0 & 0 \\ 0 & p & 0 \\ 0 & 0 & p \end{pmatrix} \tag{21}$$

1.2 Sound in perfect gases

Now we shall deal with the main theoretical topics regarding linear acoustics in perfect gases: the context where most of sound phenomena perceived by human beings take place. This will be the background which our work will be built on [2] , [3] .

1.2.1 The wave equation

We may indicate the absence of acoustical perturbations in the medium by means of the equilibrium values of the three fundamental quantities: pressure, mass density, fluid velocity (p_0, ρ_0, $\mathbf{v}_0$); however we shall remember that, in ordinary environmental conditions, the particle velocity may be thought to be zero, since the motion of the single molecules is of thermal origin.

When an acoustic source, like a vibrating object, produces a perturbation in the medium, the above mentioned quantities become: $p = p_0 + p_1$, $\rho = \rho_0 + \rho_1$, $\mathbf{v} = \mathbf{v}_1$. Eqs. (6) and (11) , in a region of space not including the source, are then written as follows

$$(\rho_0 + \rho_1)_t + \boldsymbol{\nabla} \cdot [(\rho_0 + \rho_1)\, \mathbf{v}] = 0$$

$$(\rho_0 + \rho_1)\, (\mathbf{v}_t + \mathbf{v} \cdot \boldsymbol{\nabla}\mathbf{v}) = -\boldsymbol{\nabla}\, (p_0 + p_1)$$

The linear acoustic theory is based on the assumption that pressure and density variations, p_1 and ρ_1, are small compared with the corresponding equilibrium values: this allows us to neglect all the terms of order higher than first in the equations. The result is the following pair of relations:

$$\rho_{1t} + \rho_0 \boldsymbol{\nabla} \cdot \mathbf{v} = 0 \tag{22}$$

$$\mathbf{v}_t + \frac{\boldsymbol{\nabla} p}{\rho_0} = 0 \tag{23}$$

which, in contrast to the previous ones, are linear.

Thanks to another basic simplification, this time due to thermodynamics, is then possible to establish a proportionality relationship between $p_1$and ρ_1, which represents the empirical phenomenon of the linear dependence between the normal stress and the volume change. The physical principle accounting for that is the “Laplace hypothesis”, for which sound vibration occurs without any significant heat transfer. From the Fourier equation viewpoint ($\rho T\, (s_t + \mathbf{v} \cdot \boldsymbol{\nabla} s) = \kappa\, \Delta T$) the statement is equal to setting the thermal conduction coefficient κ to zero, so that the motion is isentropic, being $s_t + \mathbf{v} \cdot \boldsymbol{\nabla} s = 0$. In the case of a medium which can be well described by a perfect gas, as for instance air at ordinary pressure and temperature ($p_0 \simeq 10^5\,\mathrm{Pa}$, $T_0 \simeq 300\,\mathrm{K}$), it follows:

$$p = C\rho^\gamma \tag{24}$$

where $\gamma = c_p/c_V$ is the specific heats ratio and C is a constant. Through a Taylor series expansion limited to first order, one then finds that pressure variations obey the following relationship

$$p_1 \equiv \mathrm{d}p = \left(\frac{\partial p}{\partial \rho}\right)_s \mathrm{d}\rho = c^2 \rho_1 \tag{25}$$

where the quantity c^2, which we will dwell upon in the following section, has the dimensions of a squared velocity. If in Eq. (22) we replace the expression of ρ_1 from Eq. (25) and differentiate with respect to time, we have

$$\frac{p_{tt}}{c^2} + \rho_0 \boldsymbol{\nabla} \cdot \mathbf{v}_t = 0$$

from which, writing $\mathbf{v}_t$ according to Eq. (23) , we get the *wave equation* (called also *d'Alembert equation*) for pressure:

$$\boldsymbol{\Delta} p - \frac{p_{tt}}{c^2} = 0 \tag{26}$$

It is easy to show that, thanks to Eq. (25) , the same equation holds for mass density as well.

1.2.2 The speed of sound

The form of Eq. (26) tells us that c is the speed of sound propagation in adiabatic conditions. From Eq. (24) we obtain the equality

$$c^2 = \frac{\partial}{\partial \rho} C \rho^\gamma = \gamma C \rho^{\gamma - 1} = \frac{\gamma p}{\rho}$$

which, according to the state equation for perfect gases: $p = \rho RT/m_{air}$ (where $R = 8314\,\mathrm{J\,kg^{-1}\,K^{-1}}$ and m_{air} is the average molecular weight of air), becomes

$$c^2 = \frac{\gamma RT}{m_{air}} \tag{27}$$

Dry air is approximately made up of $78\,\%$ N_2 ($m_{N_2} = 28$), $21\,\%$ O_2 ($m_{O_2} = 32$) and $1\,\%$ Ar ($m_{Ar} = 40$), hence $m_{air} \simeq 0.78 \times 28 + 0.21 \times 32 + 0.01 \times 40 \simeq 29$. Moreover, putting $\gamma = 1.4$ ($c_p = 1.08 \cdot 10^{-3}\,\mathrm{J\,kg^{-1}K^{-1}}$, $c_V = 5/7 c_p$), sound speed at $T = 300\,\mathrm{K}$ is found to be about $347\ \mathrm{m\,s^{-1}}$.

1.2.3 The velocity potential

If in the linearized Euler equation (Eq. (23)) we apply the rotor operator to both sides we get $(\boldsymbol{\nabla} \times \mathbf{v})_t = 0$, for $\boldsymbol{\nabla} \times \boldsymbol{\nabla} p = 0$: this admits a solution $\mathbf{v}$ whose rotor is zero:

$$\boldsymbol{\nabla} \times \mathbf{v} = 0 \tag{28}$$

hence describing an *irrotational* motion (not involving any rotation and deformation with change of shape). One easily verifies from Eq. (22) that in these conditions also the velocity vector satisfies the wave equation:

$$\boldsymbol{\Delta} \mathbf{v} - \frac{\mathbf{v}_{tt}}{c^2} = 0 \tag{29}$$

Acoustical waves are thus *longitudinal*, the particles movement being directed along $\mathbf{v}$. According to Eq. (28) , $\mathbf{v}$ itself may be expressed through the gradient of a scalar function $\phi(\mathbf{x}, t)$,

named *velocity* (or *kinetic*) *potential*; as a consequence the Euler equation may be written $\boldsymbol{\nabla}(\rho_0\phi_t + p) = 0$, from which one infers that the argument of the gradient is a function of time only:

$$\rho_0\phi_t + p = f(t)$$

If, through a gauge transformation, the potential is chosen in such a way that f is zero for every t, we find out that p_1, ρ_1, $\mathbf{v}$ may be written as functions of ϕ only:

$$\mathbf{v} = \boldsymbol{\nabla}\phi \qquad p_1 = -\rho_0\phi_t \qquad \rho_1 = -\frac{\rho_0\phi_t}{c^2} \tag{30}$$

We also note that the wave equation is fulfilled by the potential too:

$$\boldsymbol{\Delta}\phi - \frac{\phi_{tt}}{c^2} = 0 \tag{31}$$

so, thanks to Eq. (30) , we shall take Eq. (31) as the reference equation in the formal study of linear acoustic fields.

1.2.4 Sources

Now we will realize that the wave equation referred to a region containing the acoustic source has a non homogeneous form. Actually we may describe the sound origin in two ways: by means of mass source or by a pressure perturbation. If we focus our attention on the latter case it is helpful to write the perturbation as a distribution $P(\mathbf{x}, t)$; Eq. (23) then becomes

$$\rho_0\mathbf{v}_t + \boldsymbol{\nabla}p = -\boldsymbol{\nabla}P \tag{32}$$

Introducing the velocity potential, Eq. (32) is rewritten in the form $\boldsymbol{\nabla}(\rho_0\phi_t + p + P) = 0$, as it has been done in the previous section, ϕ may be chosen in order to make the gradient argument zero. If we replace $\mathbf{v} = \boldsymbol{\nabla}\phi$ into Eq. (22) we get the kinetic potential wave equation with the source term q

$$\boldsymbol{\Delta}\phi - \frac{\phi_{tt}}{c^2} = q \qquad q = \frac{P_t}{\rho_0 c^4} \tag{33}$$

Now, taking into account Eq. (30) , we obtain the expressions of the source terms appearing in the wave equations of pressure, density and particle velocity

$$q_p = -\frac{P_{tt}}{c^2} \qquad q_\rho = -\frac{P_{tt}}{c^4} \qquad \mathbf{q}_\mathbf{v} = \frac{\boldsymbol{\nabla}P_t}{\rho_0 c^2} \tag{34}$$

1.3 Elementary fields

Even though in practice it is almost always impossible to determine a solution of the wave equation describing the physical situation in an exact manner, it is useful to study some ideal cases; these can in fact be often taken as suitable models for accomplishing an approximate analysis of the acoustic system. For this reason we will now discuss two important solutions of the homogenous equation [3] .

1.3.1 Plane waves

The simplest field is given by the *plane wave*: in a proper reference frame its quantities may be described as functions of just one spatial coordinate, let's say x, and of the time t. The wave equation for plane waves is thus reduced to the one-dimensional form, whose most general solution is written

$$\phi(x,t) = f_+(x-ct) + f_-(x+ct) \tag{35}$$

where f_+ e f_- are two arbitrary functions, which are constant on planes normal to x, representing a wave traveling at speed c along the positive and negative x respectively. According to Eq. (30) pressure and velocity are

$$\begin{aligned} p(x,t) &= \rho_0 c f'_+ - \rho_0 c f'_- = p_+ + p_- \\ v(x,t) &= f'_+ + f'_- = p_+/\rho_0 c - p_-/\rho_0 c \end{aligned} \tag{36}$$

For a generic direction, the plane wave solution is written $\phi(\mathbf{x},t) = f_+(\mathbf{k}\cdot\mathbf{x}-\omega t) + f_-(\mathbf{k}\cdot\mathbf{x}+\omega t)$: in this case the propagation plane is defined by the equation $\mathbf{k}\cdot\mathbf{x} = const.$ where $\mathbf{k}$, called *wave vector*, satisfies the dispersion law $\mathbf{k}^2c^2 = \omega^2$.

In the class of the plane waves an essential role is played by *monochromatic waves*, which in polar form are written

$$\phi(\mathbf{x},t) = A\mathrm{e}^{\mathrm{i}(\mathbf{k}\cdot\mathbf{x}-\omega t)} \tag{37}$$

Note that A is a complex amplitude, independent of $\mathbf{x}$ and t.

1.3.2 Spherical waves

Spherical waves are characterized by the dependence on a distance r from a fixed point in space, called *center*. Their mathematical expression can be easily obtained writing the wave equation in spherical coordinates and neglecting the polar and azimuthal angles. The result is

$$[r\phi(r,t)]_{rr} = \frac{[r\phi(r,t)]_{tt}}{c^2} \tag{38}$$

which is just the d'Alembert equation for the function $r\phi(r,t)$. According to what we have said in the previous section a solution of Eq. (38) is of the kind

$$\phi(r,t) = \frac{f_+(r-ct) + f_-(r+ct)}{r} \tag{39}$$

Therefore the first term represents an *outgoing* wave, propagating from the origin to infinite distances and with an amplitude decreasing as r^{-1}, the second is the *ingoing* term, traveling in the opposite direction.

For a sinusoidal time dependence the sound pressure and the particle velocity are

$$p(r,t) = \frac{P_0}{r}\mathrm{e}^{[\mathrm{i}(kr-\omega t)]} \qquad v(r,t) = \frac{P_0}{\omega\rho_0 r}\left(k - \frac{\mathrm{i}}{r}\right)\mathrm{e}^{[\mathrm{i}(kr-\omega t)]} = \frac{p(r,t)}{\rho_0 c}\left(1 - \frac{\mathrm{i}}{kr}\right)$$

Unlike the case of the plane wave behavior, the phase relationship between p and v depends on a length, through the scale factor kr. It is thus customary to think of a spherical wave as roughly divided in two regions: the *near field* ($kr \ll 1$), where the velocity component in quadrature with the pressure dominates, and a *far field* ($kr \gg 1$), where the opposite occurs. As we will

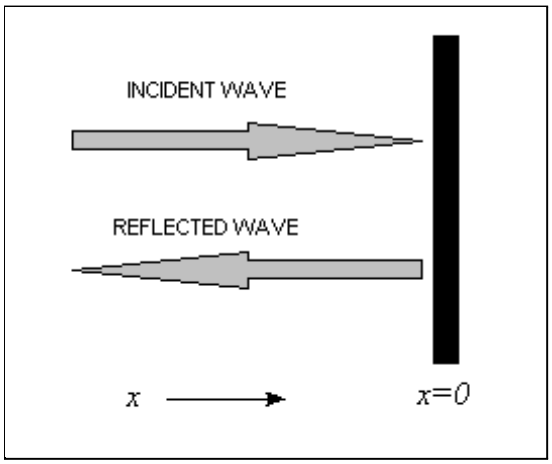

FIGURE 1. The normal reflection of a plane wave.

see below, this property has remarkable effects on the way how the energy is transferred inside the field.

1.4 The wave reflection

Up to this point we have focused our attention just on intrinsic properties of the acoustic field: we have not explained what happens when there are constraints in the environment. This is by far the most frequent situation encountered in practice: think for instance at the way how the sound propagates in rooms, where the space available is even finite. This argument will be treated more extensively in the next chapter; yet, now it is necessary to introduce the general law of reflection from the wave point of view [4] : this will allow us to understand the main effects on the energy propagation. The easiest way of doing this is to take into account the reflection of a plane monochromatic wave on a single surface, which for simplicity is considered perfectly plane, rigid and of infinite extension, but partially porous. When the wave interacts with the wall a secondary wave is created in correspondence of the air-wall separation surface. This is called *reflected wave* and has a different amplitude, phase and propagation direction, from those of the direct one. If the incident wave is normal to the surface, let's say it travels along the direction x as shown by Fig. 1 its pressure and velocity components are given by

$$p_i(x,t) = P_0 \mathrm{e}^{\mathrm{i}(\omega t - kx)} \qquad v_i(x,t) = \frac{P_0}{z}\mathrm{e}^{\mathrm{i}(\omega t - kx)}$$

where P_0 indicates the wave amplitude and $z = \rho_0 c$ (*characteristic impedance of air*). The reflected wave is then:

$$p_r(x,t) = CP_0\mathrm{e}^{\mathrm{i}(\omega t + kx + \phi)} = \mathcal{C}P_0\mathrm{e}^{\mathrm{i}(\omega t + kx)} \qquad v_r(x,t) = -C\frac{P_0}{z}\mathrm{e}^{\mathrm{i}(\omega t + kx + \phi)} = -\mathcal{C}\frac{P_0}{z}\mathrm{e}^{\mathrm{i}(\omega t + kx)}$$

where we have introduced the complex *reflection coefficient* $\mathcal{C} := C\mathrm{e}^{\mathrm{i}\phi}$ $(0 \leq C \leq 1)$; the total field is then the result of an *interference* process: $p = p_i + p_r$, $v = v_i + v_r$ (see Eq. (35)). In

particular, evaluating the above expressions in the plane given by $x = 0$:

$$p(0,t) = P_0\,(1+\mathcal{C})\,\mathrm{e}^{\mathrm{i}\omega t} \qquad v(0,t) = \frac{P_0}{z}\,(1-\mathcal{C})\,\mathrm{e}^{\mathrm{i}\omega t}$$

We emphasize three notable cases:

- $\mathcal{C} = 1$: perfectly reflecting surface with impenetrable walls ($v(0,t) = 0$);
- $\mathcal{C} = -1$: perfectly reflecting surface with pressure release ($p(0,t) = 0$);
- $\mathcal{C} = 0$: non reflecting surface ($p(0,t) = v(0,t)/z$).

1.5 Acoustic energy and momentum

The theoretical and experimental study of acoustic phenomena is often undertaken with attention on the energy and momentum carried by the waves. We will now see how to describe the behavior of these quantities in the linear context, once again with the help of the general laws of fluid dynamics processes [2] , [3] .

1.5.1 The energy conservation law

Let's expand the energy w of Eq. (16) in a Taylor series up to second order with respect to the density perturbation $\rho_1 = \rho - \rho_0$. As regards the internal energy term, we have:

$$\rho\varepsilon \simeq \rho_0\varepsilon_0 + (\rho-\rho_0)\left[\frac{\partial(\rho\varepsilon)}{\partial\rho}\right]_{\rho=\rho_0} + \frac{1}{2}(\rho-\rho_0)^2\left[\frac{\partial^2(\rho\varepsilon)}{\partial\rho^2}\right]_{\rho=\rho_0}$$

The two derivatives must be calculated at constant entropy: using the relation $dh = dp/\rho$ (Eq. (14)) and the definition of c^2 (Eq. (25)) we find

$$\left[\frac{\partial(\rho\varepsilon)}{\partial\rho}\right]_s = \left[\frac{\partial(\rho h - p)}{\partial\rho}\right]_s = h + \rho\left(\frac{\partial h}{\partial\rho}\right)_s - c^2 = h + \rho\left(\frac{\partial h}{\partial p}\right)_s\left(\frac{\partial p}{\partial\rho}\right)_s - c^2 = h$$

$$\left[\frac{\partial^2(\rho\varepsilon)}{\partial\rho^2}\right]_s = \left(\frac{\partial h}{\partial p}\right)_s = \frac{c^2}{\rho}$$

Replacing ρ_1 with p_1/c^2 and adding the kinetic term we obtain

$$w \simeq \rho_0\varepsilon_0 + \rho_1 h_0 + \frac{1}{2}\frac{p_1^2}{\rho_0 c^2} + \frac{1}{2}\rho_0\mathbf{v}^2$$

The first two terms are unessential from the acoustic point of view: in fact, $\rho_0\varepsilon_0$ is the energy density of the medium at rest while $\rho_1 h_0$ can be neglected, because its integral on the gas volume vanishes, meaning that it doesn't give any global contribution. The final approximated *acoustic energy density* w_1 is then given by the sum of the a *kinetic* part, $\rho_0\mathbf{v}^2/2$, and a *potential* (or compression) part, $p_1^2/(2\rho_0 c^2)$.

$$w_1 := \frac{1}{2}\rho_0\left(\frac{p_1^2}{z^2} + \mathbf{v}^2\right) \tag{40}$$

We now may find out the expression of the energy conservation law. Differentiating w_1 and writing p_1 and $\mathbf{v}$ by means of Eq. (30) we obtain

$$w_{1t} = \rho_0 \left(\frac{p_{1t} p_1}{z^2} + \mathbf{v}_t \cdot \mathbf{v} \right) = \rho_0 \left(\frac{\phi_{tt} \phi_t}{c^2} + \boldsymbol{\nabla} \phi_t \cdot \boldsymbol{\nabla} \phi \right) \tag{41}$$

In general ϕ obeys the non-homogeneous wave equation (Eq. (33)), therefore we may write $\phi_{tt} = c^2 (\boldsymbol{\Delta} \phi - q)$. Eq. (41) becomes then

$$w_{1t} = \rho_0 \left[\phi_t \left(\boldsymbol{\Delta} \phi - q \right) + \boldsymbol{\nabla} \phi_t \cdot \boldsymbol{\nabla} \phi \right] = -\boldsymbol{\nabla} \cdot (p_1 \mathbf{v}) + p_1 q$$

This is usually written

$$w_{1t} + \boldsymbol{\nabla} \cdot \mathbf{j}_1 = p_1 q \tag{42}$$

Thus, the role of the vector $\mathbf{j}_1 = p_1 \mathbf{v}$, called *acoustic intensity*, is that of *wave energy flux density*, while $p_1 q$ represents the energy source term, i.e. the space-time distribution of energy introduced in the environment per unit time.

1.5.2 The momentum conservation law

The wave momentum density is $\mathbf{m}_1 = \rho_1 \mathbf{v}$ (see Sect. 1.1.4): the corresponding conservation equation is

$$\mathbf{m}_{1t} + \boldsymbol{\nabla} \cdot \mathfrak{M} = \mathbf{0} \tag{43}$$

where $\mathfrak{M}$ is the *wave-stress tensor*, representing the *wave momentum flux density*: this is found to be [2]

$$\mathfrak{M} = \rho_0 \begin{pmatrix} \frac{1}{2}\left(v_x^2 - v_y^2 - v_z^2 + \frac{p^2}{z^2} \right) & v_x v_y & v_x v_z \\ v_y v_x & \frac{1}{2}\left(v_y^2 - v_z^2 - v_x^2 + \frac{p^2}{z^2} \right) & v_y v_z \\ v_z v_x & v_z v_y & \frac{1}{2}\left(v_z^2 - v_x^2 - v_y^2 + \frac{p^2}{z^2} \right) \end{pmatrix} \tag{44}$$

It is easy to see that the wave momentum density is proportional to the sound intensity:

$$\mathbf{m}_1 = \frac{\mathbf{j}_1}{c^2} \tag{45}$$

This relation is quite general (for instance it holds for electromagnetic waves if $\mathbf{j}_1$ indicates the Poynting vector and c the speed of light) and represents a link between the two conservation equations (Eqs. (42) and (43)).

From now on we will exclusively deal with acoustic quantities, hence we can write them omitting the subscript 1.

1.5.3 Radiation pressure

Integrating Eq. (43) on a volume V, enclosed by the surface S, one finds

$$\frac{\mathrm{d}}{\mathrm{d}t} \int_V \mathrm{d}^3 \mathbf{x}\, \mathbf{m} = -\int_V \mathrm{d}^3 \mathbf{x}\, \boldsymbol{\nabla} \cdot \mathfrak{M} = -\int_S \mathrm{d}^2 \mathbf{x}\, \mathfrak{M} \cdot \mathbf{n} \tag{46}$$

where the last equality follows from the divergence theorem. Denoting by $\mathbf{m}_V$ the momentum of the wave in V and by $\mathbf{F}$ the total force, Eq. (46) can be written

$$\frac{\mathrm{d}\mathbf{m}_V}{\mathrm{d}t} = \mathbf{F} \tag{47}$$

which is just the Newton law. From Eq. (47) we can gain a deeper understanding of the tensor $\mathfrak{M}$: in fact, the vector $\mathbf{p}_{rad} = -\mathfrak{M} \cdot \mathbf{n}$ is the *radiation pressure* exerted by the wave on a surface of normal $\mathbf{n}$. This is a quite important result, for its shows that the acoustic radiation pressure, often treated as a nonlinear effect [5] , is present in the linear case as well [6] .

1.6 Energy average behavior

We now approach to the main subject of the present work, the study of the average behavior of acoustic energetic quantities. The averaging procedure we will referred to in the following of the discussion is expressed in Appendix and appropriate both for deterministic signals and stationary ergodic processes.

As far as concerns the energy density, the average values of the two components are proportional to the *mean square pressure* and *mean square velocity* respectively:

$$W_U(\mathbf{x}) := \frac{1}{2}\rho_0 \frac{\langle p^2 \rangle}{z^2} \qquad W_K(\mathbf{x}) := \frac{1}{2}\rho_0 \langle \mathbf{v}^2 \rangle \tag{48}$$

thus the total energy is of course

$$W(\mathbf{x}) := \langle w \rangle = W_U + W_K = \frac{1}{2}\rho_0 \left(\frac{\langle p^2 \rangle}{z^2} + \langle \mathbf{v}^2 \rangle \right) \tag{49}$$

In general W_U and W_K are not equal: for characterizing their relative magnitude it is useful to introduce the indicator [10]

$$\sigma := \frac{2\sqrt{W_U W_K}}{W_U + W_K} = \frac{2cz\sqrt{\langle p^2 \rangle \langle \mathbf{v}^2 \rangle}}{\langle p^2 \rangle + z^2 \langle \mathbf{v}^2 \rangle} \tag{50}$$

which is the ratio of the geometric to arithmetic mean of the two energy parts. Note that $0 \leq \sigma \leq 1$.

Extremely important is also the average version of Eq. (42) : thanks to $\langle w_t \rangle = 0$, it reduces to

$$\boldsymbol{\nabla} \cdot \mathbf{A} = \langle pq \rangle \tag{51}$$

where we have defined the *mean intensity* vector: $\mathbf{A}(\mathbf{x}) := \langle \mathbf{j} \rangle$, which can be also interpreted as the sound power flux density. We can graphically represent the mean intensity vector $\mathbf{A}(\mathbf{x})$ of a steady acoustic field by mean of a pattern of *power flux streamlines* : these are built analogously to the usual streamlines adopted for describing the mass flow in a fluid. In particular, a power flux streamline is any continuous line across which the mean power flow is zero [7] , [8] . Actually, in many real situations the time average distribution $\langle pq \rangle$ is zero everywhere, apart from a limited region occupied by the source (consider for instance a loudspeaker in a room), then the most frequent form of Eq. (51) is $\boldsymbol{\nabla} \cdot \mathbf{A} = 0$. In this case the Gauss's theorem holds, meaning that the power flux through a tube formed by a bundle of streamlines is conserved.

1.7 Time independent intensities

The definition of the mean intensity suggests an important remark. The mean value $\mathbf{A}$ is strongly affected by the time-dependence of $p(\mathbf{x},t)$ as compared with that of $\mathbf{v}(\mathbf{x},t)$. For instance, if $\mathbf{A}$ vanishes, due to symmetrical oscillations of $\mathbf{j}$ around zero, it is clear that $\mathbf{A}$ by itself doesn't suffice to describe the average energy motion. Our next target will be then that of expressing $\mathbf{j}$ in such a way to evaluate also the part not associated to a net transfer of energy. We begin with the simplest case.

1.7.1 Monochromatic fields

The acoustic pressure for a monochromatic field may be written in real form as:

$$p(\mathbf{x},t) = P(\mathbf{x})\cos\left[\chi(\mathbf{x}) - \omega t\right] \tag{52}$$

through the Euler equation the velocity is then given by:

$$\mathbf{v}(\mathbf{x},t) = \frac{P(\mathbf{x})\boldsymbol{\nabla}\chi(\mathbf{x})}{\omega\rho_0}\cos\left[\chi(\mathbf{x}) - \omega t\right] - \frac{\boldsymbol{\nabla}P(\mathbf{x})}{\omega\rho_0}\sin\left[\chi(\mathbf{x}) - \omega t\right] \tag{53}$$

It is evident that $\mathbf{v}$ is formed by a sum of a term in phase and one in quadrature with the pressure; we will indicate these contributions by $\mathbf{v}_p$ and $\mathbf{v}_q$ respectively [9] . The instantaneous intensity $\mathbf{j} = p\mathbf{v}$ itself will then split into two parts: $\mathbf{a} = p\mathbf{v}_p$ e $\mathbf{r} = p\mathbf{v}_q$, in such a way that $\langle\mathbf{a}\rangle = \mathbf{A}$ and $\langle\mathbf{r}\rangle = \mathbf{0}$. In this way we have obtained a simple partition of the flux $\mathbf{j}$, suitable to our purpose: $\mathbf{a}$ represents the term responsible for the net energy transfer and $\mathbf{r}$ is the oscillation term. We will call these two vectors: *radiating intensity* and *oscillating intensity* [19] ; they may be written in this way:

$$\mathbf{a} = 2\mathbf{A}\left[\cos\left(\chi - \omega t\right)\right]^2 \qquad \mathbf{r} = \mathbf{R}\sin\left[2\left(\chi - \omega t\right)\right] \tag{54}$$

where $\mathbf{A}(\mathbf{x}) = P^2\boldsymbol{\nabla}\chi/2\omega\rho_0$ and $\mathbf{R}(\mathbf{x}) = -P\boldsymbol{\nabla}P/2\omega\rho_0$.

1.7.2 General fields

When extending the definition of $\mathbf{a}$ and $\mathbf{r}$ to the general case of non monochromatic fields, which in practice is by far the most common one, one has to bear in mind that the concept of relative phase between p and $\mathbf{v}$ looses its meaning. We can convince ourselves of this by a simple example; let's take a bichromatic field whose pressure is

$$p = p_1 + p_2 = P_1\,\cos\left[\chi_1 - \omega_1 t\right] + P_2(\mathbf{x})\,\cos\left[\chi_2 - \omega_2 t\right]$$

The velocity is here given by four terms: $\mathbf{v} = \mathbf{v}_{1p} + \mathbf{v}_{1q} + \mathbf{v}_{2p} + \mathbf{v}_{2q}$, therefore the total instantaneous intensity is formed by eight terms; among these the only ones which do not vanish on average are $p_1\mathbf{v}_{1p}$ e $p_2\mathbf{v}_{2p}$, while four of the remaining six vanish being products of different frequencies and the other two due to the quadrature relationship between equal frequencies. The oscillating intensity now depends on the relative phases of the single waves and on the cross terms given by the superposition of frequencies, so that the partition in terms of the global phase between p and $\mathbf{v}$ is no more applicable. We may find a solution to the problem noting that the term $\mathbf{v}_p$ in Eq. (53) may be rewritten as

$$\mathbf{v}_p = \frac{\boldsymbol{\nabla}\chi}{\omega\rho_0}p = \frac{P^2\boldsymbol{\nabla}\chi}{\omega\rho_0}\frac{p}{P^2}$$

which gives:

$$\mathbf{v}_p = \frac{\langle p\mathbf{v}\rangle\, p}{\langle p^2\rangle} \qquad \mathbf{v}_q = \frac{\langle p^2\rangle\, \mathbf{v} - \mathbf{A}p}{\langle p^2\rangle} \tag{55}$$

The partition of $\mathbf{v}$ is now written in such a way that $\mathbf{v}_p(\mathbf{x},t)$ shows the same time dependence of $p(\mathbf{x},t)$ and $\mathbf{v}_q(\mathbf{x},t)$ times p has zero average [12] . Yet, this definition is quite general, and may be used for any kind of field; therefore we can always write $\mathbf{j} = \mathbf{a} + \mathbf{r}$, where:

$$\mathbf{a} := p\mathbf{v}_p = \frac{\mathbf{A}p^2}{\langle p^2\rangle} \qquad \mathbf{r} := p\mathbf{v}_q = \frac{\langle p^2\rangle\, \mathbf{j} - \mathbf{A}p^2}{\langle p^2\rangle} \tag{56}$$

from which one finds $\langle\mathbf{a}\rangle = \mathbf{A}$ and $\langle\mathbf{r}\rangle = \mathbf{0}$ once again.

1.7.3 The polarization tensor

We now discuss the task regarding the quantitative evaluation of "how much" the intensity oscillates on average. Due to the fact that $\langle\mathbf{r}\rangle = \mathbf{0}$ by definition, we have to resort to the general method of second order moments, explained in Appendix (Sect. A.3.1). We start defining the tensor

$$\mathfrak{N}(\mathbf{x}) := 2\,\langle\mathbf{r}\otimes\mathbf{r}\rangle \tag{57}$$

and subsequently

$$\mathfrak{R}(\mathbf{x}) := \sqrt{\mathfrak{N}(\mathbf{x})} \tag{58}$$

which expresses the *average oscillating intensity*. This allows us to represent the indicatrix quadric [11] describing the energy oscillation: its equation is given by

$$\mathbf{q}\cdot\mathfrak{N}_+^{-1}\mathbf{q} = 1 \tag{59}$$

where $\mathfrak{N}_+$ is the restriction of $\mathfrak{N}$ to the subspace of the positive eigenvalues. The graphical rendering of the quadric, which as known may be an ellipsoid, an ellipse or a segment, offers a remarkable physical interpretation of $\mathfrak{N}$: the length l of a generic segment joining the ellipsoid center with a point on its surface, represents the average amount of flux oscillating along the direction defined by the segment. In particular, the eigenvalues of $\mathfrak{R}$, which are the ellipsoid's semiaxes, express this quantity along the three reference axes. We then realize that, when these are not equal, the oscillating flux may be thought to be *polarized*. One remarkable case where this happens is given by monochromatic fields we have analyzed in the previous section: from Eq. (54) we note we are in the case where all the components of $\mathbf{r}$ have the same time dependence, therefore, according to Eq. (177) , we have

$$\mathfrak{R}(\mathbf{x}) = \frac{\mathbf{R}(\mathbf{x})\otimes\mathbf{R}(\mathbf{x})}{|\mathbf{R}(\mathbf{x})|} \tag{60}$$

which has just $|\mathbf{R}|$ as a non vanishing eigenvalue, corresponding to the eigenvector $\mathbf{R}$. It follows that the indicatrix (59) reduces to the segment of length $2\,|\mathbf{R}|$ directed along $\mathbf{R}$.

The amount of energy oscillating in every direction (effective value of $\mathfrak{R}$) is defined introducing the Hilbert-Schmidt norm of $\mathfrak{R}$:

$$R := \|\mathfrak{R}\| = \sqrt{Tr\mathfrak{R}^2} = \sqrt{2\,\langle\mathbf{r}^2\rangle} \tag{61}$$

this is related to $\mathbf{A}$ through the general relationship

$$\mathbf{A}^2 + R^2 = \langle p^2 \rangle \langle \mathbf{v}_p^2 \rangle + 2 \langle p^2 \mathbf{v}_q^2 \rangle \tag{62}$$

In particular, for monochromatic fields one has $R = |\mathbf{R}|$, since $\langle \mathbf{r}^2 \rangle = \mathbf{R}^2/2$. Moreover, from Eqs. (54) and (62) it follows

$$\mathbf{A}^2 + R^2 = \langle p^2 \rangle \langle \mathbf{v}_p^2 \rangle + 2 \langle p^2 \rangle \langle \mathbf{v}_q^2 \rangle \tag{63}$$

1.8 Energy fluxes in elementary fields

In this section we will present some computer simulations aimed to give a deeper understanding of the energy-related quantities behavior in simple field conditions.

1.8.1 Plane wave reflection

The simplest situation where one encounters the fluxes partition is offered by the interference field created by a plane monochromatic wave normally reflected by an ideal plane (see Sect. 1.4). It is useful to write the sound pressure in polar form:

$$p(x,t) = P_0 \left[\mathrm{e}^{\mathrm{i}(\omega t - kx)} + C \mathrm{e}^{\mathrm{i}\theta} \, \mathrm{e}^{\mathrm{i}(\omega t + kx)} \right] = P_0 \, \left[\mathrm{e}^{-\mathrm{i}kx} + C \, \mathrm{e}^{\mathrm{i}\theta} \mathrm{e}^{\mathrm{i}kx} \right] \mathrm{e}^{\mathrm{i}\omega t} = \mathcal{P}(x) \mathrm{e}^{\mathrm{i}\omega t}$$

by simple trigonometric calculations the complex factor $\mathcal{P}(x)$ may be written in polar form: $\mathcal{P}(x) = P(x)\mathrm{e}^{\mathrm{i}\chi(x)}$, where:

$$P(x) = P_0 \sqrt{1 + C^2 + 2C\cos(2kx + \theta)} \qquad \chi(x) = \arctan \frac{C\sin(kx+\theta) - \sin(kx)}{C\cos(kx+\theta) + \cos(kx)}$$

Therefore, according to Sect. 1.7.1, the intensity contributions pv_p and pv_q appear. This case is particularly interesting because it shows in a simple way how the average energy flux is affected by the reflection coefficient: for instance, if $C = 0$ there is no reflection at all and the intensity is completely radiating (*progressive wave*), while if $C = 1$ the intensity is totally oscillating (*standing wave*). Moreover, in the progressive wave case, being $v = p/z$ (see Eq. (36)), the following relation holds:

$$|\mathbf{A}| = Wc \tag{64}$$

As an example we report in Fig. 2 the behavior of the instantaneous intensity in the following three cases $C = 0; 0.5; 1$ ($f = 100\,\mathrm{Hz}$, $\theta = 0$). Subsequently (Fig. 3) the quantities j, a, r for $C = 0.5$ are shown. The spatial behavior of R is then reported in Fig. 4 ($C = 0.3; 0.6; 1$). It is interesting to compare this with the indicator σ reported in Fig. 5. Actually, the two quantities present a similar oscillation pattern (the spatial period is $\lambda/2 \simeq 1.7\,\mathrm{m}$): yet, while R varies between zero and a maximum which increases with the reflected wave amplitude (note that in a progressive wave $R \equiv 0$ for every x), σ behaves in a somewhat opposite way, for its maximum remains fixed on 1 and its minimum gradually decreases (in a progressive wave $\sigma \equiv 1$).

From these observations we are led to interpret progressive and standing waves as prototypes of totally radiating and oscillating fields, respectively: in the former all the mean energy is transferred by the average intensity vector while in the latter it is completely stored in the neighborhood of the measuring point. These two extreme cases, which in practice can be ob-

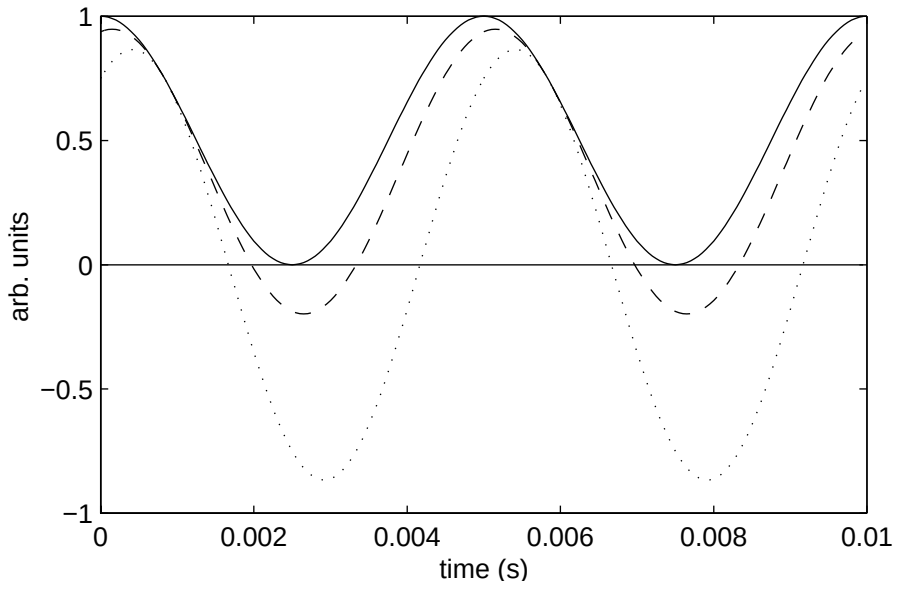

FIGURE 2. Instantaneous intensities in three normal reflection fields: $C = 0$ (continuos line), $C = 0.5$ (dashed line), $C = 1$ (dotted line). $f = 100\,\mathrm{Hz}$.

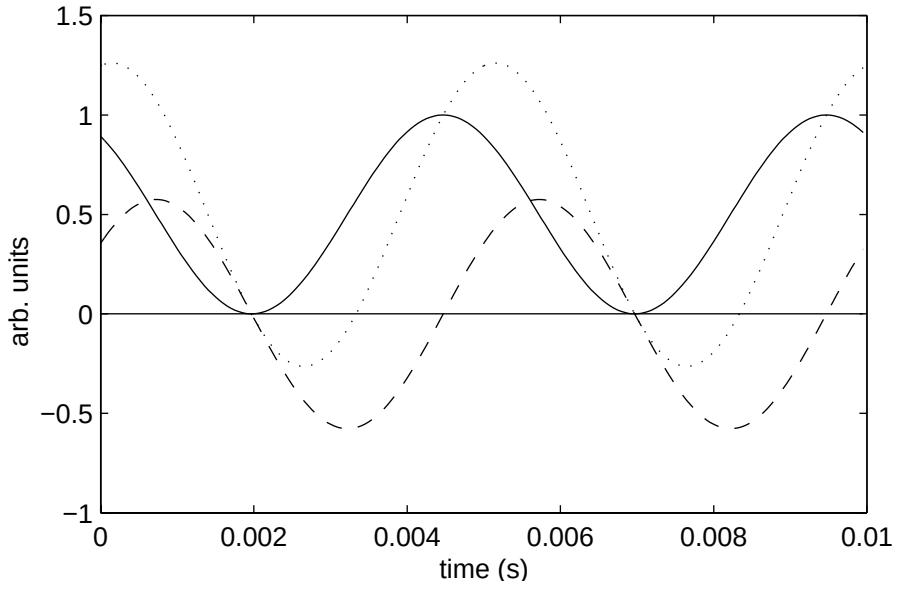

FIGURE 3. Instantaneous j (dotted line), a (continuos line), r (dashed line) in a normal reflection field ($\mathrm{R} = 0.5$).

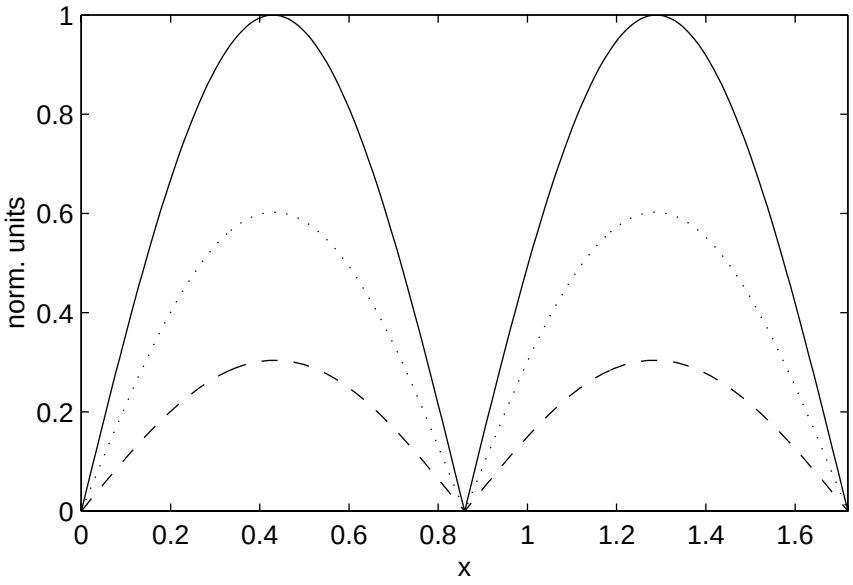

FIGURE 4. Plane wave reflection: R vs. x for three reflection coefficients. $C = 1$ (continuos line), $C = 0.6$ (dotted line), $C = 0.3$ (dashed line). The three curves are normalized with respect to the max. value of R for $C = 1$.

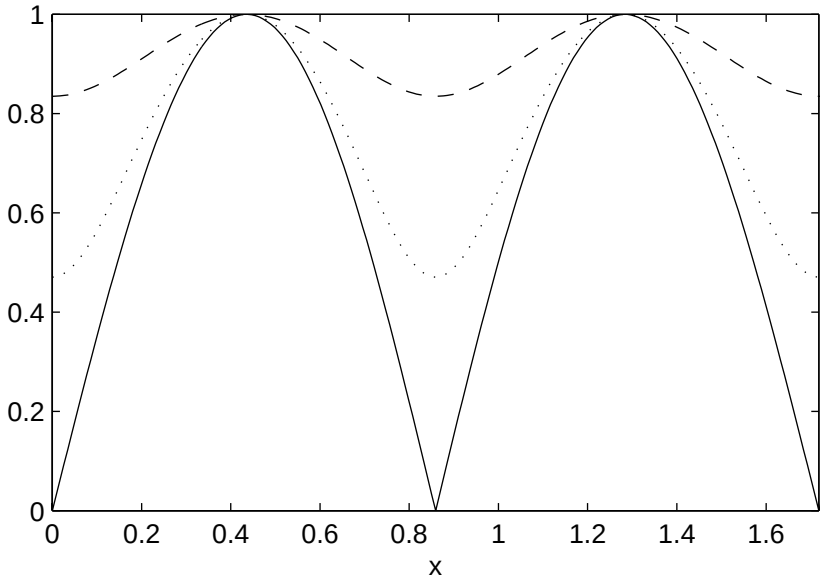

FIGURE 5. Plane wave reflection: σ vs. x in the same cases as Fig. 4.

tained just in an approximate way, define an interval where a variety of intermediate situations may occur and where, according to the boundary conditions, one of the two parts may prevail.

1.8.2 Monopole field

To analyze the flux behavior of an outgoing spherically symmetric wave it is useful to perform the calculations from the potential viewpoint. This function is written $\phi(r,t) = f(r-ct)/r$ (see Eq. (39)), hence the pressure and the two particle velocity terms are given by

$$p(r,t) = z\frac{f'}{r} \qquad \mathbf{v}_p(r,t) = \mathbf{n}\frac{f'}{r} \qquad \mathbf{v}_q(r,t) = -\mathbf{n}\frac{f}{r^2}$$

where f' is the derivative of f with respect to the argument $r-ct$ an $\mathbf{n}$ is the radial unit vector. We have then

$$\mathbf{a}(r,t) = z\mathbf{n}\frac{f'^2}{r^2} \qquad \mathbf{r}(r,t) = -z\mathbf{n}\frac{f'f}{r^3}$$

It follows

$$\mathbf{A}(\mathbf{x}) = z\mathbf{n}\frac{\langle f'^2\rangle}{r^2} \qquad \mathfrak{R}(\mathbf{x}) = z\frac{\sqrt{\langle 2f^2f'^2\rangle}}{r^3}\mathbf{n}\otimes\mathbf{n}$$

Even in this case the tensor $\mathfrak{R}$ has a single nonvanishing eigenvalue ($R = z\sqrt{\langle 2f^2f'^2\rangle}/r^3$) corresponding to an eigenvector parallel to $\mathbf{n}$. We may also easily calculate the ratio of the magnitude of $\mathbf{A}$ to the effective value of the oscillating intensity:

$$\frac{|\mathbf{A}|}{R} = \frac{r}{l} \tag{65}$$

where $l := \langle f^2\rangle / \langle f'^2\rangle$ is a sort of characteristic length (in the monochromatic case $l = 1/k$). Eq. (65) states that the far field ($r > l$) and the near field ($r < l$) are characterized by the predominance of the radiating and oscillating intensity respectively.

1.8.3 Dipole field

In the examples we have just shown, the oscillating intensity was completely polarized, for the graphical representation of the indicatrix quadric was a segment. Now we may take a little more complex field, for exhibiting the phenomenon of energy oscillation in two dimensions. The field is given by a superposition of two monopoles of different frequency (ω and $3\omega/2$) in the plane x, y:

$$p(\mathbf{x},t) = P_0\left\{\frac{\sin\left(k\left|\mathbf{x}+\mathbf{x}_0\right|+\omega t\right)}{|\mathbf{x}+\mathbf{x}_0|} + \frac{\sin\left[3\left(k\left|\mathbf{x}-\mathbf{x}_0\right|+\omega t\right)/2+\pi\right]}{|\mathbf{x}-\mathbf{x}_0|}\right\}$$

From a computer simulation, with $f = 100\,\mathrm{Hz}$, $P_0 = 10^{-4}\,\mathrm{N/m}$ and $\mathbf{x}_0 = (\lambda/4, 0)$, we show here the quadric representation and the mean intensity vectors in four points of the plane (Figs. 6 and 7). The most interesting characteristic which comes out looking at both figures is the oscillating intensity polarization along the mean intensity direction.

1.9 The energy transfer indicator

Owing to an analogy between the two conservation laws of mass and energy, which is based on the formal correspondences $\rho \leftrightarrow w$, $\mathbf{m} \leftrightarrow \mathbf{j}$, we can introduce the instantaneous *energy velocity*,

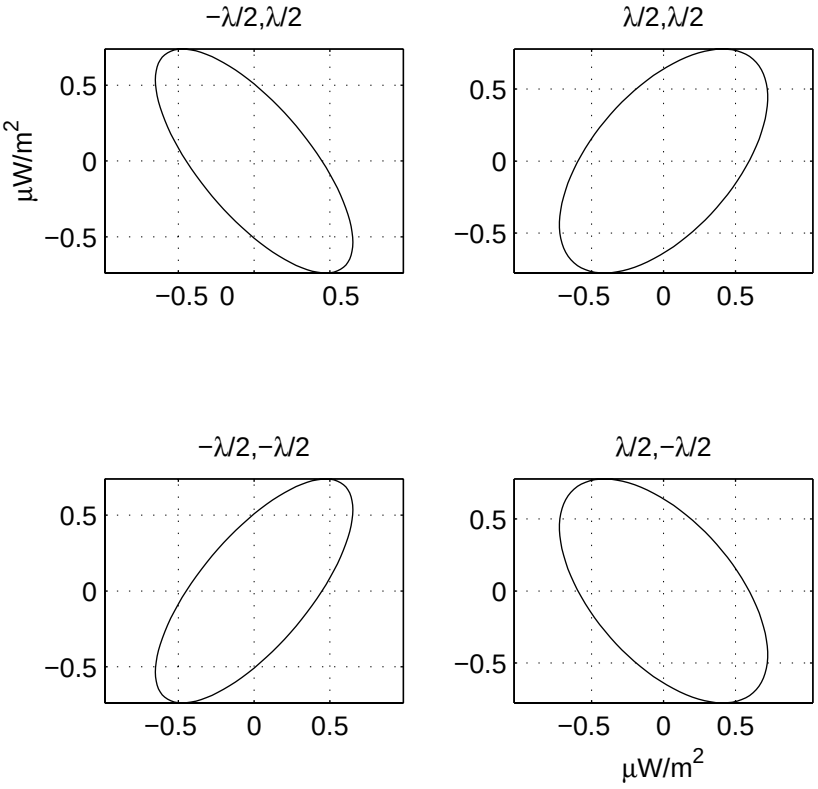

FIGURE 6. Dipole field: plots of polarization ellipses in four points symmetrical with each other.

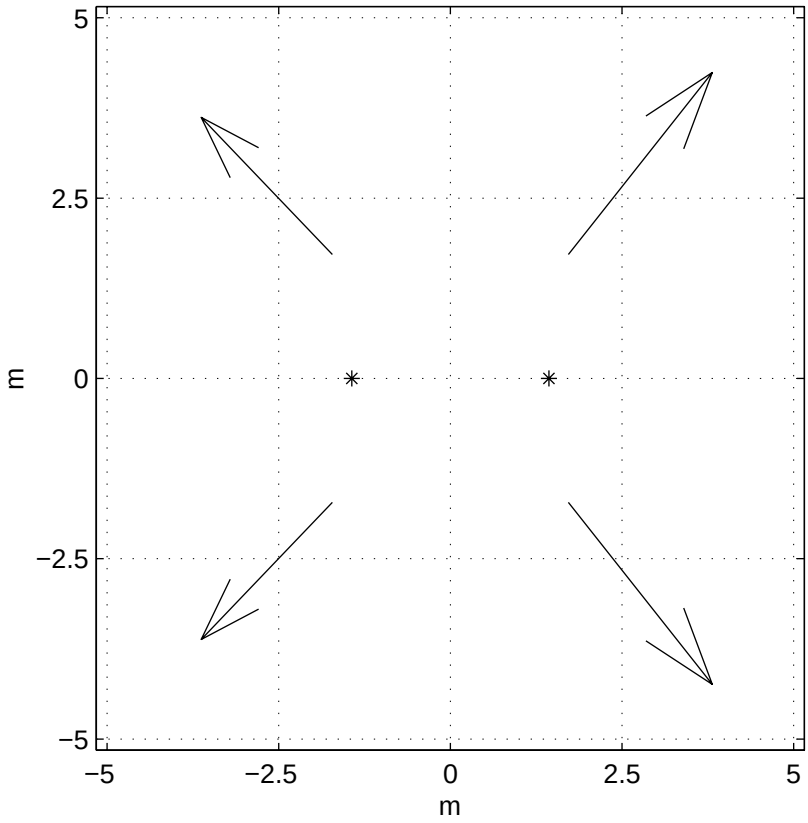

FIGURE 7. Dipole field: mean intensity vectors in the same points of Fig. 6. The two asterisks indicate the monopoles' centers.

defined as the ratio of intensity and energy density [12] :

$$\mathbf{u}_E(\mathbf{x},t) := \frac{\mathbf{j}(\mathbf{x},t)}{w(\mathbf{x},t)} = \frac{2czp\mathbf{v}}{z^2\mathbf{v}^2 + p^2} \tag{66}$$

It can be easily shown that $|\mathbf{u}_E| \leq c$: in particular the equality holds when the instantaneous kinetic and potential energies are equal.

For studying the average behavior of the energy velocity we have two possibilities. The first and most obvious one is given by the quantity $\mathbf{U}(\mathbf{x}) = \langle \mathbf{u}_E \rangle$, which represents the *mean velocity of sound energy*; on the other hand, we may also define the ratio

$$\mathbf{u}(\mathbf{x}) := \frac{\mathbf{A}(\mathbf{x})}{W(\mathbf{x})} \tag{67}$$

which can be interpreted as the *velocity of energy transferred by the average intensity*. The two averages obviously lead to different results: for instance $\mathbf{u}(\mathbf{x})$ (which will be called *u velocity*) has the same direction of $\mathbf{A}$ while in general this is not true of $\mathbf{U}$. The particular averaging rule introduced in Eq. (67) makes the calculation of the u velocity quite advantageous compared to $\mathbf{U}$. In particular, we may verify the following relationship

$$|\mathbf{u}| \leq c\sigma \leq c \tag{68}$$

where σ has been defined in Eq. (50) . The first inequality is due to

$$|\mathbf{A}| = \sqrt{\langle p^2 \rangle \left(\langle \mathbf{v}^2 \rangle - \left\langle \mathbf{v}_p^2 \right\rangle \right)} \leq \sqrt{\langle p^2 \rangle \langle \mathbf{v}^2 \rangle}$$

while the second one is a direct consequence of the inequality $(a-b)^2 \geq 0$, with $a^2 = z^2 \langle \mathbf{v}^2 \rangle$ and $b = \langle p^2 \rangle$. Moreover from Eq. (68) one finds that the joint conditions: $R = 0$ (vanishing oscillating intensity) and $z^2 \langle \mathbf{v}^2 \rangle = \langle p^2 \rangle$ (i.e. $\sigma = 1$, that is $W_K = W_U$) are equivalent to the condition $|\mathbf{u}| = c$: in particular, this happens for a plane progressive wave (see Eq. (64)).

We now present an argument displaying a deeper physical meaning of the u velocity, and allowing us to use this quantity as an important field indicator. To this purpose we have to come back to the spherical wave field considered in Sect. 1.8.2 and calculate both the potential and the kinetic energy:

$$w_U(r,t) = \frac{1}{2}\rho_0 \frac{f'^2}{r^2} \qquad w_K(r,t) = \frac{1}{2r^2}\rho_0 \left(f' - \frac{f}{r} \right)^2$$

For obtaining the time averages, we first calculate the quantity

$$\langle f f' \rangle = \lim_{T\to\infty} \frac{1}{2T} \int_{-T}^{T} \mathrm{d}t \, f(r-ct) f'(r-ct)$$

putting $\xi = r - ct$ and integrating by parts, we have

$$\langle f f' \rangle = -\lim_{T\to\infty} \frac{1}{2cT} \int_{r-cT}^{r+cT} \mathrm{d}\xi \, f(\xi) f'(\xi) = -\lim_{T\to\infty} \frac{1}{4cT} \left[f^2(r+cT) - f^2(r-cT) \right] = 0$$

whence it follows

$$W = \frac{1}{2}\rho_0 \left(\frac{2\langle f'^2 \rangle}{r^2} + \frac{\langle f^2 \rangle}{r^4} \right) \tag{69}$$

The u velocity modulus becomes then

$$|\mathbf{u}| = c\frac{2r^2}{2r^2 + l^2} \tag{70}$$

which approaches 0 or 1 when $r \ll l$ or $r \gg l$ respectively. Stated another way: at distances r large compared with l (far field) the relationship between pressure and velocity approaches that of a plane progressive wave. In fact, here the fluid velocity has the same temporal behavior of the pressure and, how it is clearly shown by Eq. (69) , all the energy density is radiating and moves at speed c. On the contrary, if we come nearer to the source, there appears an additional term (proportional to $\langle f^2 \rangle$) which is not present in $\mathbf{A}$: this can be interpreted as an oscillating energy term which does not radiate outward but is locally stored [2] .

Thanks to these arguments we may generalize the concept defining the indicator

$$\eta = \frac{|\mathbf{u}|}{c} \tag{71}$$

which, in addition of being the modulus of the u velocity in units of c, may be interpreted as the fraction of the mean energy which is radiated at the speed of sound.

CHAPTER 2

Acoustics of confined fields

We have examined the general physical laws of linear acoustic systems, disregarding almost completely the study of phenomena which take place when the field is bound, that is when the sound propagation occurs in presence of walls or other obstacles. The only question we have presented about this issue has been the simplified treatment of the general phenomena of reflection, where in particular we have realized the influence of the wave interference on the energy propagation.

It's obvious that almost always the task of determining the spatial and temporal distribution of acoustical quantities cannot be achieved exactly, due to the huge complexity exhibited by most real confined fields; for this reason a variety of approaches is often employed, each of them being reliable just at a certain level of approximation. The most typical and exact one is based on the direct study of the d'Alembert equation (*wave acoustics*) and gives fundamental information about normal modes of vibration and their relationships with transient sounds in a closed environment. On the other hand, when wavelengths are much smaller than the typical dimension of the room other approaches, like *geometrical* and *statistical acoustics*, are more helpful for describing the propagation and transmission of sound, though in a more approximate way.

The models we have just mentioned constitute the framework where the study of room acoustics problems is most frequently performed. In this section we are going to discuss their main theoretical aspects, for gaining a better understanding of the concrete cases we will later discuss from an experimental viewpoint.

2.1 Introduction to the wave theory

When the typical room dimensions are of the order of a few wavelengths the only correct way of interpreting the sound propagation is the one based on the direct study of the wave equation,

which in general takes account of a source term:

$$\boldsymbol{\Delta}\phi(\mathbf{x},t) - \frac{\phi_{tt}(\mathbf{x},t)}{c^2} = s(\mathbf{x},t) \tag{72}$$

It is often useful to transform the equation by means of the Fourier integral: this often simplifies the procedure for solving it and offers the possibility of studying the acoustic system from the frequency viewpoint. For this purpose we are going to adopt the following convention for the Fourier transform:

$$\Phi(\mathbf{x},\omega) = \int_{-\infty}^{\infty} \mathrm{d}t\, \phi(\mathbf{x},t) e^{-\mathrm{i}\omega t} \qquad \phi(\mathbf{x},t) = \frac{1}{2\pi}\int_{-\infty}^{\infty} \mathrm{d}\omega\, \Phi(\mathbf{x},\omega) e^{\mathrm{i}\omega t} \tag{73}$$

Eq. (72) becomes then

$$\left[\boldsymbol{\Delta} + \frac{\omega^2}{c^2}\right] \Phi(\mathbf{x},\omega) = S(\mathbf{x},\omega) \tag{74}$$

which is called *Helmholtz equation*: ω is here a parameter, playing the role of an eigenvalue when $S = 0$. Note that in the usual time domain the same problem arises considering a steady harmonic excitation $s(\mathbf{x},t) = q(\mathbf{x})\mathrm{e}^{-\mathrm{i}\omega_0 t}$. Thanks to linearity properties also the field is separated in the same way ($\phi(\mathbf{x},t) = \alpha(\mathbf{x})\mathrm{e}^{-\mathrm{i}\omega_0 t}$), the time phasor $\mathrm{e}^{-\mathrm{i}\omega_0 t}$ can then be dropped, so that just a spatial equation remains.

In general, the walls bounding an enclosure interact with the field, therefore a strict procedure for determining the acoustic field should be based on the coupling of the wave equation with the set of equations describing the wall movements produced by the air vibration. This situation is very difficult to deal with, but fortunately it is often possible to devise a simplified boundary condition model, which may be quite helpful in practice.

2.1.1 Specific impedance

If the walls are rigid but penetrable, the interaction can be mathematically represented by a linear relation between the velocity component normal to the surface (Σ) and the sound pressure in the same point [4] :

$$Z(\mathbf{x})\mathbf{n}(\mathbf{x}) \cdot \mathbf{v}(\mathbf{x},t) = p(\mathbf{x},t) \tag{75}$$

(with $\mathbf{x} \in \Sigma$ and $\mathbf{n}$ being the external unity vector normal to the surface). The proportionality factor Z is a complex number called *specific acoustic impedance*, whose real and imaginary parts are respectively called *specific acoustic resistance* and *reactance*. Generally this quantity depends on the frequency and the direction of incidence as well as the position. Written in terms of the potential, Eq. (75) becomes

$$Z(\mathbf{x})\mathbf{n}(\mathbf{x}) \cdot \boldsymbol{\nabla}\phi(\mathbf{x},t) = -\rho_0 \phi_t(\mathbf{x},t) \qquad (\mathbf{x} \in \Sigma) \tag{76}$$

which is just a *boundary condition* for the wave equation. In the frequency domain it is written

$$Z(\mathbf{x})\mathbf{n}(\mathbf{x}) \cdot \boldsymbol{\nabla}\Phi(\mathbf{x},\omega) = -i\omega\rho_0 \Phi(\mathbf{x},\omega) \qquad (\mathbf{x} \in \Sigma) \tag{77}$$

Now, remembering the previous brief discussion about the plane wave reflection (Sect. 1.4), it is evident that there is a strong relationship between Z and the reflection coefficient $\mathcal{C}$: in

particular, we obtain

$$Z = z\frac{1+\mathcal{C}}{1-\mathcal{C}} \tag{78}$$

The three extreme cases $\mathcal{C} = 1$, $\mathcal{C} = 0$, $\mathcal{C} = -1$ then correspond to: $|Z| = \infty$, $Z = z$, $Z = 0$.

It is worth noting that the specific impedance is an extension to the acoustic case of the analog quantity defined in vibrational mechanics and in electrodynamics.

2.1.2 Energy absorption

It's worth analyzing the different cases where the energy absorption is absent. Let's suppose the field is a monochromatic one, so that pressure and velocity may be written in polar form as $p(\mathbf{x},t) = P(\mathbf{x})\mathrm{e}^{-\mathrm{i}kt}$ and $\mathbf{v}(\mathbf{x},t) = \mathbf{V}(\mathbf{x})\mathrm{e}^{-\mathrm{i}kt}$: Eq. (75) becomes

$$Z(\mathbf{x})V_{\mathbf{n}}(\mathbf{x}) = P(\mathbf{x}) \tag{79}$$

where P and $V_{\mathbf{n}} = \mathbf{V}\cdot\mathbf{n}$ are evaluated on the boundary surface. The following table summarizes all the situations where the perfect reflection occurs.

$\mathrm{Re}(Z) = \infty$ and/or $\mathrm{Im}(Z) = \infty$	$V_{\mathbf{n}}$=0
$\mathrm{Re}(Z) = 0$ and $\mathrm{Im}(Z) \neq 0$	$V_{\mathbf{n}}$ and P in quadrature
$\mathrm{Re}(Z) = 0$ and $\mathrm{Im}(Z) = 0$	$P = 0$

On the other hand, the mean normal intensity over the boundary is given by

$$\mathbf{A}_{\mathbf{n}}(\mathbf{x}) = \langle p(\mathbf{x},t)v_{\mathbf{n}}(\mathbf{x},t)\rangle = \frac{1}{2}\,\mathrm{Re}\left[P(\mathbf{x})V_{\mathbf{n}}^{*}(\mathbf{x})\right] = \frac{1}{2}\left|V_{\mathbf{n}}(\mathbf{x})\right|^{2}\mathrm{Re}\left[Z(\mathbf{x})\right] \tag{80}$$

which confirms the fact that if the resistance is 0 the energy is not absorbed. It's also clear that for intensity to be positive, in order that energy escapes from the enclosure (passive surfaces), the resistance has to be defined as a non negative number.

In the case of the normal reflection of a plane progressive wave, Eq. (80) may be written

$$\mathbf{A}_{\mathbf{n}}(\mathbf{x}) = \frac{1}{2z}\left|P_0\right|^{2}\left(1-\left|\mathcal{C}\right|^{2}\right) \tag{81}$$

Since the term $\left|P_0\right|^{2}/2z$ represents the incident mean intensity, while the same quantity times $\left|\mathcal{C}\right|^{2}$ gives the intensity related to the reflected wave, Eq. (81) expresses the energy conservation law at the boundary surface. It is then customary to call $\left|\mathcal{C}\right|^{2}$ *energy reflection coefficient*, and contemporarily define the quantity $\alpha = 1-\left|\mathcal{C}\right|^{2}$, representing the *energy absorption coefficient*.

2.2 Sound in ducts

To introduce some examples where the wave treatment of sound is employed, we will discuss the transmission inside *waveguides* and in finite ducts with partially absorbing ends. The analysis will be carried out focusing the attention on the homogeneous problem in the frequency domain, in order to investigate the relationship between the eigenfunctions of the Helmholtz equation and the boundary conditions [4] .

2.2.1 Waveguides

Let's consider a semi-infinite straight duct of constant section, aligned along x ($0 \leq x < \infty$) and having perfectly reflecting walls. For simplicity we will consider here the case where $V_{\mathbf{n}} = \mathbf{n} \cdot \boldsymbol{\nabla}\phi$ is 0 on the surface Σ. In order to study the solutions in the frequency domain we define the following eigenvalue problem for the Laplacian operator:

$$\begin{cases} \left[\boldsymbol{\Delta} + \dfrac{\omega^2}{c^2}\right] \Phi(\mathbf{x},\omega) = 0 \\ \mathbf{n} \cdot \boldsymbol{\nabla}\Phi(\mathbf{x},\omega) = 0 \qquad (\mathbf{x} \in \Sigma) \end{cases} \tag{82}$$

where we suppose that the surface Σ is formed by the four planes of equations $y = 0$, $y = l_y$ ($0 \leq z \leq l_z$), $z = 0$, $z = l_z$ ($0 \leq y \leq l_y$).

It is helpful to look for a solution having the axial variable x separated from the others. Dropping the frequency dependence in the notation we assume

$$\Phi(x,y,z) = X(x)\Psi(y,z) \tag{83}$$

as a consequence, we obtain a transversal equation and an axial equation:

$$\left(\boldsymbol{\Delta}_{yz} + \alpha^2\right) \Psi = 0 \tag{84}$$

$$X'' + \left(k^2 - \alpha^2\right) X = 0 \tag{85}$$

where $k^2 = \omega^2/c^2$. In the first case Ψ and α are eigenfunctions and eigenvalues of a two-dimensional Helmholtz equation corresponding to reflecting walls: the α^2 are then non negative real numbers taking a discrete set of values α_n^2, and the corresponding Ψ_n form a complete orthonormal set of functions

$$\alpha_n^2 = \pi^2 \left[\left(\frac{n_y}{l_y}\right)^2 + \left(\frac{n_z}{l_z}\right)^2 \right] \qquad \Psi_n(y,z) = K(n_y,n_z) \cos\frac{n_y \pi y}{l_y} \cos\frac{n_z \pi z}{l_z} \tag{86}$$

where $K(n_y,n_z)$ are normalization constants.

The general solution of Eq. (85) depends on the eigenvalue α_n^2 in two possible ways

$$X_n(x) = B\mathrm{e}^{\mathrm{i}\beta_n x} \qquad \beta_n = \begin{cases} \sqrt{k^2 - \alpha_n^2} & \text{if} \quad k^2 > \alpha_n^2 \\ \mathrm{i}\sqrt{\alpha_n^2 - k^2} & \text{if} \quad \alpha_n^2 > k^2 \end{cases} \tag{87}$$

We are now able to write explicitly the solution of the spatial component Φ in the two cases:

$$\Phi(x,y,z) = B\mathrm{e}^{\mathrm{i}\beta_n x}\Psi_n(y,z) \qquad \Phi(x,y,z) = B\mathrm{e}^{-|\beta_n|x}\Psi_n(y,z) \tag{88}$$

The second case differs from the first one because it describes an excitation dying out exponentially along the axis x. Two kinds of modes are then present inside the duct: the *propagating modes*, defined for $\alpha_n^2 < k^2$ and being finite in number, and the *evanescent modes*, which cannot propagate. Among the first ones there is the so-called *fundamental mode*, corresponding to $\alpha_n = 0$, which is a plane wave without any transversal excitation. We are then led to the conclusion that a given frequency ω excites more than one mode, but among these the only ones

being able to propagate will be those for which ω is greater than the *cutoff frequency* $\omega_n = c\alpha_n$. Furthermore, if ω is so low that $\omega < c\alpha_n$ for each $n > 0$, the only propagating mode will be the fundamental one: for instance, in the particular case of square section duct the propagation inside will occur in the form of plane waves whenever

$$\omega < \omega_0 = \frac{c\pi}{l} \tag{89}$$

where l is the side of the square. The condition expressed by Eq. (89) is obviously equivalent to $l < \lambda/2$.

2.2.2 Finite length ducts

Now we consider a finite length duct in a frequency range satisfying Eq. (89) and with both ends having an impedance Z. Due to the plane wave nature, the acoustic quantities may be considered functions of just the axial coordinate (x), therefore the system may be taken as a simple example of one dimensional room for it gives us the opportunity of finding the relationship between the modes' behavior and the wall impedance.

The problem we have to solve is

$$\Phi''(x) + \frac{\omega^2}{c^2}\Phi(x) = 0 \qquad \begin{cases} Z\Phi'(0) - \mathrm{i}\omega\rho_0\Phi(0) = 0 \\ Z\Phi'(L) + \mathrm{i}\omega\rho_0\Phi(L) = 0 \end{cases}$$

where L represents the duct length. The general solution of the equation is $\Phi(x) = a\mathrm{e}^{\mathrm{i}(\omega/c)x} + b\mathrm{e}^{-\mathrm{i}(\omega/c)x}$ which must be inserted into the boundary conditions in order to find the constants a and b. The result is the following system

$$\begin{cases} (Z-z)a - (Z+z)b = 0 \\ \mathrm{e}^{\mathrm{i}(\omega/c)L}(Z+z)b - \mathrm{e}^{-\mathrm{i}(\omega/c)L}(Z-z)b = 0 \end{cases}$$

The condition for a non trivial solution is then

$$\mathrm{e}^{-2\mathrm{i}(\omega/c)L} = \left(\frac{Z+z}{Z-z}\right)^2 \tag{90}$$

The calculation of k may be accomplished by distinguishing two physical situations.

Perfectly reflecting walls

In this context Z must satisfy one of the three conditions indicated in the table above (Sect. 2.1.2): it is then easy to verify that the quantity on the right-hand side of Eq. (90) has unit magnitude. It follows that ω forms a discrete set of real numbers. In particular, in the first and third case ($P = 0$ or $V_\mathrm{n} = 0$) we obtain $\cos(2\omega L/c) - i\sin(2\omega L/c) = 1$, so

$$\omega_n = \frac{n\pi c}{L} \qquad n = 0, \pm 1, \pm 2 \ldots \tag{91}$$

The eigenfunctions are thus expressed by

$$\Phi_n(x) = \mathrm{e}^{\mathrm{i}(\omega_n/c)x} + \mathrm{e}^{-\mathrm{i}(\omega_n/c)x}$$

and it can easily be demonstrated that they are not orthogonal, the boundary conditions being dependent on the eigenvalue; therefore, it is not possible to express the general solution as an

infinite series using $\Phi_n(x)$. Anyway, from the particular solutions of the homogeneous problem, which may be written

$$\Phi(x,\omega) = \delta(\omega - \omega_n)\Phi_n(x)$$

it is possible to deduce some interesting properties through the transformation in the time domain. From Eq. (73) we then obtain

$$\phi_n(x,t) = \frac{1}{2\pi}\int_{-\infty}^{\infty} \mathrm{d}\omega\delta(\omega-\omega_n)\Phi_n(x)\mathrm{e}^{\mathrm{i}\omega t} = \frac{\Phi_n(x)}{2\pi}\mathrm{e}^{\mathrm{i}\omega_n t} \tag{92}$$

which is a standing wave of angular frequency ω_n. It is thus clear that in this systems the sound doesn't need any power to be sustained, for the solution of the homogeneous problem doesn't show a transient behavior. By the discussion presented in Sect. A.2 we can infer that the Green function is not finite, meaning that the system cannot be considered stable. We'll come back to this subject below, when speaking about Green functions in detail.

Partially absorbing walls

In this case Z is a complex number, so ω must be a complex number too: let's write it $\omega = \widetilde{\omega} + i\gamma$. It follows

$$\mathrm{e}^{2\mathrm{i}\gamma L}\left[\cos(2\widetilde{\omega}L/c) - \mathrm{i}\sin(2\widetilde{\omega}L/c)\right] = \left(\frac{Z+z}{Z-z}\right)^2$$

from which, putting for simplicity $\mathrm{Im}(Z) = 0$, we have

$$\widetilde{\omega}_n = \frac{n\pi c}{L} \qquad \gamma = \frac{1}{2L}\left(\frac{Z+z}{Z-z}\right)^2 \tag{93}$$

γ is positive and independent of n, but we can write $\omega_n = \widetilde{\omega}_n + \mathrm{i}\gamma_n$ all the same, because in general Z is implicitly dependent on frequency; γ_n has then asymptotic behaviors given by $\lim_{Z\to z}\gamma_n = \infty$ (maximum absorption) and $\lim_{Z\to\infty}\gamma_n = 0$ (zero absorption). The eigenfunctions are

$$\Phi_n(x) = (Z+z)\mathrm{e}^{\mathrm{i}(\omega_n/c)x} + (Z-z)\mathrm{e}^{-\mathrm{i}(\omega_n/c)x}$$

corresponding to

$$\phi_n(x,t) = \Phi_n(x)\mathrm{e}^{\mathrm{i}\omega_n t}\mathrm{e}^{-(\gamma_n/c)t} \tag{94}$$

We now see how absorption affects the time behavior of eigenfunctions: these decrease exponentially with the slope $\tau_n = c/\gamma_n$. In fact, this is a first simple example of the phenomenon of the decay of sound, which will be treated in more detail in the following.

2.3 Solutions in terms of Green functions

We now want to deal with the resolution of the wave equation when an acoustic source is present: for this we will rely on the Green function method, whose theoretical foundations are presented in Appendix. The first point we need to discuss now is the extension to the space-time domain of the concepts introduced for time-invariant dynamic systems.

Referring to Sect. 2.1, we can affirm there are two ways of defining Green functions in linear acoustics. The first one is related to the usual wave equation and is employed for determining fields of generic time behavior. The second one is a special case regarding the time independent

wave equation (Helmholtz equation) and can be directly interpreted as the Green function for obtaining the space distribution of simple-harmonic fields. Anyway, as shown above, the two formulations are linked to each other by the Fourier transform.

In the first case we have to find the space-time behavior of a field $\phi(\mathbf{x},t)$, produced by the source distribution $s(\mathbf{x},t)$, in such a way that the wave equation is

$$\boldsymbol{\Delta}\phi - \frac{\phi_{tt}}{c^2} = s \tag{95}$$

The source has then to be subdivided into an ensemble of elementary terms being point-like in space and impulsive in time. The Green function $g(\mathbf{x},t)$ represents the field observed in position $\mathbf{x}$ at time t due to one of these elementary sources. Of course, the simplest case is the one encountered in free space, where the function satisfies Eq. (95) with $s(\mathbf{x},t) = \delta(\mathbf{x})\delta(t)$ and no boundary conditions. It can be demonstrated [13] that the Green function satisfying the causality condition is

$$g(\mathbf{x},t) = -\frac{c}{4\pi|\mathbf{x}|}\delta(|\mathbf{x}| - ct) \tag{96}$$

which is an impulsive spherical outgoing wave, traveling at speed c. The global field, called *delayed potential*, is obtained by means of a space-time convolution

$$\phi(\mathbf{x},t) = (s * g)\,(\mathbf{x},t) = -\frac{1}{4\pi c}\int_{R^3} \mathrm{d}^3\mathbf{y}\,\frac{s(\mathbf{y}, t - |\mathbf{x}-\mathbf{y}|/c)}{|\mathbf{x}-\mathbf{y}|} \tag{97}$$

Nevertheless, if boundary conditions are present, the field has to be written

$$\phi(\mathbf{x},t) = \int_V \mathrm{d}^3\mathbf{y}\int_{-\infty}^{t} \mathrm{d}\tau\, g(\mathbf{x},\mathbf{y};t-\tau)s(\mathbf{y},\tau) \tag{98}$$

so that we can no more speak of convolution because the translational invariance in space has disappeared. g now depends on the impulse position and must satisfy the boundary conditions: it is defined by the equation

$$\boldsymbol{\Delta}_{\mathbf{x}} g(\mathbf{x},\mathbf{y},t) - \frac{g_{tt}(\mathbf{x},\mathbf{y};t)}{c^2} = \delta(\mathbf{x}-\mathbf{y})\delta(t) \qquad g(\mathbf{x},\mathbf{y};t<0) = 0$$

As regards the Helmholtz equation, the Green function G is the solution of

$$\left[\boldsymbol{\Delta}_{\mathbf{x}} + \frac{\omega^2}{c^2}\right] G(\mathbf{x};\mathbf{y}) = \delta(\mathbf{x}-\mathbf{y}) \tag{99}$$

In the most general case, the space distribution $\Phi(\mathbf{x})$ of the field $\phi(\mathbf{x},t) = \Phi(\mathbf{x})\mathrm{e}^{\mathrm{i}\omega t}$, produced by the excitation $s(\mathbf{x},t) = S(\mathbf{x})\mathrm{e}^{\mathrm{i}\omega t}$, is given by

$$\Phi(\mathbf{x}) = \int_V \mathrm{d}^3\mathbf{y}\, G(\mathbf{x};\mathbf{y})S(\mathbf{y}) \tag{100}$$

which in the free space becomes

$$\Phi(\mathbf{x}) = (G * S)(\mathbf{x}) \tag{101}$$

Now we examine a particular case allowing us to simplify the way how ϕ is written. Let us suppose the source distribution is separable in the form

$$s(\mathbf{x},t) = \alpha(\mathbf{x})\beta(t) \tag{102}$$

We then have

$$\phi(\mathbf{x},t)=\int_{-\infty}^{t}\mathrm{d}\tau\,\beta(\tau)\int_V \mathrm{d}^3\mathbf{y}\,g(\mathbf{x},\mathbf{y};t-\tau)\alpha(\mathbf{y})=\int_{-\infty}^{t}\mathrm{d}\tau\,g_\alpha(\mathbf{x};t-\tau)\beta(\tau)=g_\alpha*\beta$$

that is a temporal convolution between the time part of s and the spatial integral expressed by:

$$g_\alpha(\mathbf{x},t)=\int_V \mathrm{d}^3\mathbf{y}\,g(\mathbf{x},\mathbf{y};t)\alpha(\mathbf{y}) \tag{103}$$

The result is obvious if we think of the equation with the source term $s(\mathbf{x},t)=\alpha(\mathbf{x})\delta(t)$, whose solution is just g_α, which can be then interpreted as a kind of Green function valid for fixed spatial dependence. One meaningful case, often useful in practice, is encountered when $\alpha(\mathbf{x})=\delta(\mathbf{x}-\mathbf{x}_0)$: this gives $g_\delta(\mathbf{x};t)=g(\mathbf{x},\mathbf{x}_0;t)$.

2.4 Green functions in rooms

In this section we are going to present a brief discussion about Green functions in rooms provided with absorbing walls, both from the point of view of harmonic and general fields; we anticipate we are not aiming at an exhaustive treatment of the subject: further details and more precise explanations may be found on specialistic works [14] , [3] .

2.4.1 Helmholtz equation

We are going to express the Green function by a series of orthonormal eigenfunctions inside the region where the equation is defined. In practice, these come out by the problem

$$\begin{cases}\left[\boldsymbol{\Delta}+\dfrac{\Omega^2}{c^2}\right]\Phi(\mathbf{x};\omega)=0 & \mathbf{x}\in V\\ Z(\mathbf{x})\mathbf{n}(\mathbf{x})\cdot\boldsymbol{\nabla}\Phi(\mathbf{x};\omega)=-\mathrm{i}\omega\rho_0\Phi(\mathbf{x};\omega) & \mathbf{x}\in\Sigma\end{cases} \tag{104}$$

where the frequency in the equation has been given a value different from that in the boundary condition, in order to find a complete set of orthogonal eigenfunctions Ψ_n; hence, ω has to be regarded as a parameter, whose value may be given by the driving frequency of a sound source, so that Ω_n are the ω-dependent eigenvalue. The general solution of Eq. (104) is then given by

$$\Phi(\mathbf{x})=\sum_{n=0}^{\infty}f_n\Psi_n(\mathbf{x})\qquad f_n=\int_V\mathrm{d}\mathbf{x}\,\Phi(\mathbf{x})\Psi_n(\mathbf{x})$$

where the frequency dependence has been omitted. Let's now take into consideration the homogeneous problem (74) and expand the source term S

$$S(\mathbf{x})=\sum_{n=0}^{\infty}s_n\Psi_n(\mathbf{x})\qquad s_n=\int_V\mathrm{d}\mathbf{x}\,S(\mathbf{x})\Psi_n(\mathbf{x})$$

If we know the s_n we can obtain the f_n substituting the two series expansions into the equation. We get:

$$\sum_{n=0}^{\infty}f_n\left(\boldsymbol{\Delta}+\frac{\omega^2}{c^2}\right)\Psi_n=\sum_{n=0}^{\infty}s_n\Psi_n$$

and because of Eq. (104)

$$\sum_{n=0}^{\infty} f_n \left(\frac{\omega^2}{c^2} - \frac{\Omega_n^2}{c^2} \right) \Psi_n = \sum_{n=0}^{\infty} s_n \Psi_n$$

We have

$$f_n = \frac{c^2 s_n}{\omega^2 - \Omega_n^2}$$

The Green function is given by $S(\mathbf{x}) = \delta(\mathbf{x} - \mathbf{y})$ so that $s_n = \Psi_n(\mathbf{y})$; we then have

$$G(\mathbf{x}, \mathbf{y}; \omega) = c^2 \sum_{n=0}^{\infty} \frac{\Psi_n(\mathbf{x};\omega)\Psi_n(\mathbf{y};\omega)}{\omega^2 - \Omega_n^2(\omega)} \tag{105}$$

where in general the eigenvalue Ω_n is a complex number, meaning that energy absorption occurs at the boundary. If the acoustic system is driven by a source $s(\mathbf{x}, t) = q(\mathbf{x})\mathrm{e}^{-\mathrm{i}\omega_0 t}$ the solution of the wave equation is then

$$\phi_{\omega_0}(\mathbf{x},t) = \left(c^2 \sum_{n=0}^{\infty} \frac{\Psi_n(\mathbf{x};\omega_0)}{\omega_0^2 - \Omega_n^2(\omega_0)} \int_V \mathrm{d}^3\mathbf{y}\, \Psi_n(\mathbf{y};\omega_0) q(\mathbf{x}) \right) \mathrm{e}^{-\mathrm{i}\omega_0 t} \tag{106}$$

The function ϕ_{ω_0}, as well G, is singular when the implicit equation $\omega_0^2 = \Omega_n^2(\omega_0)$ is satisfied, that is when the eigenvalue problem expressed by Eq. (104) is solved maintaining the equality between the frequency appearing in the equation and that of the boundary condition (as it has been done in Sect. 2.2.2 for the one dimensional case); in this case, the eigenvalues are $\omega_n = \widetilde{\omega}_n + \mathrm{i}\gamma_n$. Therefore, if $\gamma_n = 0$ (no absorption), G has poles on the real axis and as the driving frequency ω approaches one of the $\widetilde{\omega}_n$, the corresponding amplitude tends to diverge; on the contrary, if $\gamma_n \neq 0$ the amplitude is high but not infinite. For this reason the $\widetilde{\omega}_n$ are usually called: *eigenfrequencies of the room*.

2.4.2 Time dependent wave equation

The Green function for determining fields with any time dependence is obtained applying the inverse Fourier transform to Eq. (105) . This is calculated by means of the *residues theorem* and turns out to be

$$g(\mathbf{x}, \mathbf{y}; t) = \begin{cases} 0 & t < 0 \\ \sqrt{\dfrac{\pi}{2}} c^2 \displaystyle\sum_{n=0}^{\infty} e^{-\gamma_n t}\, \mathrm{Im}\left[\frac{\Psi_n(\mathbf{x};\omega)\Psi_n(\mathbf{y};\omega)}{\widetilde{\omega}_n} \mathrm{e}^{-\mathrm{i}\widetilde{\omega}_n t} \right] & t \geq 0 \end{cases} \tag{107}$$

Remembering that the Green function is the response to an impulsive source, we can now realize the physical meaning of the coefficient γ_n: the higher γ_n is (i.e. the higher the absorption) the faster is the decay of the corresponding modal vibration in the impulse. Therefore, it is reasonable to name this quantity *damping constant*. Thus, we can now better explain also the short remark we have made in Sect. 2.2.2 about sound decay . Let us suppose the room be excited by a stationary signal switched off at $t = 0$ and having, for simplicity, a point-like extension:

$$s(\mathbf{x},t) = \begin{cases} \delta(\mathbf{x} - \mathbf{x}_0)\beta(t) & t < 0 \\ 0 & t \geq 0 \end{cases}$$

Referring to the Eq. (98) , we have

$$\phi(\mathbf{x},t)=\sqrt{\frac{\pi}{2}}c^2\sum_{n=0}^{\infty}\mathrm{e}^{-\gamma_n t}\int_{-\infty}^{0}\mathrm{d}\tau\,\mathrm{e}^{\gamma_n\tau}\,\mathrm{Im}\left[\frac{\Psi_n(\mathbf{x};\omega)\Psi_n(\mathbf{x}_0;\omega)}{\widetilde{\omega}_n}\mathrm{e}^{-\mathrm{i}\widetilde{\omega}_n(t-\tau)}\right] \tag{108}$$

which shows that all the eigenfrequencies appear in the transient response observed soon after $t=0$, each of them decaying with its own particular damping constant γ_n. The process we have just introduced, probably the most important phenomenon of room acoustics, is usually called *reverberation*.

2.5 Impulse responses and convolutions

Now we are going to learn how to employ the Green function method when dealing with the acoustic quantities p and $\mathbf{v}$ rather than ϕ. First we shall show that the manner of writing these by means of a relation analogous to Eq. (98) is twofold. For instance, if we make use of Eq. (30) we get the two relations:

$$\begin{aligned}
\mathbf{v}(\mathbf{x},t) &= \boldsymbol{\nabla}\phi(\mathbf{x},t)=\int_V \mathrm{d}^3\mathbf{y}\int_{-\infty}^{t}\mathrm{d}\tau\boldsymbol{\nabla}_{\mathbf{x}}g(\mathbf{x},\mathbf{y};t-\tau)s(\mathbf{y},\tau)\\
&= \int_V \mathrm{d}^3\mathbf{y}\int_{-\infty}^{t}\mathrm{d}\tau\,\widetilde{\mathbf{g}}_{\mathbf{v}}(\mathbf{x},\mathbf{y};t-\tau)s(\mathbf{y},\tau)\\
p(\mathbf{x},t) &= -\rho_0\phi_t(\mathbf{x},t)=\int_V \mathrm{d}^3\mathbf{y}\int_{-\infty}^{t}\mathrm{d}\tau\,\left[-\rho_0 g_t(\mathbf{x},\mathbf{y};t-\tau)\right]s(\mathbf{y},\tau)\\
&= \int_V \mathrm{d}^3\mathbf{y}\int_{-\infty}^{t}\mathrm{d}\tau\,\widetilde{g}_p(\mathbf{x},\mathbf{y};t-\tau)s(\mathbf{y},\tau)
\end{aligned} \tag{109}$$

Hence, with respect to Eq. (98) , the source term s remains the same, while the potential's Green function g is replaced by $\widetilde{\mathbf{g}}_{\mathbf{v}}=\boldsymbol{\nabla}_{\mathbf{x}}g$ and $\widetilde{g}_p=-\rho_0 g_t$: these are not the Green functions of p and $\mathbf{v}$ respectively, but just the pressure and velocity corresponding to an impulsive excitation of the kinetic potential ϕ. Yet, this fact is not surprising, since a δ-source for the kinetic potential doesn't generate a δ also for p and $\mathbf{v}$, as shown by Eq. (34) .

An alternative way of writing p can be obtained changing the integration variable from τ to $t'=t-\tau$ in Eq. (98) : this makes the time derivative to act on s instead of g. The result is:

$$p(\mathbf{x},t)=\int_V \mathrm{d}^3\mathbf{y}\int_0^{\infty}\mathrm{d}t' g(\mathbf{x},\mathbf{y},t')\left[-\rho_0 s_t(\mathbf{y};t-t')\right]=\int_V \mathrm{d}^3\mathbf{y}\int_{-\infty}^{t}\mathrm{d}\tau\,g(\mathbf{x},\mathbf{y};t-\tau)s_p(\mathbf{y},\tau) \tag{110}$$

where in the second equality we have used Eq. (30) . Thanks to the source term s_p we can interpret Eq. (110) as the analogous of Eq. (98) in the pressure domain, which we could have there obtained simply by taking p instead of ϕ. The fact that the Green function is the same in the two relations is justified if we consider that in both cases g is the solution of the wave equation with source term equal to $\delta(\mathbf{x}-\mathbf{y})\delta(t)$ and the same boundary conditions: in fact, ϕ must satisfy the relation $Z(\mathbf{x})\mathbf{n}(\mathbf{x})\cdot\boldsymbol{\nabla}\phi(\mathbf{x},t)=-\rho_0\phi_t(\mathbf{x},t)$, which can be written

$$-Z(\mathbf{x})\mathbf{n}(\mathbf{x})\cdot\frac{1}{\rho_0}\int_{-\infty}^{t}\mathrm{d}\tau\boldsymbol{\nabla}p(\mathbf{x},\tau)=p(\mathbf{x},t)$$

Taking the time derivative, this becomes:

$$Z(\mathbf{x})\mathbf{n}(\mathbf{x}) \cdot \boldsymbol{\nabla} p(\mathbf{x},t) = -\rho_0 p_t(\mathbf{x},t)$$

that is the same condition with p in place of ϕ.

Velocity comes out from the Euler equation (Eq. (23)) with p given by Eq. (110) :

$$\mathbf{v}(\mathbf{x},t) = -\frac{1}{\rho_0}\int_{-\infty}^{t} \mathrm{d}t' \int_V \mathrm{d}^3\mathbf{y} \int_{-\infty}^{\mathbf{t'}} \mathrm{d}\tau\, \boldsymbol{\nabla}_{\mathbf{x}} g(\mathbf{x},\mathbf{y};t'-\tau) s_p(\mathbf{y},\tau)$$

Being $g(t \leq 0) = 0$ for the causality principle, we can write:

$$\begin{aligned}
\mathbf{v}(\mathbf{x},t) &= -\frac{1}{\rho_0}\int_{-\infty}^{t} \mathrm{d}t' \int_V \mathrm{d}^3\mathbf{y} \int_{-\infty}^{\infty} \mathrm{d}\tau\, \boldsymbol{\nabla}_{\mathbf{x}} g(\mathbf{x},\mathbf{y};t'-\tau) s_p(\mathbf{y},\tau) \\
&= -\frac{1}{\rho_0}\int_V \mathrm{d}^3\mathbf{y} \int_{-\infty}^{+\infty} \mathrm{d}\tau\, s_p(\mathbf{y},\tau) \int_{-\infty}^{t} \mathrm{d}t'\, \boldsymbol{\nabla}_{\mathbf{x}} g(\mathbf{x},\mathbf{y};t'-\tau) \\
&= -\frac{1}{\rho_0}\int_V \mathrm{d}^3\mathbf{y} \int_{-\infty}^{+\infty} \mathrm{d}\tau\, s_p(\mathbf{y},\tau) \int_{-\infty}^{t-\tau} \mathrm{d}t''\, \boldsymbol{\nabla}_{\mathbf{x}} g(\mathbf{x},\mathbf{y};t'')
\end{aligned}$$

where in the last equality we have made the substitution $t'' = t' - \tau$. Since the integral in t'' differs from zero only if $t - \tau \geq 0$, we obtain:

$$\mathbf{v}(\mathbf{x},t) = \int_V \mathrm{d}\mathbf{y} \int_{-\infty}^{t} \mathrm{d}\tau \left[-\frac{1}{\rho_0}\int_0^{t-\tau} \mathrm{d}t'' \boldsymbol{\nabla}_{\mathbf{x}} g(\mathbf{x},\mathbf{y};t'') \right] s_p(\mathbf{y},\tau) \tag{111}$$

Defining the function

$$\mathbf{g}_{\mathbf{v}}(\mathbf{x},\mathbf{y},t) = -\frac{1}{\rho_0}\int_0^t \mathrm{d}\tau\, \boldsymbol{\nabla}_{\mathbf{x}} g(\mathbf{x},\mathbf{y};\tau) \qquad t \geq 0 \tag{112}$$

Eq. (111) may be rewritten as

$$\mathbf{v}(\mathbf{x},t) = \int_V \mathrm{d}^3\mathbf{y} \int_{-\infty}^{t} \mathrm{d}\tau\, \mathbf{g}_{\mathbf{v}}(\mathbf{x},\mathbf{y},t-\tau) s_p(\mathbf{y},\tau) \tag{113}$$

In short, we have expressed the velocity vector through a relation resembling Eq. (110) for the pressure; a remarkable fact to be noticed is that Eq. (113) combines the pressure excitation s_p with the function $\mathbf{g}_{\mathbf{v}}$, which can be thought of as the velocity response produced by a pressure impulsive source. In the following of our discussion we will often refer to Eqs. (110) and (113) , it is thus practical to call g and $\mathbf{g}_{\mathbf{v}}$ *pressure impulse response* and *velocity impulse response* respectively, at any rate remembering that the latter does not represent a Green function for $\mathbf{v}$.

2.6 Geometric-statistical treatment of reverberation

We will now focus the attention on the study of the sound reverberation adopting a method completely different from the one adopted in the previous treatment, where the process was explained in terms of decaying modes. In fact, the wave approach has to be employed when the sound wavelength is not too small with respect to the room spatial dimensions: if this is

not the case, as it sometimes happens, the modal density increases too much and the number of resonances becomes so large that this theory is no more useful. It is clear that in this condition it is not possible to give an exact representation of acoustical phenomena: as we are going to see, the only thing one can do is to invoke a geometric-statistical model for obtaining a rough quantitative evaluation of the physical quantities [15] .

The situation where an approximation to the wave theory is needed, occurs when, due to the multiple reflections from the walls, the sound field is given by a superposition of a large number of plane waves traveling in all directions. Let's take for simplicity the single frequency case: the total pressure and velocity amplitudes in each point $\mathbf{x}$ may then be given by

$$P(\mathbf{x}) = \int_0^{2\pi} \mathrm{d}\varphi \int_{\mathbf{0}}^{\boldsymbol{\pi}} d\vartheta \, \sin\vartheta \, \widehat{p}(\mathbf{x};\varphi,\vartheta) \mathrm{e}^{\mathrm{i}k\mathbf{n}(\varphi,\vartheta)\cdot\mathbf{x}} \tag{114}$$

$$\mathbf{V}(\mathbf{x}) = \frac{1}{\rho_0 c} \int_0^{2\pi} \mathrm{d}\varphi \int_{\mathbf{0}}^{\boldsymbol{\pi}} d\vartheta \, \sin\vartheta \mathbf{n}(\varphi,\vartheta) \widehat{p}(\mathbf{x};\varphi,\vartheta) \mathrm{e}^{\mathrm{i}k\mathbf{n}(\varphi,\vartheta)\cdot\mathbf{x}} \tag{115}$$

where $\mathbf{n}(\varphi,\vartheta) = [\sin\vartheta\cos\varphi, \sin\vartheta\sin\varphi, \cos\vartheta]$ and $\widehat{p}(\mathbf{x};\varphi,\vartheta)$ is the complex amplitude of a single wave, which depends on the direction φ,ϑ as well as on the position. We now want to find the mean intensity and the mean energy density: limiting the latter to the potential part for simplicity, we have:

$$W_U(\mathbf{x}) = \frac{\rho_0}{4z^2} |P(\mathbf{x})|^2 \qquad \mathbf{A}(\mathbf{x}) = \frac{1}{2} \mathrm{Re}\left[P(\mathbf{x})\mathbf{V}^*(\mathbf{x})\right] \tag{116}$$

where (simplifying the integral notation by putting $\int_0^{2\pi} \mathrm{d}\varphi \int_0^{2\pi} \mathrm{d}\varphi' \int_{\mathbf{0}}^{\boldsymbol{\pi}} \mathrm{d}\vartheta \sin\vartheta \int_{\mathbf{0}}^{\boldsymbol{\pi}} \mathrm{d}\vartheta' \sin\vartheta' = \int_{4\pi} \mathrm{d}\Omega \int_{4\pi} \mathrm{d}\Omega'$)

$$|P|^2 = \int_{4\pi} \mathrm{d}\Omega \int_{4\pi} \mathrm{d}\Omega' \left[\widehat{p}(\mathbf{x};\varphi,\vartheta)\widehat{p}^*(\mathbf{x};\varphi',\vartheta') \mathrm{e}^{\mathrm{i}k\cdot[\mathbf{n}(\varphi,\vartheta)-\mathbf{n}(\varphi',\vartheta')]\cdot\mathbf{x}}\right] \tag{117}$$

$$P\mathbf{V}^* = \frac{1}{\rho_0 c} \int_{4\pi} \mathrm{d}\Omega \int_{4\pi} \mathrm{d}\Omega' \left[\mathbf{n}(\varphi',\vartheta')\widehat{p}(\mathbf{x};\varphi,\vartheta)\widehat{p}^*(\mathbf{x};\varphi',\vartheta') \mathrm{e}^{\mathrm{i}k\cdot[\mathbf{n}(\varphi,\vartheta)-\mathbf{n}(\varphi',\vartheta')]\cdot\mathbf{x}}\right] \tag{118}$$

In such a kind of fields the behavior of the physical quantities is properly described in an approximate way by means of *local spatial averages* (l.s.a.), i.e. averages computed over a volume with dimensions substantially larger than the typical wavelength, but much smaller than those of the whole room. We may indicate the l.s.a. operation on a generic quantity $h(\mathbf{x})$ by $L(h)(\mathbf{x})$, where the dependence on $\mathbf{x}$ now refers to the position of the elementary integration volume in the room. If we now calculate the l.s.a. of Eqs. (117) and (118) we may assume that due to the oscillatory terms the integrand is nonvanishing just for $\mathbf{n}(\varphi,\vartheta) = \mathbf{n}(\varphi',\vartheta')$ i.e. for $\varphi = \varphi'$ and $\vartheta = \vartheta'$. We then have

$$\left[L\left(|P|^2\right)\right](\mathbf{x}) = \int_{4\pi} \mathrm{d}\Omega \left[L\left(|\widehat{p}|^2\right)\right](\mathbf{x};\varphi,\vartheta)$$

$$\left[L\left(P\mathbf{V}^*\right)\right](\mathbf{x}) = \frac{1}{\rho_0 c} \int_{4\pi} \mathrm{d}\Omega \, \mathbf{n}(\varphi,\vartheta) \left[L\left(|\widehat{p}|^2\right)\right](\mathbf{x};\varphi,\vartheta)$$

the l.s.a of energy and intensity are given by the integral of the l.s.a of the energies $|\widehat{p}|^2/\rho_0 c^2$ and intensities $|\widehat{p}|^2/\rho_0 c$ corresponding to the single waves. Therefore, the l.s.a. picture shows that in a short wavelength field where multiple reflections occur, it can be assumed that the sound

energies and intensities of the wave packets can be simply added together, so that any diffraction or interference effect can be simply neglected. Therefore, the sound field can be geometrically approximated by a large number of superimposed *rays* traveling at speed c along straight lines in all possible directions: in practice, waves behave as they were *incoherent* packets without a definite phase relationship. For this reason, we can omit the explicit indication of l.s.a. and define the angular distributions of sound energy and intensity as

$$\frac{\mathrm{d}W}{\mathrm{d}\Omega} = w_{\mathbf{n}} \qquad \frac{\mathrm{d}\mathbf{A}}{\mathrm{d}\Omega} = \mathbf{n}\, c w_{\mathbf{n}} \tag{119}$$

where $w_{\mathbf{n}} = L\left(|\widehat{p}|^2\right)/\rho_0 c^2$.

2.6.1 Diffuse sound fields

In order to develop a geometric interpretation of the sound decay process we have to make a fundamental assumption: the sound rays have to be distributed so much at random that the quantity $w_{\mathbf{n}}$ is a constant independent of $\mathbf{x}$, φ and ϑ. As a consequence, also the mean energy density is independent of $\mathbf{x}$, so that $W = 4\pi w$ and the power incident on any unit area is a constant as well; in particular, this is found to be isotropic, in the sense that it does not depend on the plane orientation. Its value is given by

$$J = cw \int_0^{2\pi} \mathrm{d}\varphi \int_0^{\pi/2} \mathrm{d}\vartheta \cos\vartheta \sin\vartheta = \pi c w = \frac{1}{4} c W$$

A field satisfying the above property is said to be *diffuse*.

As regards the way energy is absorbed at the walls boundary, according to the laws of reflection which we have previously explained, it is customary to quantify this by means of the coefficient α, i.e. the fraction of incident acoustic power absorbed by the surface; in general, this depends on the position, the incidence angle ϑ and the sound frequency.

2.6.2 Mean free path

From the concept of sound particle one may develop a model for explaining reverberation using elementary calculations of statistical mechanics. The first quantity we are going to introduce is that of *mean free path* of an acoustic ray in a room. Let us take a particle which undergoes N wall reflections in a time interval t: its mean free path is given by

$$m = \frac{ct}{N} = \frac{c}{n} \tag{120}$$

where n is the average number of reflections per second. Since m and n are time average values referred to a single particle we ask ourselves how to pass to a picture where all the particles are taken into account. The answer to the question is immediate if the field behaves in a diffuse way: in this case, the particle-wall interactions don't follow a deterministic law (e.g. the Snell law); on the contrary, the process determines a non predictable change in the particle direction. Hence, the reflection angle ϑ, measured with respect to a straight line normal to the surface, may be expressed by a probability density function $P(\vartheta)$, so that $\int_{\Omega_0} \mathrm{d}\Omega P(\vartheta)$ represents the probability of a particle to be reflected into Ω_0. The assumption that $P(\vartheta)$ is independent of the incident angle ϑ_0 is well-founded when the walls have irregularities whose size is roughly equal

to the wavelength: in this case, the sound reflection does not follow the law we have described in Sect. 1.4 but it occurs through a multiplicity of scattering processes.

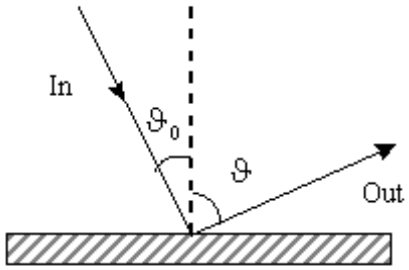

$P(\vartheta)$ is usually taken equal to the so-called *Lambert's cosine law*

$$P(\vartheta) = \frac{\cos\vartheta}{\pi} \tag{121}$$

Due to Eq. (121) we can then affirm that after the reflection a particle loses its individuality because its previous history does not affect its new trajectory; as a consequence, the time average of the paths of one single particle is fully indistinguishable from the average calculated over the all ensemble of particle paths: stated another way, the particle paths ensemble is treated as an ergodic stochastic process. In this framework it is possible to calculate the mean free path by averaging the connecting segment $r(\vartheta, \mathbf{x})$ on the whole reflection angle and on the enclosure surface S.

$$\begin{aligned} m &= \frac{1}{S}\int_S \mathrm{d}^2\mathbf{x}\int_{2\pi}\mathrm{d}\Omega\, r(\vartheta,\mathbf{x})P(\vartheta) = \frac{1}{\pi S}\int_S \mathrm{d}^2\mathbf{x}\int_{2\pi}\mathrm{d}\Omega\, r(\vartheta,\mathbf{x})\cos\vartheta \\ &= \frac{1}{\pi S}\int_{2\pi}\mathrm{d}\Omega\int_S \mathrm{d}^2\mathbf{x}\; r(\vartheta,\mathbf{x})\cos\vartheta \end{aligned}$$

the inner integral is the double of the room volume, since its integrand is the volume of the infinitesimal cylinder of height r and basis $\mathrm{d}\mathbf{x}\cos\vartheta$. It follows

$$m = \frac{4V}{S} \tag{122}$$

which is a remarkable results, because it depends just on the geometrical parameters of the room. By Eq. (120) we then obtain $n = cS/4V$.

2.6.3 Eyring's decay law

Using the concepts illustrated in the two following sections we now report a simple deduction of the energy decay law, which is appropriate when the field may be considered diffuse. Let us suppose for simplicity that the boundary consist of two parts only, having area S_1 and S_2 and absorption coefficients $\alpha_1$and α_2 respectively, both independent of position and angle of incidence. Thanks to diffuseness, the energy flows equally in every direction and subsequent wall reflections are stochastically independent of each other, so that the ratios S_1/S and S_2/S, where $S = S_1 + S_2$, express the probability of hitting the two surfaces. We may take one particle

and follow the path covered over N reflections: if this is reflected N_1 times by the first wall and $N - N_1$ from the second one, its energy will be given by

$$W_N(N_1) = W_0(1-\alpha_1)^{N_1}(1-\alpha_2)^{N-N_1}$$

while the probability for this to happen is obtained from the binomial distribution

$$P_N(N_1) = \binom{N_1}{N}\left(\frac{S_1}{S}\right)^{N_1}\left(\frac{S_2}{S}\right)^{N-N_2}$$

We may now take the expectation value of the energy: the results is

$$\overline{W_N} = \sum_{N_1=0}^{N} P_N(N_1)W_N(N_1) = W_0\left[\frac{S_1}{S}(1-\alpha_1) + \frac{S_2}{S}(1-\alpha_2)\right]^N = W_0(1-\widetilde{\alpha})^N$$

where we have defined the average absorption coefficient $\widetilde{\alpha} = (S_1\alpha_1 + S_2\alpha_2)/S$. In the last expression we may now explicit the time using Eq. (120) , with m given by Eq. (122) . The result, which represents the time dependent ensemble average of the decaying global energy in the room, is the well-known *Eyring's decay formula*

$$\overline{W(t)} = W_0(1-\widetilde{\alpha})^{cSt/4V} = W_0\mathrm{e}^{-t/\tau} \tag{123}$$

where $\tau = -\frac{4V}{cS}/\ln(1-\widetilde{\alpha})$. We have thus realized that the geometrical treatment of reverberation foresees an exponential decay with a single value of the slope (τ). In particular, we note that τ decreases when the absorption increases, approaching ∞ when $\widetilde{\alpha} \to 1$. In practice, it is customary to characterize the decay slope by defining the quantity $T_{60} = 6\tau\ln 10$ (*reverberation time*), which is the time required for energy to reach a millionth of its initial value:

$$\frac{\overline{W(T_{60})}}{W_0} = 10^{-6} \tag{124}$$

2.7 Sound decay and energy transfer

In the wave and statistical theory of room acoustics we have just discussed, the reverberation process was explained in terms of the relationship between the sound field and the boundary properties: in both cases a simplified representation was given, in order to easily account for the effects of sound reflection. These approaches are useful insofar as they allow us to obtain an approximate decay law and to find its relationship to the structural characteristics of the environment. In particular, from the wave theory one gains a correct understanding of the field behavior $\phi(\mathbf{x}, t)$ in very simple environmental situations; while the statistical treatment is based on a model which may be useful when dealing with complicate sound field patterns where the typical wavelength is small compared to the reflecting obstacles in the room. Anyway, the interpretation of the phenomenon does not really involve the fundamental physical law on which it is based, that is the energy conservation equation. In fact, this viewpoint is somewhat adopted just when in the geometrical description of sound absorption one makes the hypothesis that the reflected sound particles transmit to the wall a fraction of their energy; furthermore, the model becomes less obvious when the energy loss is supposed to depend on the parameter $\widetilde{\alpha}$, whose

physical meaning is not simply related to the one inferred in the case of a single plane wave reflection on a perfectly rigid and flat surface, which is the only system for which one can give a clear definition of absorption coefficient.

We may now try to give a better explanation of the phenomenon using the concepts we have introduced when speaking about the energy propagation. Let us consider a room of volume V and surface S where the space-time distribution of sound energy is given by $w(\mathbf{x},t)$; the time dependent global energy will be

$$E(t) = \int_V \mathrm{d}^3\mathbf{x}\, w(\mathbf{x},t) \tag{125}$$

If in V there are sound sources emitting at a constant power, the global energy in the room has a constant value, which is due to the equilibrium condition between the amount of energy introduced and the one absorbed. In fact, this is exactly the meaning of the average formulation of the non homogeneous energy conservation equation (Eq. (51)).

Let us suppose the excitation be switched off at $t = 0$, so that the energy starts to decrease. In general the decay rate is time dependent. It is calculated differentiating Eq. (125)

$$E'(t) = \frac{\mathrm{d}}{\mathrm{d}t}\int_V \mathrm{d}^3\mathbf{x}\, w(\mathbf{x},t) = \int_V \mathrm{d}^3\mathbf{x}\, w_t(\mathbf{x},t) = -\int_V \mathrm{d}^3\mathbf{x}\, \boldsymbol{\nabla}\cdot\mathbf{j}(\mathbf{x},t) = -\int_S \mathrm{d}^2\mathbf{x}\ \mathbf{n}(\mathbf{x})\cdot\mathbf{j}(\mathbf{x},t) \tag{126}$$

where in the third equality the energy conservation law has been used. This relation tells us that the time rate of change of the energy inside V is equal to the energy which escapes through S in unit time. An important quantity we may calculate without any statistical or boundary hypothesis is the decay velocity relative to the initial energy soon after $t = 0$. Indicating the initial elementary time interval by Δt the quantity is expressed by $\mu_0 = -\left[E(\Delta t) - E(0)\right]/E(0)\Delta t$ and replacing the incremental ratio by the derivative of Eq. (126) :

$$\mu_0 \simeq \frac{\int_S \mathrm{d}^2\mathbf{x}\ \mathbf{n}(\mathbf{x})\cdot\mathbf{j}(\mathbf{x},0)}{\int_V \mathrm{d}^3\mathbf{x}\, w(\mathbf{x},0)} = \frac{S}{V}\frac{\left[\mathbf{n}(\mathbf{x})\cdot\mathbf{j}(\mathbf{x},0)\right]_S}{\left[w(\mathbf{x},0)\right]_V} \tag{127}$$

where we have defined the volume and surface averages respectively of energy density and intensity ($[F]_S = \int_S \mathrm{d}^2\mathbf{x}F(\mathbf{x},t)/S$, $[F]_V = \int_V \mathrm{d}^3\mathbf{x}F(\mathbf{x},t)/V$). Now we can make the statistical hypothesis that if for $t < 0$ the excitation is a random stationary signal, the respective $\mathbf{j}(\mathbf{x},t)$ and $w(\mathbf{x},t)$ are both stationary ergodic processes until $t = 0$. In this condition the whole study is better performed from the ensemble averages viewpoint:

$$\mu_0 = \frac{S}{V}\frac{\left[\mathbf{n}(\mathbf{x})\cdot\overline{\mathbf{j}(\mathbf{x},0)}\right]_S}{\left[\overline{w(\mathbf{x},0)}\right]_V} = \frac{S}{V}\frac{\left[\mathbf{n}(\mathbf{x})\cdot\mathbf{A}(\mathbf{x})\right]_S}{\left[W(\mathbf{x})\right]_V} \tag{128}$$

Where in the first equality we have expressed the ensemble averages of $\mathbf{j}(\mathbf{x},0)$ and $w(\mathbf{x},0)$, which have been then replaced by the corresponding time averages for $t < 0$. We have then realized that the initial decay rate is inversely proportional to the characteristic length of the environment (V/S) and directly proportional to the ratio of mean intensity surface average to the mean energy density volume average. It is worth noting that when the acoustic system is such that the decay law is exponential (like foreseen by the diffuse field model) the parameter μ_0 corresponds to τ^{-1} and does not depend on the time interval on which it is evaluated.

As far as concerns the possibility of experimentally checking the above relation, we must stress that in principle the task is quite hard, for it would require an extended measurement of the energy density and the intensity all over the space and on the surfaces of the room respectively. Nevertheless, it is sometimes possible to gain an insight into the relationship of the sound decay process with respect to the energy absorption if measurements are performed locally: in fact, if we look at Eq. (128) , we note that this parameter shows a sort of resemblance with the local indicator $\eta(\mathbf{x}) = \mathbf{A}(\mathbf{x})/cW(\mathbf{x})$ introduced in the first chapter. Remembering that the latter is defined as the energy fraction of mean energy density locally radiating outward in consequence of the average intensity $\mathbf{A}$, it can be inferred that its value in a point of the space far enough from the source (in such a way the near field effects are negligible), is somewhat physically linked to the amount of energy which is absorbed at the boundary. In order to verify this, in the last chapter of this work we are going to present a series of simple experiments performed on some test fields, where the total energy decay and the most significant energy related quantities during a stationary excitation, among which the η parameter, have been measured.

We conclude this discussion by saying that a local investigation of the transient properties of sound fields is extremely useful mostly from a practical point of view, since a global description is often not suited in those situations where it is necessary to understand the process on a local basis. This may for instance happen when one wants to consider the energy decay just in the point where the listener is placed.

2.8 Transient energy and impulse responses

Now we are about to explain a fundamental relationship between the impulse response of a system and the ensemble average of a sound signal produced by a broad band excitation: we will see that through this relation it will be possible to undertake the local study of a transient field in an empirical manner, both during the rise and the fall of the signal. This principle was originally introduced by M. Schroeder in the mid Sixties and implemented for determining the decay curve of squared pressure [16] : here, we are going to show that the same reasoning holds for the squared velocity and the sound intensity as well.

Let us suppose that a generic environment be excited by a source which, for the sake of simplicity, is taken separable as described by Eq. (102) ; let us also indicate its temporal dependence by $s(t)$. A quantity h, like the pressure p or one of the velocity components, in a certain point of the space, will be given by the convolution:

$$h(t) = g * s = \int_{-\infty}^{t} \mathrm{d}t'\, g(t-t')s(t') \tag{129}$$

where the spatial dependence has been omitted for briefness, while g indicates the impulse response related to h.

As a first case, let us assume that the stimulus signal be interrupted at $t = 0$ after a stationary excitation, and calculate the quantity h^2 for $t \geq 0$:

$$h^2_{dec}(t) = \int_{-\infty}^{0} \mathrm{d}t'\, g(t-t')s(t') \int_{-\infty}^{0} \mathrm{d}t''\, g(t-t'')s(t'') \tag{130}$$

If the above-mentioned signal is an ergodic broad band white noise (that is with a constant spectral density), a description of the process free of random fluctuations is obtained taking the

ensemble average of Eq. (130) . It follows

$$\begin{aligned}\overline{h^2_{dec}(t)} &= \int_{-\infty}^{0} \mathrm{d}t'\, g(t-t') \int_{-\infty}^{0} \mathrm{d}t''\, g(t-t'')\overline{s(t')s(t'')} \\ &= \int_{-\infty}^{0} \mathrm{d}t'\, g(t-t') \int_{-\infty}^{0} \mathrm{d}t''\, g(t-t'')\delta(t'-t'') \\ &= \int_{-\infty}^{0} \mathrm{d}t'\, [g(t-t')]^2 = -\int_{\infty}^{t} \mathrm{d}\tau\, [g(\tau)]^2 = \int_{t}^{\infty} \mathrm{d}\tau\, [g(\tau)]^2\end{aligned}$$

where the second equality holds thanks to the property of white noise: $\mathfrak{R}_s(t) = \delta(t)$. It is then clear that from pressure and velocity impulse responses one can go back to the decay curve of the total energy $\overline{w(t)}$ occurring after having switched off a stationary broad band source. A remarkable fact to be emphasized, which makes $\overline{w(t)}$ suitable for expressing the energy decay, is the fact that this quantity is a monotonic decreasing function, as shown by its first derivative:

$$\frac{\partial \overline{w(t)}}{\partial t} = -\frac{1}{2}\rho_0 \left[\frac{[g_p(\tau)]^2}{z^2} + [\mathbf{g}_\mathbf{v}(\tau)]^2\right] \leq 0 \tag{131}$$

The statistical evolution of the intensity vector $\mathbf{j}(t)$ is given in an equally simple manner: it suffices to multiply $p(t)$ and $\mathbf{v}(t)$ ($t \geq 0$), both written in terms of their impulse responses

$$\overline{\mathbf{j}(t)} = \overline{p(t)\mathbf{v}(t)} = \int_{t}^{\infty} d\tau\, g_p(\tau)\mathbf{g}_\mathbf{v}(\tau) \tag{132}$$

Note that now the curves are not in general monotonic, since g_p and the components of $\mathbf{g}_\mathbf{v}$ not always have the same sign.

Reasoning in an analogous way, one can realize what happens if the excitation is switched on at $t = 0$ and goes on infinitely. In this case the starting point is the relation

$$h^2_{rise}(t) = \int_0^t \mathrm{d}t' g(t-t')s(t') \int_0^t \mathrm{d}t'' g(t-t'')s(t'')$$

and the final result is given by

$$\overline{h^2_{rise}(t)} = \int_0^t \mathrm{d}\tau\, [g(\tau)]^2 \tag{133}$$

In short, this gives us the possibility of calculating the energy also during the rise following the start of the signal. Of course, the time derivative will now be positive.

We also immediately find out the following symmetry relationship between the two transient quantities

$$\overline{h^2_{rise}(t)} = H_0^2 - \overline{h^2_{dec}(t)} \tag{134}$$

where $H_0^2 = \int_0^\infty d\tau [g(\tau)]^2$ may be interpreted as the asymptotic value reached during the stationary excitation. For figuring this out in another way, we may think of sending to the environment the same excitation s used before, this time keeping it steady. The squared value of h is then

$$h^2_{stat}(t) = \int_{-\infty}^t \mathrm{d}t' g(t')s(t-t') \int_{-\infty}^t \mathrm{d}t'' g(t'')s(t-t')$$

If the process is ergodic the time average coincides with the ensemble average (see Appendix); it follows:

$$\begin{aligned} \left\langle h_{stat}^2 \right\rangle &= \overline{h_{stat}^2} = \int_{-\infty}^{t} \mathrm{d}t' \int_{-\infty}^{t} \mathrm{d}t'' g(t-t') g(t-t'') \overline{s(t')s(t'')} \\ &= \int_{-\infty}^{t} \mathrm{d}t' \int_{-\infty}^{t} \mathrm{d}t'' g(t-t') g(t-t'') \delta(t'-t'') = \int_{0}^{\infty} \mathrm{d}\tau \ [g(\tau)]^2 = H_0^2 \end{aligned} \quad (135)$$

CHAPTER 3

Measurement techniques

We now intend to discuss the practical methods which may be used for measuring the energetic parameters we have previously defined. The first subject to be treated will be that of the intensity measurements: in this context we will focus our attention mainly on the explanation of the current techniques, both from the transduction principle and the hardware viewpoint. Then, we will deal with the measurement of the other fundamental quantity we have met in the theoretical exposition, that is the impulse response. In particular, after having illustrated the general methods (cross-correlation algorithms), which are usually adopted for obtaining responses related to pressure signals, we will explain how these can be easily employed for measuring also the velocity impulse responses. The devised procedure has two main applications: the first one concerns the possibility of performing energy decay studies involving also the kinetic term, the second one is related to an improvement of the above mentioned intensity measurements. In fact, nowadays the traditional intensimetry is almost exclusively based on the determination of the so-called *active intensity* $\langle p\mathbf{v}\rangle$, which actually coincides with the quantity we have named average radiating intensity; as regards the study of oscillating fluxes, the several attempts made in order to define a measurable quantity, being significant from a physical point of view, has not given satisfactory results up to now: for instance, the concept of *reactive intensity*, defined as the imaginary part of the complex intensity $\mathbf{j}_c(x) = \frac{1}{2}p(x)\mathbf{v}^*(x)$, can be interpreted as an oscillation term just for monochromatic fields [17] , [18] , [19] . In order to make up for this drawback we will see how to implement an indirect measurement of our oscillating intensity: the procedure is based on the "reconstruction" of the sound field by means of the convolution between excitation signals and impulse responses.

3.1 The condenser microphone

Before dealing with the intensity measurement technique, it will be useful to dwell upon the most important element for acquiring acoustic signals, both in a standard and in a research context. We are referring to the microphone, an electroacoustic transducer able to convert sound vibrations into electric signals. Here we will deal just with the condenser microphone, since this is the type usually employed for building the most common intensimetric probes [20] .

The transduction element of this microphone is given by a condenser with plane and parallel faces, kept at a constant charge (let's say Q_0) by an external voltage (typically of the order of $200\ \mathrm{V}$). One of the two faces, called diaphragm, consists of a thin metal layer (some $\mu\mathrm{m}$ thick) exposed outside in order to receive the sound pressure oscillations of the nearby field. The entire structure is usually enclosed in a cylindrical capsule as shown by the figure below.

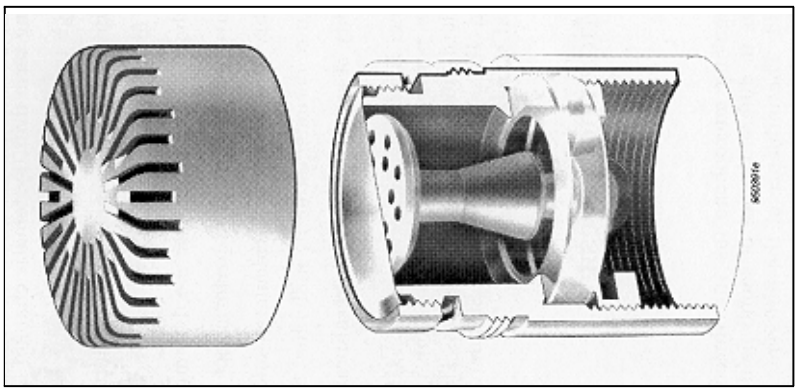

The mechanical vibrations occurring due to the sound pressure variations change the rest distance D_0 between the two faces, so that the condenser's capacity is changed; therefore, a series of voltage oscillations arises at the two condenser ends, the amplitude of these being linearly dependent on the distance variations d. In fact

$$VC = Q_0 \Longrightarrow (V_0 + v)\,\frac{\varepsilon_0 S}{D_0 + d} = V_0 \frac{\varepsilon_0 S}{D_0} \Longrightarrow v = V_0 \frac{d}{D_0} \tag{136}$$

where C is the condenser capacity and v is the voltage fluctuation with respect to the equilibrium value V_0. It is interesting to note that being D_0 quite small, about $20\,\mu\mathrm{m}$, the internal field may reach a very high value, that is about $10\,\mathrm{kV/mm}$, which is more or less three times the dielectric strength of air: nevertheless, the small distance itself prevents the ion cascade so that no discharge takes place.

An important parameter characterizing the microphone performance is the *sensitivity*, that is the voltage amplitude corresponding to a given acoustic pressure: it is measured in $\mathrm{V/Pa}$ (or in dB relative to $1\,\mathrm{V/Pa}$) and usually varies between $1\,\mathrm{V/Pa}$ and $100\,\mu\mathrm{V/Pa}$. The sensitivity is inversely proportional to the mechanical tension of the diaphragm and directly proportional to its diameter: for instance, the standard microphones of diameter $1.27\,\mathrm{cm}$ $(1/2'')$ and $0.64\,\mathrm{cm}$ $(1/4'')$, commonly used for intensity measurements, have sensitivities of the order of 12 and $6\,\mathrm{mV/Pa}$ respectively.

It is obvious that by means of a single microphone one may perform measurements on just the potential part of the acoustic field energy.

3.2 Intensity measurements

From the instantaneous intensity expression ($\mathbf{j} = p\mathbf{v}$) one easily understands that an ideal measurement instrument would require, besides a pressure transducer, a device able to detect the particle velocity. Actually, there exists a kind of probe directly implementing this principle, called *p*-**v** (pressure-velocity): it is constituted by a microphone for pressure measurements coupled to an ultrasound transducer for **v** [7] . Anyway, this technique is not very practical, because the probe, being sensitive to the air turbulence along with the sound pressure, has to be carefully protected by a proper shield, which sometimes may produce some unwanted refraction effects. On the contrary, the most common intensimetric technique employs the *p-p* (pressure-pressure) principle; this is based on the processing of signals coming from an array of microphones. Since we shall make a large use of this method, we now intend to explain its working principles in some details.

Let us consider a one dimensional field: the Euler equation may be written as follows

$$\frac{\partial v(x,t)}{\partial t} = -\frac{1}{\rho_0}\frac{\partial p(x,t)}{\partial x}$$

From this we get the velocity v

$$v(x,t) = -\frac{1}{\rho_0}\int_{-\infty}^{t} \mathrm{d}\tau\, \frac{\partial p(x,\tau)}{\partial x} \tag{137}$$

If the frequency is not too high, it is possible to approximate the derivative by an incremental ratio. Therefore

$$v(t) \simeq -\frac{1}{\rho_0}\int_{-\infty}^{t} \mathrm{d}\tau \left[\frac{p(x+\mathrm{d}x,\tau) - p(x,\tau)}{\mathrm{d}x}\right] = \frac{1}{\rho_0 d}\int_{-\infty}^{t} \mathrm{d}\tau\, [p_2(\tau) - p_1(\tau)] \tag{138}$$

where in the second equality we have written $p_1(t)$ for $p(x+\mathrm{d}x,t)$, $p_2(t)$ for $p(x,t)$ and d for $\mathrm{d}x$. In practice, one can measure the signals p_1 and p_2 by means of two condenser microphones placed at a distance d apart, then perform the time integral and finally obtain the approximate velocity component along the direction defined by the axis joining the two transducer centers. It is customary to refer the value given by Eq. (138) to the mid point between the two microphones: the corresponding pressure is given by the spatial average

$$p(t) \simeq \frac{p_1(t) + p_2(t)}{2} \tag{139}$$

The approximate instantaneous intensity is then obtained multiplying the above two quantities:

$$j(t) = p(t)v(t) = \frac{1}{2\rho_0 d}\,[p_1(t) + p_2(t)] \int_{-\infty}^{t} d\tau\, [p_1(\tau) - p_2(\tau)] \tag{140}$$

3.2.1 Outline of measurement errors

We now want to discuss the main sources of systematic errors intervening in the intensity measurements performed with the *p-p* technique.

Finite difference approximation

The first inaccuracy related to the measurement of p and v is obviously due to the way how Eqs. (138) and (139) are obtained, which is commonly called *finite difference approximation*. In particular, if the pressure gradient varies rapidly with respect to the two microphones distance, the velocity estimate from the incremental ratio becomes inadequate. The error size depends mostly on the type of the field which is being measured and on the probe orientation inside it, therefore it is not possible to give an absolute evaluation of the measurement correctness valid in all cases: anyway, following a rough but reasonable rule, we can say that the smaller is the transducers distance with regard to the wavelength, the more the measurement is accurate. A rigorous way for showing this is that of expanding in a Taylor series, with respect to the parameter $kd \ll 1$, the pressure field which a known field would produce in the two points. As an example, we here report the expansion for a plane progressive monochromatic field, dropping for briefness the detailed calculations. Following Fahy, the expansion is done with respect to kh ($h = d/2$). The results for p, v and j are

$$\begin{aligned} e(p) &= \frac{p_e - p}{p} \simeq -\frac{(kh)^2}{2} + \frac{(kh)^4}{24} + \ldots = \cos(kh) - 1 \\ e(v) &= \simeq -\frac{(kh)^2}{6} + \frac{(kh)^4}{120} + \ldots = \frac{\sin(kh)}{kh} - 1 \\ e(j) &\simeq -\frac{2}{3}(kh)^2 + \frac{2}{15}(kh)^4 + \ldots \end{aligned}$$

These relations confirm that the error is reduced by decreasing the microphones distance: for example, one may find that the conditions for the three normalized errors to be less than $5\,\%$ ($10\log(1+e) = -0.2$ dB) are: $kd < 0.66,\ 1.1,\ 0.55$. An analogous result is obtained for a plane wave interference field.

From these considerations one might think that the best result would be achieved reducing the microphones distance to the minimum; unfortunately, there is an another systematic effect which prevents us from doing this.

Phase mismatch

In addition to the inaccuracy introduced by the approximated gradient, which is an unavoidable intrinsic effect due to the measurement principle, there is a source of error which is caused by the hardware itself: it is the *phase mismatch* which arises between the two signals due to both the transducers and the readout system. A first condition to be satisfied for this to be low is that the probe is built employing a pair of microphones having similar phase responses. Nevertheless, phase discrepancy cannot be completely removed in this way, for it depends strongly from the analyzer channels as well: further expedients are then required. The following example will be of help for focusing the issue: let us consider a monochromatic field, with pressure given by $p(\mathbf{x}, t) = P(\mathbf{x})\cos[\chi(\mathbf{x}) - \omega t]$, and call χ_r the real phase difference between two points distant d apart ($d \leq \lambda$). It may be easily seen that this quantity depends on the field itself and on the direction n of the line joining the two points with respect to the wave front normal $\boldsymbol{\nabla}\chi$: for example, in a plane progressive wave, χ_r varies between a maximum equal to kd ($k = \omega/c$) and a minimum equal to zero, when performing a rotation of 90° about the propagation axis of the wave; on the other hand, if the orientation is kept fixed, χ_r vanishes also when the field becomes a perfect standing wave. To consider a specific case, let us suppose that the field be

a plane progressive stationary wave: the approximate mean intensity along n, calculated from Eq. (140) , is given by

$$A = -\frac{1}{\rho_0 d}\left\langle p_1(t)\int_{-\infty}^{t} \mathrm{d}\tau\, p_2(\tau)\right\rangle \tag{141}$$

where we have made use of the relations $\langle p_1 p_{1t}\rangle = 0$ and $\langle p_1 p_{2t}\rangle = -\langle p_2 p_{1t}\rangle$, due to stationarity (the proof follows on integrating by parts). Besides, if the wave is monochromatic, we can write $p_1(t) = P_1\cos(\chi_1 - \omega t)$, $p_2(t) = P_2\cos(\chi_2 - \omega t)$ and $\chi_r = \chi_1 - \chi_2 = kd$. Then, Eq. (141) becomes

$$A = \frac{P_1 P_2 \sin kd}{2\rho_0 c k d} = I_0\frac{\sin kd}{kd} \tag{142}$$

(where $I_0 = P_1 P_2/2\rho_0 c$). Now, let us suppose the phase mismatch error be θ: the above relation will be

$$A_m = I_0\frac{\sin(kd+\theta)}{kd}$$

so that, if $kd \ll 1$, we evaluate the relative error by the ratio

$$e(\theta) = \frac{|A_m - A|}{|A|} \simeq \left|\frac{\sin(kd+\theta)}{kd} - 1\right|$$

from which we see that the discrepancy due to a fixed θ increases when kd decreases, that is when the microphone spacing is small with respect to the wavelength. A typical phase error encountered in practice is of the order of 0.1°, this means that when for instance $f = 100\,\mathrm{Hz}$ and $d = 5\,\mathrm{cm}$ (which, as we are going to see, is on of the standard spacer lengths), $e\theta$ is of the order of $2\,\%$.

When measurements are done in critical field conditions, that is in quasi-standing waves ($\chi_r \ll kd$) or extremely low frequencies, besides using an appropriate spacer, it may be necessary to adopt a more effective method for limiting the phase discrepancy. By this technique, called *probe reversal* [21] , the mean intensity is measured two times: the first one along one direction and the second one after having changed by 180° the orientation of the probe, in order to change the phase difference from χ_r to $-\chi_r$. The two results (A_{m+}, A_{m-}) are

$$A_{m\pm} = I_0\frac{\sin(\pm\chi_r+\theta)}{kd} \simeq \pm\frac{I_0\sin\chi_r}{kd} + \frac{I_0}{kd}\cos\chi_r\sin\theta$$

In this way, taking the half-difference of the two values one can obtain a good evaluation to the average intensity

$$A = \frac{I_0\sin\chi_r}{kd} \simeq \frac{A_{m+} - A_{m-}}{2}$$

3.2.2 Probes configuration and signals readout

Intensity probes are built by mounting from one to three pairs of microphones on a single support, depending on the number of dimensions one wants to study; for 3D measurements the three axes are normal to each other in order to measure the particle velocity components in a Cartesian frame of reference. We emphasize that each pair is a one dimensional probe and therefore must be constituted by two microphones of amplitude and phase responses as similar as possible. These are arranged in such a way as to minimize the diffraction effects: the most common configurations, depicted in Fig. 8, are called *face-to-face* and *side-by-side*. As regards the

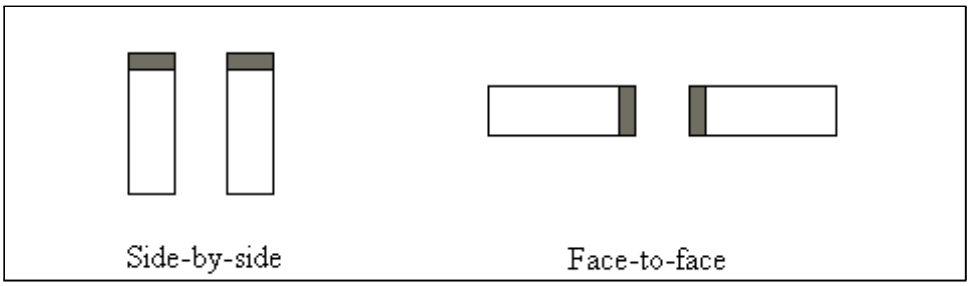

FIGURE 8. The two most common microphones' configuration in the intensity probes.

microphones distance, we have to keep in mind that, as previously explained, an optimal phase coupling and a low finite difference approximation error lead to opposite solutions; therefore, this important parameter must be chosen in order to reach a satisfactory compromise between the two needs. The distances into the probes we are going to use in our experiments (the *Brüel & Kjær 4181* and *4135*, reported in Figs. 9 and 10) are generally set, by means of proper spacers, to 5 and $1.2\,\mathrm{cm}$. This allows us to perform measurements with an accuracy of the order of $\pm\,1\,\mathrm{dB}$ (relative to $10^{-12}\,\mathrm{W/m^2}$) into the two frequency ranges: $31.5\,\mathrm{Hz} \div 1.25\,\mathrm{kHz}$ and $125\,\mathrm{Hz} \div 5\,\mathrm{kHz}$ [22] .

The electrical signals produced by the probe microphones have to be transferred to some device able to analyze them; yet, they are first sent to proper preamplifiers for changing their impedance, due to the fact that the microphones output capacity (variable from about 3 to $70\,\mathrm{pF}$, depending on the diaphragm's diameter) is not sufficiently small compared to the impedance of the chain formed by cables and the readout system ($R \sim 1\,\mathrm{M\Omega}$, $C \sim 50\,\mathrm{pF}$). The microphone capsules are thus directly connected to the preamplifiers, which contain the condensers power supply too.

The next step regards the signals elaboration for obtaining sound pressure, particle velocity and finally their time average product. Actually, there are two methods for accomplishing this. In one case the Euler equation (see Eq. (138)) is directly implemented in the time domain (as it is done for instance by the intensity analyzers *B&K 2133* and *4433*), so that after having obtained p and $\mathbf{v}$ their product is calculated according to Eq. (140) . The other method works in the frequency domain (e.g. *Onosokki CF 360*): it is based on an indirect spectral analysis of the intensity performed by means of the FFT (*Fast Fourier Transform*) of the probe signals. The basic relation implemented is $A(\omega) = \mathrm{Im}\left[G_{p_2p_1}(\omega)\right]/\rho_0\omega s$, where $G_{p_2p_1}$ is the one-sided cross-spectrum of p_2 and p_1.

In both cases the results are presented by means of spectra, but with an important difference: in the first case data are shown in *constant percentage bands*, i.e. the amplitude distribution is composed of values referred to adjacent frequency bands (like octaves or third-octaves), whose width is such that the ratio of the upper to the lower frequency is constant; in the second case the distribution is obtained in the form of *constant bands* : here levels are referred to equal frequency intervals, whose width depends on the signal sampling rate.

As an example of the first type, the block diagram of the *B&K 2133* analyzer is reported in Fig. 11. It is arranged in three main parts: signal conversion, elaboration and averaging. In the first stage the input signals are amplified and, after having been sampled and quantized through two ADC modules, they are sent to a digital filter bank (e.g. one third-octave). Afterwards the sum and difference operations of signals are performed; in particular the pressure difference is

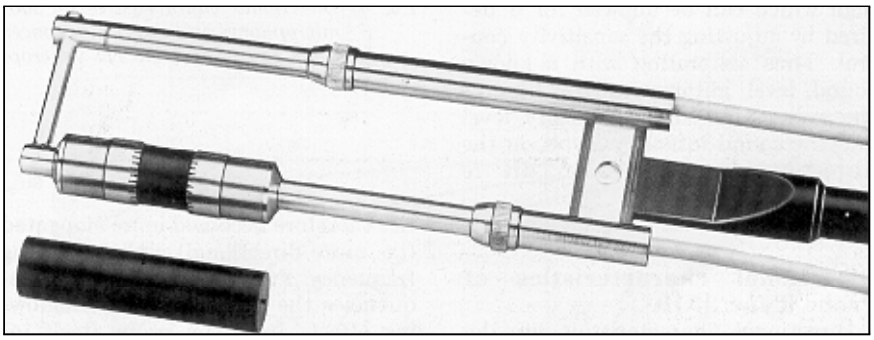

FIGURE 9. The *B&K 4181* 1D intensity probe (mic. diam.: $1.27\,\mathrm{cm}$), provided with two different spacers.

integrated and normalized in order to obtain the particle velocity signal, subsequently multiplied by the middle pressure for obtaining the instantaneous intensity. In the last stage the averages are then calculated and displayed.

An essential operation to be done before any measurement series is the channels calibration. Its purpose is twofold: firstly it compensates the inevitable sensitivity differences between channels (due both to the microphones and to the acquisition line), then it gives the possibility to display the final results in physical units or in levels (dB) referred to proper reference values ($2\times10^{-5}\mathrm{Pa}$ for pressure, $5\times10^{-8}\,\mathrm{m/s}$ for velocity and $10^{-12}\,\mathrm{W/m^2}$ for intensity). The calibration can be done in a variety of ways: the simplest one is achieved by sending to each channel a signal with a known pressure, through a sound generator called *pistonphone*; by a special procedure implemented in the analyzer the corresponding sensitivity (Pa vs. V) is then stored and subsequently used for converting the acquired signal into the correct units.

3.3 Impulse responses

From the theoretical treatment of the previous chapter we have realized that the impulse response has a twofold relevance. Let us first spend a few words about its most immediate application: that of the energy decay study, achieved making use of the fundamental relationship between the signal ensemble average and the squared impulse time integration. We underline that this was introduced as an effective method for removing the typical drawbacks of the direct investigation technique, which is based on the direct measurement of the signal (sound pressure) after a steady excitation (e.g. a white noise) [15] . The decay curves so obtained are often of little help, due to the fact they are not monotonic: as a matter of fact a plenty of oscillations, caused by the instantaneous wavefronts passages, are superimposed on a rough decreasing behavior. This stochastic-like property often makes the decay parameters calculation (e.g. the reverberation time or the early decay time) quite hard to perform, due to the difficulty encountered when trying to fit the curve. On the contrary, the Schroeder's method does not suffer from this limitation, since the ensemble average obtained integrating the impulse response eliminates any random fluctuation. Moreover, as we have previously illustrated, the same technique can be extended to get the kinetic energy decay too, which is a quite important feature from a physical viewpoint: in fact, the kinetic term is usually neglected in a practical context; nevertheless, no experimental evidences supporting the assumption of the equivalence between its behavior and that of the potential term, have ever been found.

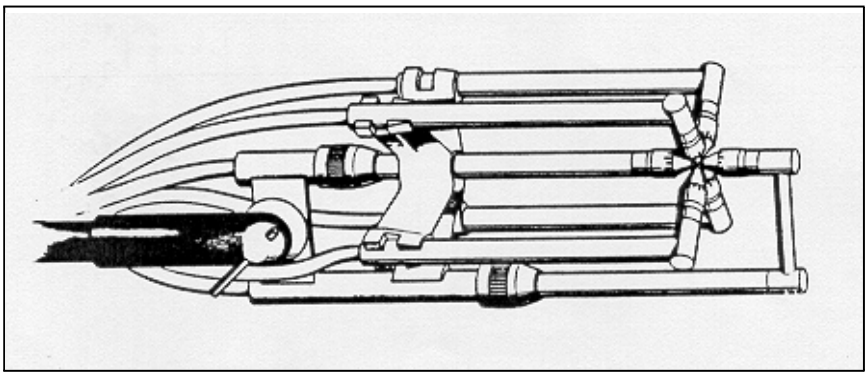

FIGURE 10. Scketch of the *B&K 4135* 3D intensity probe (mic. diam. $0.64\,\mathrm{cm}$).

We then emphasize the other important use which the impulse response may employed for. This is the indirect study of stationary parameters, which is made available by the acoustic field reconstruction through convolution algorithms, in accordance with the theory exposed in Chap. 2. We will treat the practical details of the procedure after having explained the experimental technique for measuring impulse responses.

3.3.1 Main principles

In the past, pressure impulse response measurements were done using real acoustic impulses, as the ones produced by gun shots or by loudspeakers excited by short and high voltages [15] . Although very practical, this technique is characterized by some serious disadvantages: one of these is the high crest factor of the impulsive signal, for which a high excitation energy, indispensable for maintaining the signal-to-noise ratio at an adequate level, is concentrated in a very short time. When using an electroacoustic source, this can lead to bad distortions compromising the linearity of the system: an improvement may be given reducing the frequency range by means of filters or using, instead of a crude impulse, a sinusoidal signal delimited by a particular envelope (like a Hanning, Hamming or a pseudo-Gaussian window). This method is based on the general principle for which increasing the signal length, and as a consequence spreading the excitation energy on a longer time interval, is tantamount to decreasing the frequency band.

A more recent method makes use of the cross-correlation properties between input and output of a linear system excited by a white noise. With respect to the previous one, this is much more effective because it allows us to measure indirectly a response arbitrarily large in frequency, without using an impulsive excitation. To see how it works, let us again consider the general convolution expression for a time invariant linear system

$$s_o(t) = \int_{-\infty}^{+\infty} \mathrm{d}t' g(t-t') s_i(t') \tag{143}$$

here s_i and s_o are the input and output signals respectively. Now let us calculate the cross-correlation between s_i and s_o, supposing these are random stationary ergodic processes (see Appendix)

$$\mathfrak{R}_{s_i s_o}(\tau) = \langle s_i(t) s_o(t+\tau) \rangle = \left\langle s_i(t) \int_{-\infty}^{+\infty} \mathrm{d}t' s_i(t') g(t+\tau-t') \right\rangle$$

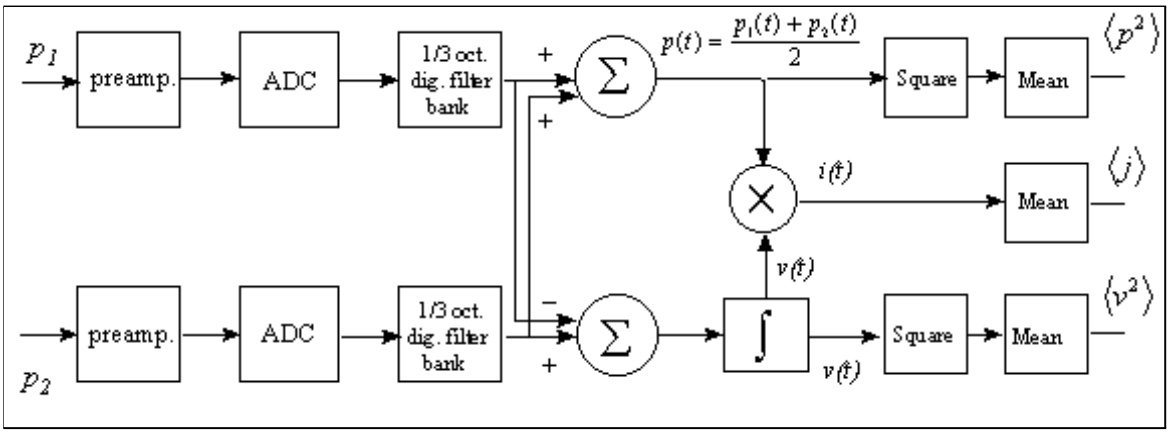

FIGURE 11. Block diagram of the *B&K 2133* real time intensity analyzer.

performing the substitution: $y = t + \tau - t'$, which implies $t' = t + \tau - y$ and $dt' = -dy$, we have:

$$\mathfrak{R}_{s_i s_o}(\tau) = \left\langle s_i(t) \int_{-\infty}^{+\infty} \mathrm{d}y \, s_i(t + \tau - y) g(y) \right\rangle = \int_{-\infty}^{+\infty} \mathrm{d}y \, g(y) \left\langle s_i(t) s_i(t + \tau - y) \right\rangle$$

this gives:

$$\mathfrak{R}_{s_i s_o}(\tau) = \int_{-\infty}^{+\infty} \mathrm{d}y \, g(y) \mathfrak{R}_{s_i}(\tau - y) \tag{144}$$

which tells us that the cross-correlation between input and output is given by the convolution between the system impulse response and the auto-correlation of the input. If we use a white noise as the input, thanks to the property $\mathfrak{R}_w(t) = \delta(t)$, it follows

$$g(t) = \mathfrak{R}_{w s_o}(t) \tag{145}$$

In the figure below, a block scheme of the typical experimental setup used for this kind of measurements is reported.

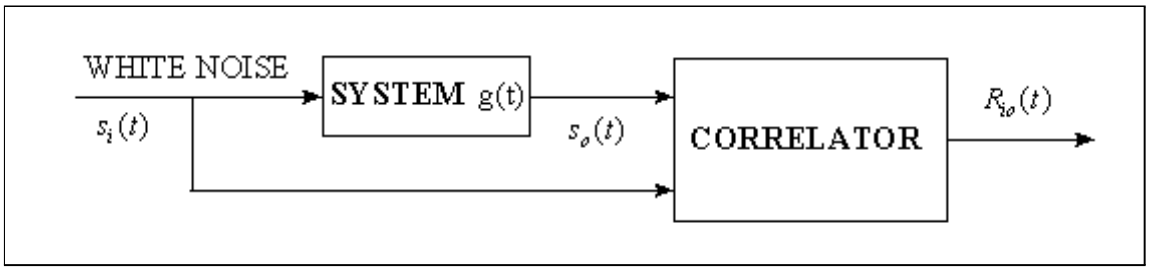

3.3.2 The MLS signal

A further improvement of the white noise technique was suggested by Schroeder himself in 1979 [23] : instead of a common white noise it may be used a special discrete excitation, called *Maximum Length Sequence* (MLS). The main characteristics which make this signal preferable are its repeatability, which allows us to reduce the statistical fluctuations of the response, and

its mathematical properties, which give the possibility of performing a fast computation of the cross-correlation.

The MLS is formally represented by a particular discrete binary periodic sequence of elements $+1$ and -1: in practice, it is generated in a deterministic way by a feedback shift register as the one shown in Fig. 12 (see [24]). Here a modulo-two adder (XOR gate) sends to the first memory unit a retroactive signal combining the l^{th} and the last bit of the slot sequence: in this way, the device generates a repeating discrete output with a period of length $N = 2^m - 1$, where m is the number of slots (*sequence order*): the rate at which these the sequence elements are produced is the same as the clock frequency f_s driving the system. A very important parameter to be set for obtaining a correct sequence, whose mathematical properties will be described in a moment, is the position of the tap inside the register: in particular, especially for long sequences, it may be necessary to arrange the cells structures inserting multiple feedbacks according to a specific pattern. Just as an example, if $m = 3$ and $l = 1$ the obtained sequence is of the kind depicted

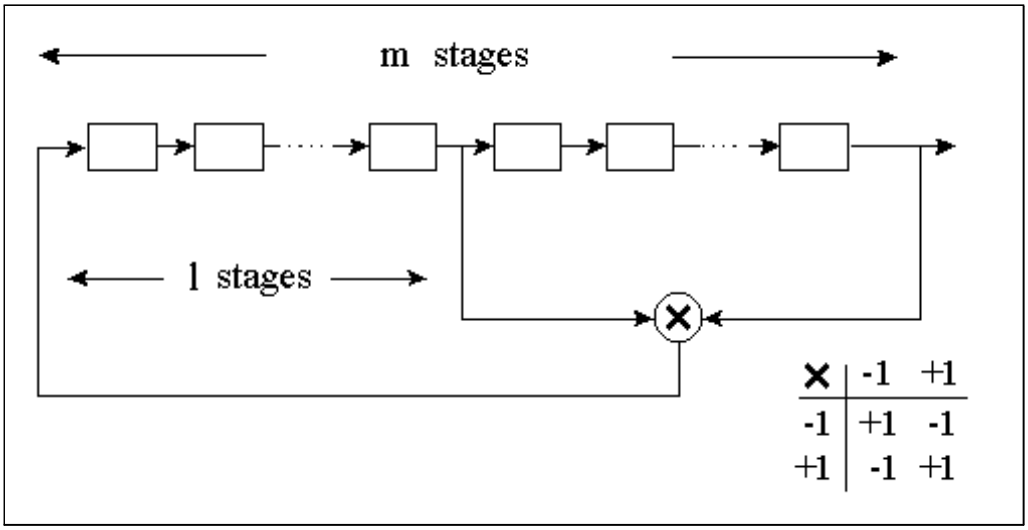

FIGURE 12. Schematic block diagram of an MLS generator.

below

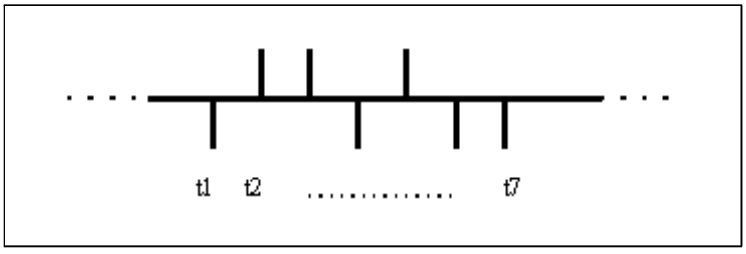

An important characteristic of the MLS is its flat spectrum (see Appendix). Hence, in spite of its non random nature, it can be considered equivalent to a white noise excitation. In particular, the auto-correlation is found to be

$$\mathfrak{R}_s(n) = \frac{1}{N}\sum_{l=0}^{N-1} s(l)s(l+n) = \begin{cases} 1 & \text{if } n = 0, N, 2N \\ -\dfrac{1}{N} & \text{otherwise} \end{cases} \tag{146}$$

The technique for obtaining the impulse response using the MLS as an excitation is analogous to that employed for a generic white noise: nevertheless, it is useful to rewrite the basic relations, for they will allow us to explain the special algorithm employed for implementing the cross-correlation procedure. Let us suppose that a loudspeaker, supposed ideal for simplicity ($g_{speak.} = \delta(t)$), be excited by an MLS, in such a way that the two values of the sequence correspond to as many values as those of the voltage applied. Then, the signal received by the transducer (for instance a microphone) can then be written as

$$p(t) = s * g = \sum_{n=0}^{N-1} s(n) g(t - n\Delta t) \tag{147}$$

If this is sampled at the same frequency as the one of the excitation ($f_s = 1/\Delta t$), Eq. (147) is just a discrete periodic convolution [25] , and we may write

$$p(k) = \sum_{n=0}^{N-1} s(n) g(k - n) \tag{148}$$

Now we calculate the input-output cross-correlation

$$\begin{aligned}
\mathfrak{R}_{sp}(k) &= \frac{1}{N} \sum_{n=0}^{N-1} s(n) \left[(s * g)(k + n) \right] \\
&= \frac{1}{N} \sum_{n=0}^{N-1} s(n) \left[\sum_{h=0}^{N-1} s(h) g(k + n - h) \right] \\
&= \frac{1}{N} \sum_{n=0}^{N-1} s(n) \left[\sum_{h=0}^{N-1} s(k + n - h) g(h) \right] \\
&= \sum_{h=0}^{N-1} g(h) \left[\frac{1}{N} \sum_{n=0}^{N-1} s(n) s(k + n - h) \right] = g * \mathfrak{R}_s
\end{aligned} \tag{149}$$

From Eq. (146) we finally get

$$\mathfrak{R}_{sp}(k) = g(k) - \frac{1}{N} \sum_{n=0}^{N-1} g(n) \tag{150}$$

Therefore, the cross-correlation directly gives the sampled impulse response, with the offset automatically subtracted from the expression.

Now let us see in detail how the entire procedure is performed. First of all we note that, according to the antisymmetry property of cross-correlation ($\mathfrak{R}_{xy}(\tau) = \mathfrak{R}_{yx}(-\tau)$), we may write

$$\mathfrak{R}_{sp}(n) = \frac{1}{N} \sum_{k=0}^{N-1} s(k) p(k + n) = \frac{1}{N} \sum_{k=0}^{N-1} s(k - n) p(k)$$

From this equality it is possible to write the algorithm in matrix form

$$\mathbf{G} = \frac{1}{N} \mathbb{M}_N \mathbf{P} \tag{151}$$

where $\mathbf{G}$ and $\mathbf{P}$ are the N-elements vectors of the impulse response and measured signal respectively, and $\mathbb{M}_N$ is the square matrix ($N\times N$) containing the circular shifts of the sequence $s(k)$. The formalism can be easily appreciated taking the sequence $M_7 \equiv [-1,1,1,-1,1,-1,-1]$ as an example: if for simplicity we write $+$ and $-$ instead of 1 and -1, Eq. (151) becomes

$$\begin{bmatrix} g(0) \\ g(1) \\ g(2) \\ g(3) \\ g(4) \\ g(5) \\ g(6) \end{bmatrix} = \frac{1}{7} \begin{bmatrix} - & + & + & - & + & - & - \\ + & + & - & + & - & - & - \\ + & - & + & - & - & - & + \\ - & + & - & - & - & + & + \\ + & - & - & - & + & + & - \\ - & - & - & + & + & - & + \\ - & - & + & + & - & + & - \end{bmatrix} \begin{bmatrix} p(0) \\ p(1) \\ p(2) \\ p(3) \\ p(4) \\ p(5) \\ p(6) \end{bmatrix} \tag{152}$$

Note that the right length N of the sequence depends on the length t_{ir} of the impulse response: in practice, $N\Delta t \geq t_{ir}$. Moreover if this has to be analyzed considering all the frequencies up to $f_{\max}$, due to the Shannon theorem [25] , it has to be sampled with a rate f_s being at least twice $f_{\max}$. In practice, one must have $N \geq 2 f_{\max} t_{ir}$.

3.3.3 The Fast Hadamard Transform

A significant advantage offered by the MLS technique is that the calculation of Eq. (151) may be performed in a very efficient way employing an algorithm called *Fast Hadamard Transform*. We will now briefly explain this procedure, following a work by W.T. Chu [26] .

The starting point of the Hadamard transform method applied to the impulse response calculation is the transformation of the matrix $\mathbb{M}_N$ into an Hadamard matrix (from now on called $\mathbb{H}$). This is a square even-dimensional matrix ($2^m \times 2^m$), whose elements are all ± 1 [27] ; in particular, it is defined by the relation

$$\mathbb{H}_{2^m}^2 = 2^m \cdot \mathbb{I}_{2^m} \tag{153}$$

where $\mathbb{I}_{2^m}$ is the identity matrix of order 2^m. As an example, we here write the matrix $\mathbb{H}_8$:

$$\mathbb{H}_8 = \begin{bmatrix} + & + & + & + & + & + & + & + \\ + & - & + & - & + & - & + & - \\ + & + & - & - & + & + & - & - \\ + & - & - & + & + & - & - & + \\ + & + & + & + & - & - & - & - \\ + & - & + & - & - & + & - & + \\ + & + & - & - & - & - & + & + \\ + & - & - & + & - & + & + & - \end{bmatrix} \tag{154}$$

As a consequence of the above definition, the following recursive property holds

$$\mathbb{H}_{2^m} = \left[\begin{array}{c|c} \mathbb{H}_{2^{m-1}} & \mathbb{H}_{2^{m-1}} \\ \hline \mathbb{H}_{2^{m-1}} & -\mathbb{H}_{2^{m-1}} \end{array}\right] \tag{155}$$

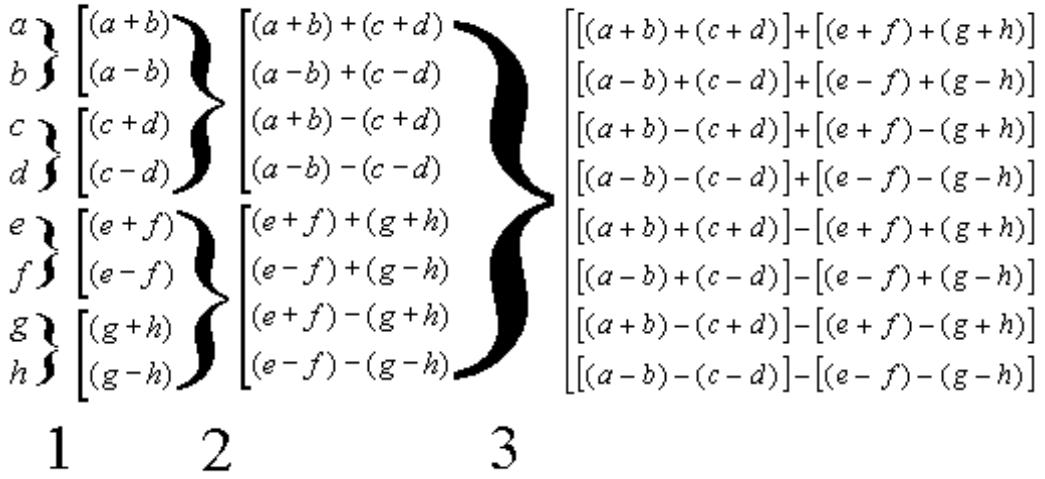

FIGURE 13. Flowgraph of the Hadamard transform of order 8.

The product of the matrix by a 2^m elements vector ($\mathbb{H}_{2^m}\mathbf{x}$) consists of $2^m(2^m-1)$ arithmetical operations: in particular, for the $\mathbb{H}_8$ 56 of them are needed:

$$\mathbb{H}_8\mathbf{x} = \begin{bmatrix} + & + & + & + & + & + & + & + \\ + & - & + & - & + & - & + & - \\ + & + & - & - & + & + & - & - \\ + & - & - & + & + & - & - & + \\ + & + & + & + & - & - & - & - \\ + & - & + & - & - & + & - & + \\ + & + & - & - & - & - & + & + \\ + & - & - & + & - & + & + & - \end{bmatrix} \begin{bmatrix} a \\ b \\ c \\ d \\ e \\ f \\ g \\ h \end{bmatrix} = \begin{bmatrix} a+b+c+d+e+f+g+h \\ a-b+c-d+e-f+g-h \\ a+b-c-d+e+f-g+h \\ a-b-c+d+e-f-g+h \\ a+b+c+d-e-f-g-h \\ a-b+c-d-e+f-g+h \\ a+b-c-d-e-f+g+h \\ a-b-c+d-e+f+g-h \end{bmatrix} \tag{156}$$

Nevertheless, it easy to see that, thanks to Eq. (155) , the same product can be calculated through $2^m m$ operations only, using an algorithm made up by m steps, each of them containing m additions and subtractions: this is just the Hadamard transform. Instead of giving a formal description of the general algorithm [28] , we prefer to illustrate, with the help of the flowgraph of Fig. 13, the way how the procedure is applied in our example ($m = 3$). It can be seen that the number of operation has decreased to 24.

Now we show how to transform the matrix $\mathbb{M}$ into a $\mathbb{H}$, in such a way that the product of Eq. (151) can be calculated by means of the Hadamard transform. To this aim we may follow, without demonstrations, the procedure suggested by Cohn and Lempel [29] , where the representation $\pm 1 \rightarrow 0, 1$ and the modulo-two arithmetic are used. First of all, we note that the Hadamard matrix can be factorized in this way

$$\mathbb{H} = \mathbb{B}\mathbb{B}^T \tag{157}$$

where $\mathbb{B}$ ($\mathbb{B}^T$) is a $2^m \times m$ ($m \times 2^m$) matrix and is built in such a way that its i^{th} row (column) is the base-2 representation of the integer i (we remind the reader that $i = 0, 1, \ldots, 2^m - 1$, so

that the total number of bits is 2^m). Therefore, for $\mathbb{H}_8$ we have

$$\mathbb{H}_8 = \begin{bmatrix} 0 & 0 & 0 & 0 & 0 & 0 & 0 & 0 \\ 0 & 1 & 0 & 1 & 0 & 1 & 0 & 1 \\ 0 & 0 & 1 & 1 & 0 & 0 & 1 & 1 \\ 0 & 1 & 1 & 0 & 0 & 1 & 1 & 0 \\ 0 & 0 & 0 & 0 & 1 & 1 & 1 & 1 \\ 0 & 1 & 0 & 1 & 0 & 1 & 0 & 1 \\ 0 & 0 & 1 & 1 & 1 & 1 & 0 & 0 \\ 0 & 1 & 1 & 0 & 1 & 0 & 0 & 1 \end{bmatrix} = \underbrace{\begin{bmatrix} 0 & 0 & 0 \\ 0 & 0 & 1 \\ 0 & 1 & 0 \\ 0 & 1 & 1 \\ 1 & 0 & 0 \\ 1 & 0 & 1 \\ 1 & 1 & 0 \\ 1 & 1 & 1 \end{bmatrix}}_{\mathbb{B}} \begin{matrix} 0 \\ 1 \\ 2 \\ 3 \\ 4 \\ 5 \\ 6 \\ 7 \end{matrix} \underbrace{\begin{bmatrix} 0 & 0 & 0 & 0 & 1 & 1 & 1 & 1 \\ 0 & 0 & 1 & 1 & 0 & 0 & 1 & 1 \\ 0 & 1 & 0 & 1 & 0 & 1 & 0 & 1 \end{bmatrix}}_{\mathbb{B}^T} \begin{matrix} \\ \\ \\ 0 \ 1 \ 2 \ 3 \ 4 \ 5 \ 6 \ 7 \end{matrix}$$

We now notice that also the $N \times N$ matrix $\mathbb{M}$ may be expressed as a product of the same kind as Eq. (157) : we have

$$\mathbb{M} = \mathbb{R}\mathbb{C} \tag{158}$$

where $\mathbb{C}$ ($m \times N$) is formed by the first m rows of $\mathbb{M}$ and $\mathbb{R}$ ($N \times m$) is formed by the m columns of $\mathbb{M}$, such that the first m rows of $\mathbb{R}$ give the $m \times m$ unit matrix. Let us verify this for the matrix appearing in Eq. (154) :

$$\mathbb{M}_7 = \begin{bmatrix} 1 & 0 & 0 & 1 & 0 & 1 & 1 \\ 0 & 0 & 1 & 0 & 1 & 1 & 1 \\ 0 & 1 & 0 & 1 & 1 & 1 & 0 \\ 1 & 0 & 1 & 1 & 1 & 0 & 0 \\ 0 & 1 & 1 & 1 & 0 & 0 & 1 \\ 1 & 1 & 1 & 0 & 0 & 1 & 0 \\ 1 & 1 & 0 & 0 & 1 & 0 & 1 \end{bmatrix} = \underbrace{\begin{bmatrix} 1 & 0 & 0 \\ 0 & 1 & 0 \\ 0 & 0 & 1 \\ 1 & 1 & 0 \\ 0 & 1 & 1 \\ 1 & 1 & 1 \\ 1 & 0 & 1 \end{bmatrix}}_{\mathbb{R}} \begin{matrix} 4 \\ 2 \\ 1 \\ 6 \\ 3 \\ 7 \\ 5 \end{matrix} \underbrace{\begin{bmatrix} 1 & 0 & 0 & 1 & 0 & 1 & 1 \\ 0 & 0 & 1 & 0 & 1 & 1 & 1 \\ 0 & 1 & 0 & 1 & 1 & 1 & 0 \end{bmatrix}}_{\mathbb{C}} \begin{matrix} \\ \\ \\ 4 \ 1 \ 2 \ 5 \ 3 \ 7 \ 6 \end{matrix}$$

We now call **r** and **c** respectively the two sequences of numbers indicating the decimal representations of the rows of $\mathbb{R}$ (from left to right) and of the columns of $\mathbb{C}$ (from top to bottom): it is easy to see that the two matrices are exactly two different permutations of the $1 \div N$ rows of $\mathbb{B}$ and of the $1 \div N$ columns of $\mathbb{B}^T$. We then may define two permutation matrices: $\mathbb{L} = \{\delta_{r(i),i}\}$, $\mathbb{Q} = \{\delta_{i,c(i)}\}$ in order to obtain

$$\mathbb{M}' = \mathbb{L}\mathbb{M}\mathbb{Q} = \mathbb{L}\mathbb{R}\mathbb{C}\mathbb{Q} = \mathbb{R}'\mathbb{C}' \tag{159}$$

The product $\mathbb{M}\mathbf{P}$ can then be written

$$\mathbb{M}\mathbf{P} = \mathbb{L}^T\mathbb{L}\mathbb{M}\mathbb{Q}\mathbb{Q}^T\mathbf{P} = \mathbb{L}^T\mathbb{M}'\mathbb{Q}^T\mathbf{P} = \mathbb{L}^T\mathbb{M}'\mathbf{P}' \tag{160}$$

where the first equality holds because the permutation matrices are orthogonal. Since $\mathbb{M}'$ contains the same elements of the $(1,1)$ minor of $\mathbb{H}_{N+1}$, expanding $\mathbb{M}'$ with a row and a column of zeros it is possible to apply the Hadamard transform upon the $N+1$ vector $[0, \mathbf{P}']$. The procedure is now complete; we can summarize it in the following way:

(1) factorize the matrix $\mathbb{M}$ according to Eq. (158) ;
(2) permute the rows of $\mathbb{R}$ and the columns of $\mathbb{C}$ in such a way that their numerical content ($1 \div N$) is ordered in an increasing manner (Eq. (159));

(3) define the Hadamard matrix adding a row and a column of zeros to $\mathbb{M}'$

$$\mathbb{H} = \begin{bmatrix} 0 & \cdots & 0 \\ \vdots & \mathbb{M}' & \\ 0 & & \end{bmatrix}$$

(4) obtain the vector $\mathbf{P}'$ reordering the elements of $\mathbf{P}$ through the same permutation used for obtaining $\mathbb{C}'$ (i.e. $\mathbb{P}' = \mathbb{Q}^T\mathbf{P}$);

(5) define the vector

$$\mathbf{P}'' = \begin{bmatrix} 0 \\ \mathbf{P}' \end{bmatrix}$$

(6) use the Hadamard transform to calculate the vector $\mathbf{G}''$:

$$\mathbf{G}'' = \frac{1}{N}\mathbb{H}\mathbf{P}''$$

(7) obtain the vector $\mathbf{G}'$ omitting the first element of $\mathbf{G}''$;

(8) reorder the elements of $\mathbf{G}'$ according to the permutation used for obtaining $\mathbb{R}'$ (i.e. $\mathbf{G} = \mathbb{L}^T\mathbf{G}'$).

3.3.4 Experimental setup

The most widely diffuse commercial instrument for the MLS measurements is a PC board called MLSSA (Maximum-Length-Sequence System Analyzer), developed at DRA laboratories (Sarasota, FL, U.S.A.). It is supplied with an output, whose signal is provided by an internal MLS generator, and with an analog input: measurements are performed sending the stimulus to a loudspeaker (through an amplifier) and contemporarily acquiring the environment response from a microphone placed in the desired position. This is first sent to an anti-aliasing filter, then sampled at the same rate at which the excitatory impulses are generated: thus, by means of a software implementing the Hadamard transform, the impulse response is obtained.

Up to now, it has been implicitly assumed that such a kind of measurements regard the sound pressure only: actually, the MLSSA system, which is a one channel instrument, has been projected for the acquisition of a single response (anyway not limited to acoustics). Nevertheless, we have shown that a complete analysis of the energetic properties of the sound field requires also the knowledge of the particle velocity. According to the explanation presented in Sect. 2.5, a function suitable to this purpose is given by the velocity impulse response $\mathbf{g_v}$. Actually, this quantity can be measured even by a single channel instrument: for each coordinate it is sufficient to directly implement Eq. (112) by first measuring one at a time two pressure impulse responses corresponding to two different locations and subsequently performing the time integral of their incremental ratio. In practice, two methods may be adopted: the first one is that of moving one microphone in the two locations, the second, and easiest one, is that of using the two channels of an intensity probe, as shown in the picture below. Of course, this procedure cannot be employed for measuring the particle velocity signal of an external field, because when using the Euler equation it is absolutely necessary that the two pressure signals are acquired contemporarily. Nevertheless, in this specific situation we are dealing with a pair of signals which, though obtained at different times, are due to a deterministic repeatable excitation and not to a random process: therefore, if we suppose that the system under analysis is time invariant we are permitted to treat the two responses as if they were taken at the same time. Moreover, the applicability is further justified by the computational procedure. In fact, the cross-correlation

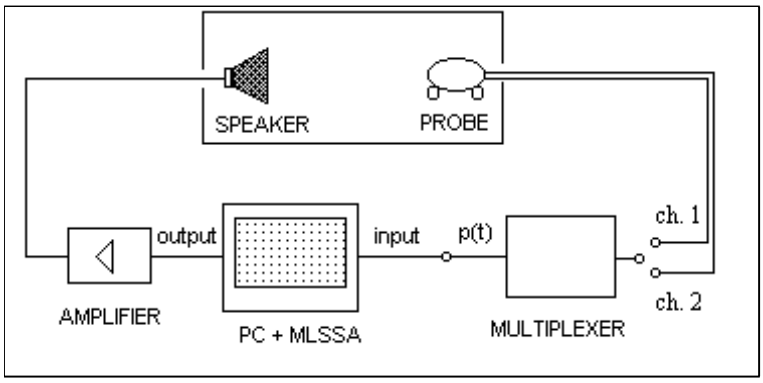

FIGURE 14. Schematic view of the experimental setup used for measuring pressure and velocity impulse responses.

between input and output strongly reduces the background noise, so that the final outcome may be considered a signal almost perfectly faithful to the desired one: in practice, one may think that during each acquisition the environment undergoes the same reflection pattern.

Obviously, if the measurement is performed by means of different microphones (as it happens when using the probe), it is essential to carefully calibrate each acquired signal, adopting a procedure similar to the one described in Sect. 3.2.2. In any case, we must stress that the impulse responses found in this way have to be thought as defined except for a common constant factor. In fact, we remind that the signals involved in the cross-correlations (see Eq. (143)) are the sequences s_i (system input) and $s_o = g * s_i$ (system output), respectively: if an MLS stimulus s is used, it may be assumed that $s_i = Ks$, K being a constant factor dependent on the excitation amplitude. Therefore, the cross correlation gives

$$\mathfrak{R}_{s_i s_o} = Kg$$

We finally emphasize that, since we are dealing with finite discrete signals, the velocity impulse response is given by (see Eq. (138))

$$g_v(n) = \frac{1}{\rho_0 d} \sum_{m=0}^{n} [g_{p_2}(m) - g_{p_1}(m)] \tag{161}$$

3.4 “Recovery” of stationary sound signals

We now want to illustrate the procedure that, given the pressure and velocity impulse responses and the explicit mathematical form of the excitation, allows us to find the corresponding stationary signals. This method may be of great interest, since by the knowledge of both pressure and velocity time histories it is possible to derive the oscillating intensity just by applying the definition of Eq. (58) ; in fact, we underline that a direct measurement of this quantity would require a specific instrumentation, which currently is not commercially available. Moreover, the convolution technique may be applied for accomplishing a kind of “virtual” study of the sound field: starting from a specific set of impulse responses one can retrieve the time histories of any kind of signal, and subsequently calculate the parameters which would have been obtained putting a real source into the environment.

Of course, also the inverse Hadamard transform can be regarded as a simple application of the convolution technique. In fact, this allows us to recompute the basic period of the pressure and velocity sequences determined by the MLS stimulus: all the quantities calculated from these signals are then related to the field produced by the indefinite iteration of the excitation sequence and may be employed for performing a broad band analysis (according to the limitations imposed by the sampling rate). Actually, it is evident that the procedure is redundant if one is interested in just the stationary parameters, for it is possible to acquire the signals without executing the forward transform; in this way one may obtain the velocity signals by directly applying the discrete form of the Euler equation on a set of finite pressure time histories (e.g. two or six of them). In practice

$$v(n) = \frac{1}{\rho_0 d} \sum_{m=0}^{n} [p_2(m) - p_1(m)]$$

Nevertheless, we will implement the first method explicitly, since this will give us the opportunity of performing an analysis involving both the transient and the stationary state in the same frequency band.

Anyway, the most general purpose of the convolution method is that of reconstructing a generic excitation. In this case, knowing the mathematical form of the signal s, one may obviously calculate the expression directly in the time domain. On the other hand, this method is in general quite cumbersome, because it requires an enormous amount of arithmetical operations (see Appendix). A more effective way is the one based on the implementation of the convolution in the frequency domain, thanks to the possibility of employing the Fast Fourier Transform algorithms. For this reason, we will check the feasibility of the convolution equation by applying the formula presented in Sect. A.7: the task will be particularly simple, since our aim will be just the reconstruction of simple harmonic fields.

It is clear that the essential requirement we have to satisfy is that of obtaining sufficiently long steady signals, in order to approach the stationary condition as better as possible. This can be achieved convolving the impulse responses with long excitation segments, for instance by means of the overlap-add method, and subsequently rejecting the initial and final transient parts.

CHAPTER 4

Experimental analysis

The purpose of the set of experiments we will be discussing is the study of the local properties of energy transfer inside acoustic fields of different kinds. As anticipated above, a particular attention will be devoted to the relationship between the behavior of the transient phase and the energy related quantities measured during the stationary excitation of the environment. The issue will be approached with the aid of the theory of energy fluxes division: we will show that the knowledge of both radiating and oscillating intensity, along with the associated indicators, makes it possible to achieve a physical interpretation of absorption and reflection phenomena on a local basis. In our opinion, this could represent the first step of a new complementary approach to the usual geometrical treatment employed in room acoustics.

4.1 Study of the sound field of an organ pipe

The first experiment concerns the measurement of $\mathbf{A}$ and W in the one-dimensional field inside an organ pipe: the main scope is that of giving a simple introductory example where one can directly understand the meaning of the indicator η when passing from the inner field to the outer field, thus drastically changing the boundary conditions and, consequently, the radiation characteristics.

The sound production mechanism of an organ pipe is based on a stream of air at constant speed, which through a slit (called the *mouth*) placed in the bottom and directed upward, is sent against a sharp edge (the *lip*): this interaction produces a series of regularly periodic vortices blowing in an alternate way at the two sides of the lip. If the vortices' period (*edge tone*) corresponds to one of the resonances of the upper duct (see [30]), the column of air contained inside it undergoes an excitation and starts to vibrate with the same frequency. The jet-lip system is thus the excitation source of the instrument while the air column is the corresponding resonator and the real source of the organ sound. Moreover, these two parts are tightly matched together so

that altering the former one would alter the latter and vice versa. Once the driving mechanism, which is usually supposed to act in a steady manner, has established, the sound field within the pipe (that is after the so called *settling time*) reaches a permanent condition (called *steady sound*): it is thus possible to perform an analysis of the field involving the air particle velocity, the sound pressure and the joint behavior of the two.

A rough explanation of the spectral content of an organ pipe field follows from the study of resonances inside a finite duct. In particular, as a first approximation it is assumed that the lower end is always a pressure-release surface ($\mathcal{C} = -1$, $Z = 0$) while the upper end is perfectly reflecting when the pipe is closed ($\mathcal{C} = 1$, $Z = \infty$) and a pressure-release surface when it is open. Accordingly, for a pipe of length L, the spectra in the two cases are given respectively by

$$\omega_n^{(Cl.)} = \frac{(2n-1)\pi c}{2L} \qquad \omega_n^{(Op.)} = \frac{n\pi c}{L} \tag{162}$$

4.1.1 Methods

The energetic analysis was accomplished along a straight path beginning near the mouth of the pipe (see Fig. 15) and ending over its top: the measurement spatial range started at the excitation region, where some of the characteristics of the driving mechanism clearly appear, to the farthest part of the pipe and also outside it, where the inner field starts matching with the remaining of the room.

We used a wooden flue open organ pipe, about $1.80\,\mathrm{m}$ long. Its tune was the E_2 of the musical scale (fundamental frequency: $82.5\,\mathrm{Hz}$). This particular choice was suggested mainly by practical reasons; in fact, wood was particularly convenient, for we had to perform several holes along the pipe in order to insert the microphones of the intensimetric probe.

Measurements were carried out under steady sound conditions, while air-supplying the pipe by a small blowing machine (Fig. 16); we employed a *B&K 4135* sound intensity probe in the "side by side" configuration, with the two microphones tightly fixed together in a plastic holder and inserted into pairs of adjacent holes all along the pipe axis. All the unused holes had been well sealed by means of metal screws and rubber washers, to avoid any internal sound field change due to air escape. The choice of a low frequency sound was done with the aim of keeping the bias errors, typical of the *p-p* intensimetric technique, as low as possible, especially for upper harmonics; for the same reason we even set the distance between the probe microphones to the non standard value of $4\,\mathrm{cm}$, so assuring minimum errors up to about $2\,\mathrm{kHz}$ and no damage on the pipe walls while making the holes. As far as concerns the data taken outside the pipe, it is worth underlining that a correct procedure would have required free field conditions (as in an anechoic chamber); anyway, for practical reasons, we performed the measurements in a big shed, which, even if certainly not anechoic, proved to be suitable for this first investigation.

The probe signal was sent to a *B&K 2133* intensity meter that gave us the average sound pressure, particle velocity and mean intensity levels. We performed the analysis in a wide frequency band, ranging from $46\,\mathrm{Hz}$ to $2.74\,\mathrm{kHz}$; besides, we kept the integration time quite long ($30\,\mathrm{s}$), to maintain statistical errors lower than $0.1\,\mathrm{dB}$ for all the quantities. The data were then transferred to a PC, then converted into physical units and processed.

The main problem encountered during the experiment was due to the channels' phase mismatch, which in fact is a particularly important source of systematic errors in low frequency standing wave fields. We realized it just at the beginning, when we saw that a tiny displacement of the probe from its right position produced a not negligible sound intensity level variation

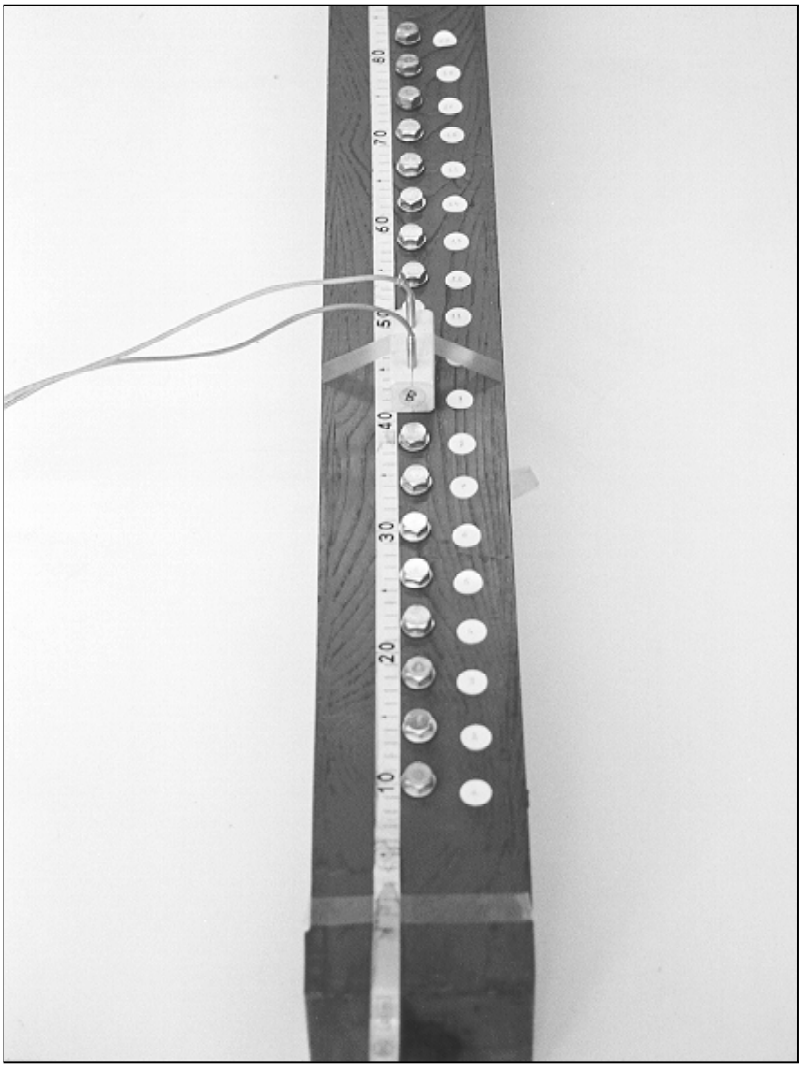

FIGURE 15. The organ pipe seen from the measurement's side. Note the screws plugging the holes and the probe placed in the middle.

($\sim 0.5 \div 1\,\mathrm{dB}$). In order to make up for this effect, we decided to collect data adopting the probe reversal technique (see Sect. 2): for all the quantities and in each point along the pipe, we took two values, corresponding to the two opposite probe axis directions. The final corrected intensity was then given by: $A = (A_1 - A_2)/2$, where the subscript 1 refers to the measurement done with the probe axis in the same direction as the pipe axis (from bottom to top), and the subscript 2 to the opposite direction.

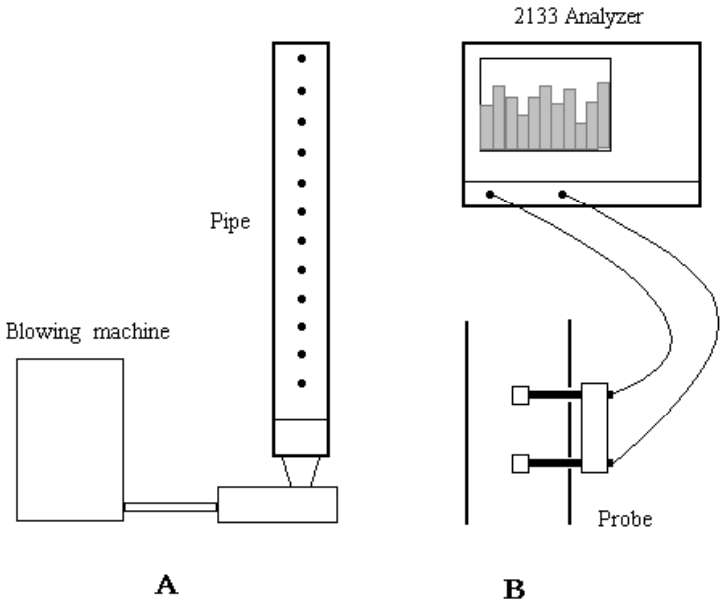

FIGURE 16. A: The organ pipe setup. **B:** side view of the probe inserted in a couple of holes.

4.1.2 Results

We performed measurements on 21 points, $12\,\mathrm{cm}$ far from each other: the first one and the last one were $12\,\mathrm{cm}$ and $252\ \mathrm{cm}$ from the base respectively. The last six were outside the pipe.

The first result we report is a typical sound level spectrum (Fig. 18), obtained sending one channel of the probe to an *Onosokki CF 360* FFT spectrum analyzer. This served us just for a few remarks about the frequency content of the pipe: first of all, it can be seen that the role of the fundamental tone is predominant, even if the value of $f_0 = 82.5$ Hz is not the one given by the second relation of Eq. (162) , meaning that the effective length where the oscillation of the column of air occurs is greater than the physical length of the duct. Nonetheless, apart from this discrepancy, the spectrum is perfectly harmonic, with all the even and odd components clearly visible until the fifth one.

Below we report all the energetic quantities versus position (Fig. 17). Graphic **A** shows the acoustic squared pressure and the normalized velocity ($z^2\mathbf{v}^2$), whose behaviors confirm that the field is almost completely built by the fundamental frequency. The same characteristic is evident looking at graphic **B**, where the indicator σ is reported (see Sect. 1.6): it oscillates on a space scale whose period is about $\lambda_0/2 \simeq 2\,\mathrm{m}$ ($\lambda_0 = c/f_0 = 4.17\,\mathrm{m}$).

C shows the average sound intensity. The most important feature to be noted here is that this quantity reaches very high values, especially in the region close to the mouth ($0.2\,\mathrm{W/m^2} \simeq 123\,\mathrm{dB}$ rel. to $10^{-12}\,\mathrm{W/m^2}$): this confirms that the inner field is not formed by perfect standing waves and, as a consequence, a certain energy flow takes place (otherwise we could not hear the sound !). Unlike the energy density, which is roughly constant inside (about $0.1\,\mathrm{J/m^3}$), the sound intensity varies with position; actually, this is not surprising, since we took data just in the middle of the sound source, which is distributed exactly over the zone where the vortices interact with the column of air (remember that in a one-dimensional field the property is mathematically expressed by the relation $\partial A/\partial x = \langle pq \rangle$). On the other hand, being the field almost completely monochromatic, a kind of "standing–wave degree" is represented also by the oscillation amplitude of σ, going from 1 to a minimum value of about 0.2: as we have pointed out in Sect. 1.8.1, in a perfectly standing monochromatic wave σ varies periodically between 0 and 1, while the more the field becomes progressive, the more σ is quenched to 1. Finally, the plot for the energetic indicator η is shown in **D.** We remind that this is defined as the u velocity modulus in units of c and it is supposed to give a synthetic quantitative evaluation of the radiating degree of the acoustic field. In our case, η is very small inside (~ 0.05) but it undergoes a considerable increase outside (it reaches 0.2 at $2.5\,\mathrm{m}$), as we expect from a field which abruptly becomes more progressive and radiating; actually, what exactly happens when passing from the inner to the outer field, is that both the intensity and the energy density fall off, because we are getting far from the source, nevertheless, their ratio increases.

Measurement of oscillating intensity

In order complete the study of the pipe field we measured also the oscillating intensity [31] . Since none of the commercially available instruments currently implements the measure of this quantity, we used an intensity meter specifically built for this purpose [32] . This is based on a software tool, developed within the *Labview* ® environment, which processes the signals coming from the probe channels: along with the oscillating intensity it can measure also the usual radiating intensity, the sound pressure and the particle velocity. Data acquisition (digitization and sampling) is performed via a 12 bits acquiring card, while analysis ($1/3$ octave filtering and algorithms) takes place in the host PC, where results are stored for subsequent rendering.

The new set of measurements was accomplished on 33 points of the axis, $8\,\mathrm{cm}$ far from each other, of which the last 11 were in the outer region. In Fig. 19 the overall levels of A and R, both on a dB scale, are shown. Note that inside, the R level is much higher than that of A, as expected from an almost-standing wave field. Moreover, its behavior resembles that of σ; in particular, the two maxima of R coincide with the points where kinetic and potential energy densities are equal ($\sigma = 1$). When passing from the last inner point to the outer region, following the pipe axis, one then finds that the two quantities exhibit a remarkable drop but with a different slope, so that at about $85\,\mathrm{cm}$ from the upper edge they intersect.

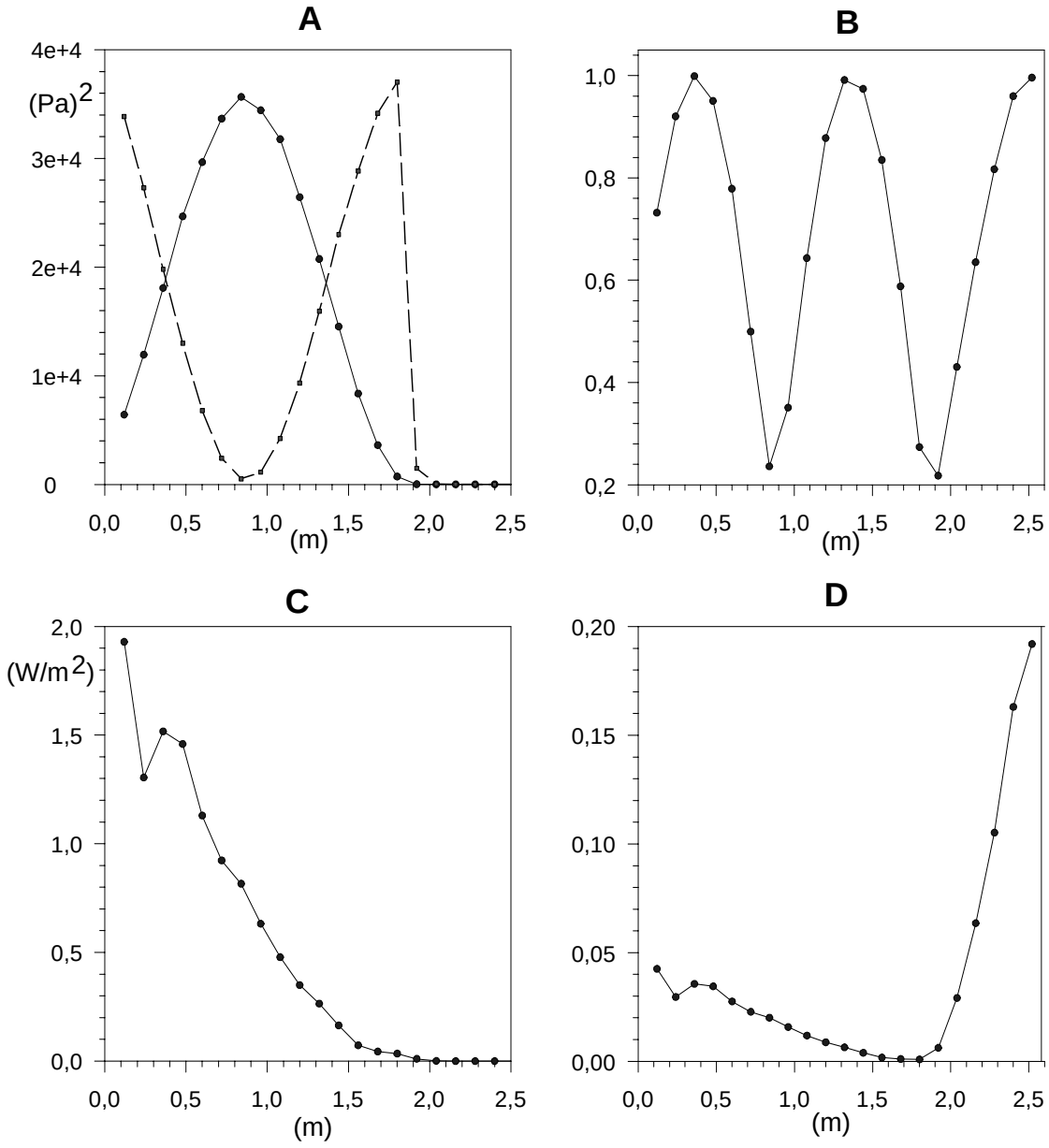

FIGURE 17. A: Sound pressure (solid line) and normalized velocity (dashed line) vs. position. **B**: σ indicator. **C**: mean intensity. **D**: η indicator.

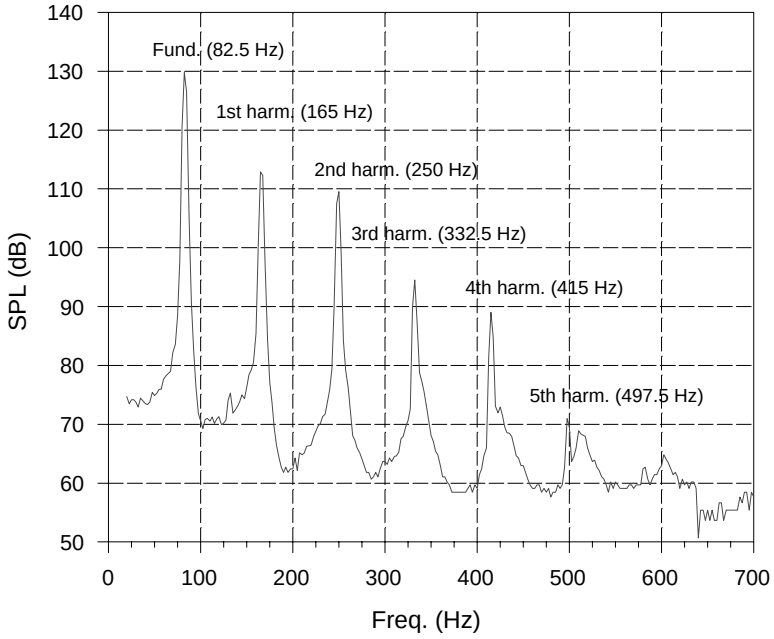

FIGURE 18. Sound pressure level spectrum of the pipe's internal field (12 cm from the duct base).

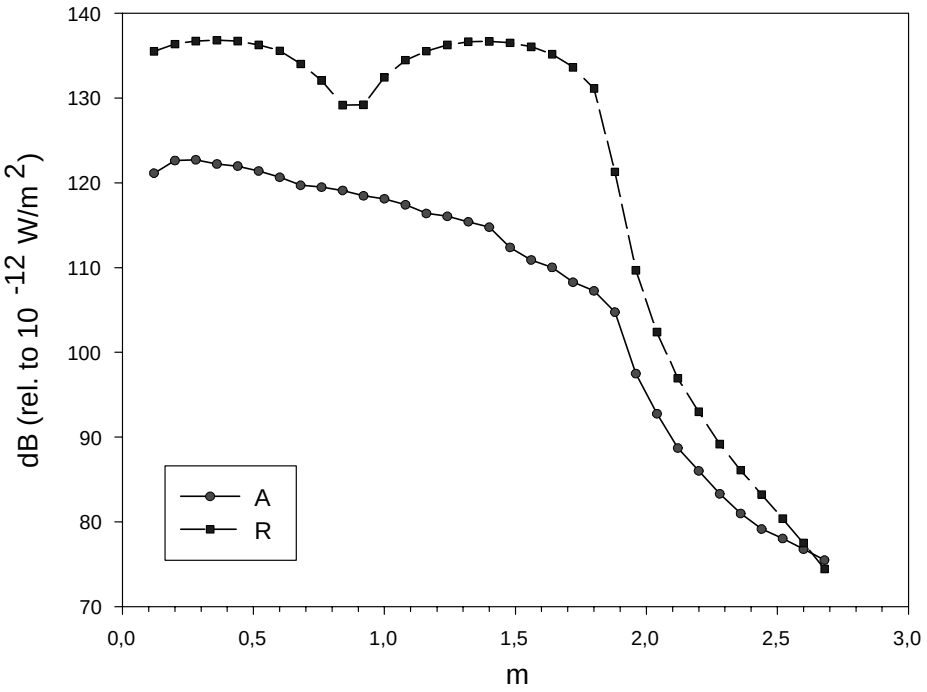

FIGURE 19. Overall values of radiating (A) and oscillating (R) intensities along the pipe axis (the last 11 measurements are taken outside).

4.2 Measurements in a duct

A complete sound field characterization in a closed environment was accomplished measuring pressure and velocity impulse responses in a plexiglass duct, of dimensions $4\,\mathrm{m} \times 0.28\,\mathrm{m} \times 0.28\,\mathrm{m}$ (see Fig. 20). The quantities, obtained by means of the MLS technique, were used to perform an analysis comprising both a study of the transient state (reverberation) and the calculations of the energetic parameters during the stationary excitation.

This particular acoustic environment, where the sound source was a loudspeaker placed at one of the two openings of the duct (see Fig. 21), was chosen for exploiting the possibility of working in two different field conditions, that is one and three-dimensional (from now on 1D and 3D), according to the sound propagation properties of waveguides excited with different frequencies (see Sect. 2.2.1). The two conditions were achieved by filtering the measured signals under and above the minimum cutoff frequency ($f_c \simeq 615\,\mathrm{Hz}$). Therefore, in order to consider just low frequencies in one dimension or high frequencies in three dimensions we had to perform two separate groups of measurements: in the first one we made use of an axial probe (*B&K 4181* - microphone diameter: $1.27\,\mathrm{cm}$) with a long spacer ($5\,\mathrm{cm}$) and of a vectorial probe (*B&K 4135* - mic. diam.: $0.64\,\mathrm{cm}$) with a short spacer ($1.2\,\mathrm{cm}$) in the second one.

Another physical characteristic we wanted to vary was the absorption property of the duct end (the one opposite the source): this was first left open, then closed by two different materials: a foam rubber layer ($\sim 5\,\mathrm{cm}$ thick) and an aluminum panel ($1\,\mathrm{cm}$ thick). In this way, we created three acoustic fields with quite different radiation properties, which allowed us to perform a comparative analysis upon the physical quantities obtained.

In Fig. 22 we report the outline of the experimental apparatus. The purpose of the *B&K 2133* analyzer is that of monitoring the acoustical quantities during the stationary excitation. This was done mainly for performing a particular test about the system ergodicity, which will be described in more detail below. Note also that for simplicity just two channels are shown in the picture; anyway, we remind the reader that in the 3D field measurements we used a vectorial probe, consisting of three pairs of channels, all of them sent to the same preamplifier-power supply system (*B&K 2811*). The probe reference frame is depicted in Fig. 23: the x coordinate is aligned along the duct axis and oriented from the speaker ($x = 0$) to the opposite end.

4.2.1 Part I: qualitative analysis of transient states

In the following table we summarize the experimental parameters adopted for measuring impulse responses in the two frequency ranges: these were $90 \div 560\,\mathrm{Hz}$ and $710 \div 4470\,\mathrm{Hz}$, each of them covering an integer number of third-octave bands (8 in both cases). Note also that the stimulus frequencies f_s was set in such a way to satisfy the Nyquist criterion $f_s \geq 2f_{\max}$ ($f_{\max} = 560\,\mathrm{Hz}$ and $4470\,\mathrm{Hz}$, respectively).

Field	Filter Bandwith	MLS freq.	Probe type	Probe spacer
1D	$90 \div 560\,\mathrm{Hz}$	$8000\,\mathrm{Hz}$	*B&K 4181* (axial)	$5\,\mathrm{cm}$
3D	$710 \div 4470\,\mathrm{Hz}$	$12000\,\mathrm{Hz}$	*B&K 4135* (vectorial)	$1.2\,\mathrm{cm}$

We start our study with a set of qualitative considerations about the field behavior during the decay. First of all we present some examples of impulse responses in both field conditions: in Fig. 24 the overall pressure and velocity of the 1D case with the aluminum panel and in Fig. 25 the quantities g_p, g_{v_x} and g_{v_y} relating to the 3D field in the same condition (the g_{v_z} term is not shown because, as expected from symmetry properties, it is similar to g_{v_y}). These plots are reported

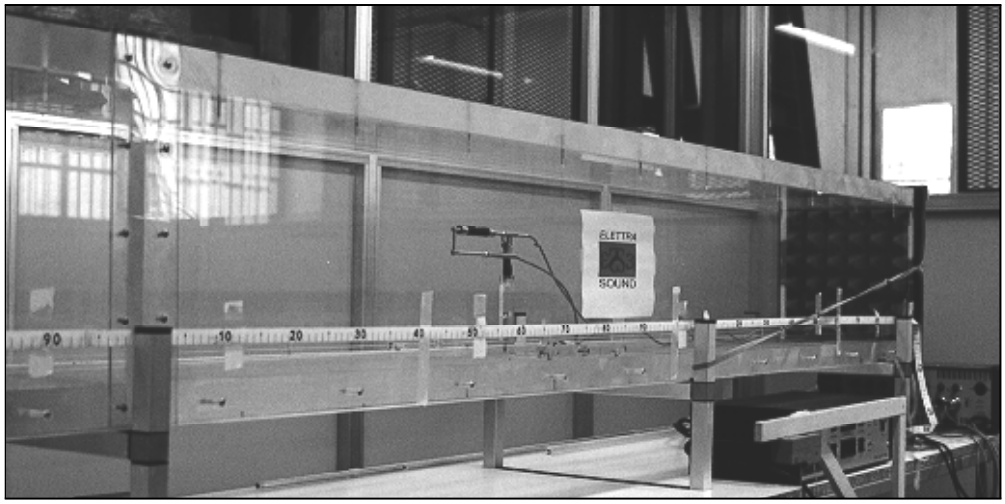

FIGURE 20. The plexiglass duct with the 1D probe inside. On the right it is visible the foam rubber layer termination.

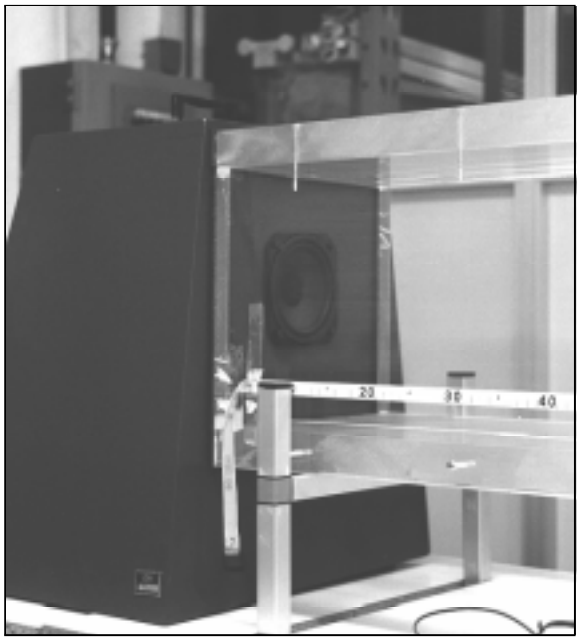

FIGURE 21. The box speaker facing one of the duct's openings.

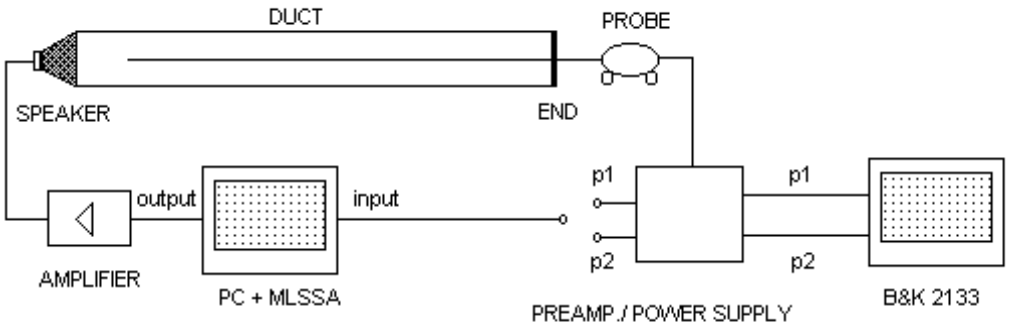

FIGURE 22. Schematic view of the experimental setup used for the measurements in the duct.

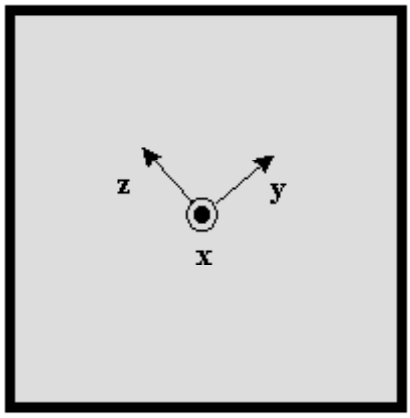

FIGURE 23. The reference frame seen from the opening opposite to the speaker.

just for a few introductory remarks. The first regards the way how the different field behavior affects the appearance of the impulse responses: in the 1D case a clear reflection pattern is clearly visible while the same is not true in 3D, apart from a slight structure appearing just in the plot of g_{v_x}. This happens because the total mode number is much higher, due to the wider frequency range and to the higher modal density (the sound propagation in 3D involves transversal modes). A proof of this feature is given by at the two spectra reported in Fig. 26, which were obtained by calculating the discrete Fourier transform of the pressure impulse responses. In particular, from the upper plot, showing the frequency interval between 100 and $500\,\mathrm{Hz}$, it may be seen the resonant pattern of a confined 1D field: the separation between adjacent peaks is $\Delta f \simeq 40\,\mathrm{Hz} \simeq c/2L$, L being the duct length ($4\,\mathrm{m}$).

p & v impulse responses and energy decays

The first thing we wanted to deal with was the study of the kinetic energy's behavior with respect to the potential energy. In fact, as we pointed out previously, it is customary to neglect the kinetic term when studying the sound decay: this happens both for practical reasons (the potential term is derived directly from a single sound pressure signal) and also because it is generally believed that the two curves coincide.

In practice, we here represent the decay curves on logarithmic scales, i.e. plotting the level with respect to the initial value:

$$L_W(t) = 10 \log \frac{\overline{W(t)}}{W_0}$$

In Fig. 27 is reported an interesting case (relative to 1D field in the aluminum panel), for it shows that strictly speaking the assumption of the equivalence of the two decays cannot be considered valid in general: in fact, it is evident that the slopes of $\overline{W_K}$ and $\overline{W_U}$ are clearly distinct. In order to give a quantitative evaluation of this fact, we note that at least in the first time interval (some tenths of second), the logarithmic decay can be considered linear, so that the typical exponential law $\overline{W(t)} = W_0 \mathrm{e}^{-t/\tau}$ may be applied (see Sect. 2.6.3). We can determine the two decay constants τ directly from the slopes: in particular, we consider the first $0.4\,\mathrm{s}$, where the levels of $\overline{W_U}$ and $\overline{W_K}$ are about $-20\,\mathrm{dB}$ and $-23\,\mathrm{dB}$ respectively, corresponding to $\tau_K \simeq 0.085\,\mathrm{s}$ and $\tau_U \simeq 0.075\,\mathrm{s}$. The difference between the first two is thus not negligible, being of the order of $10\,\%$ and this is approximately maintained until the noise threshold appears in the kinetic energy curve ($\sim -40\,\mathrm{dB}$). Fig. 28 shows the 3D field case: it is interesting to note that also the three kinetic terms (x, y, z) behave in a quite different manner. On the bottom part of the Figure the total energy decay is reported: note that its slope is intermediate between that of the potential energy and that of total kinetic energy. A different phenomenon is shown in Fig. 29 (1D field in the open duct): fitting the first $0.3\,\mathrm{s}$ we obtain $\tau_K \simeq 0.052\,\mathrm{s}$ and $\tau_U \simeq 0.062\,\mathrm{s}$ ($\Delta\tau/\tau_U \simeq 15\,\%$) but the curves meet again at about $0.6\,\mathrm{s}$, i.e. they come to a condition where $\overline{W_K}$ and $\overline{W_U}$ have the same ratio as the initial one. Moreover, though not shown here, they go on like that until the noise threshold is reached. Hence, in this case we may assume the equivalence between the decays of the kinetic and the potential terms, but just on a large time scale, because at the beginning the two decays occur in a different way. As regards the 3D behavior (Fig. 30), the total kinetic energy follows almost perfectly the potential one, apart from some tiny deviations.

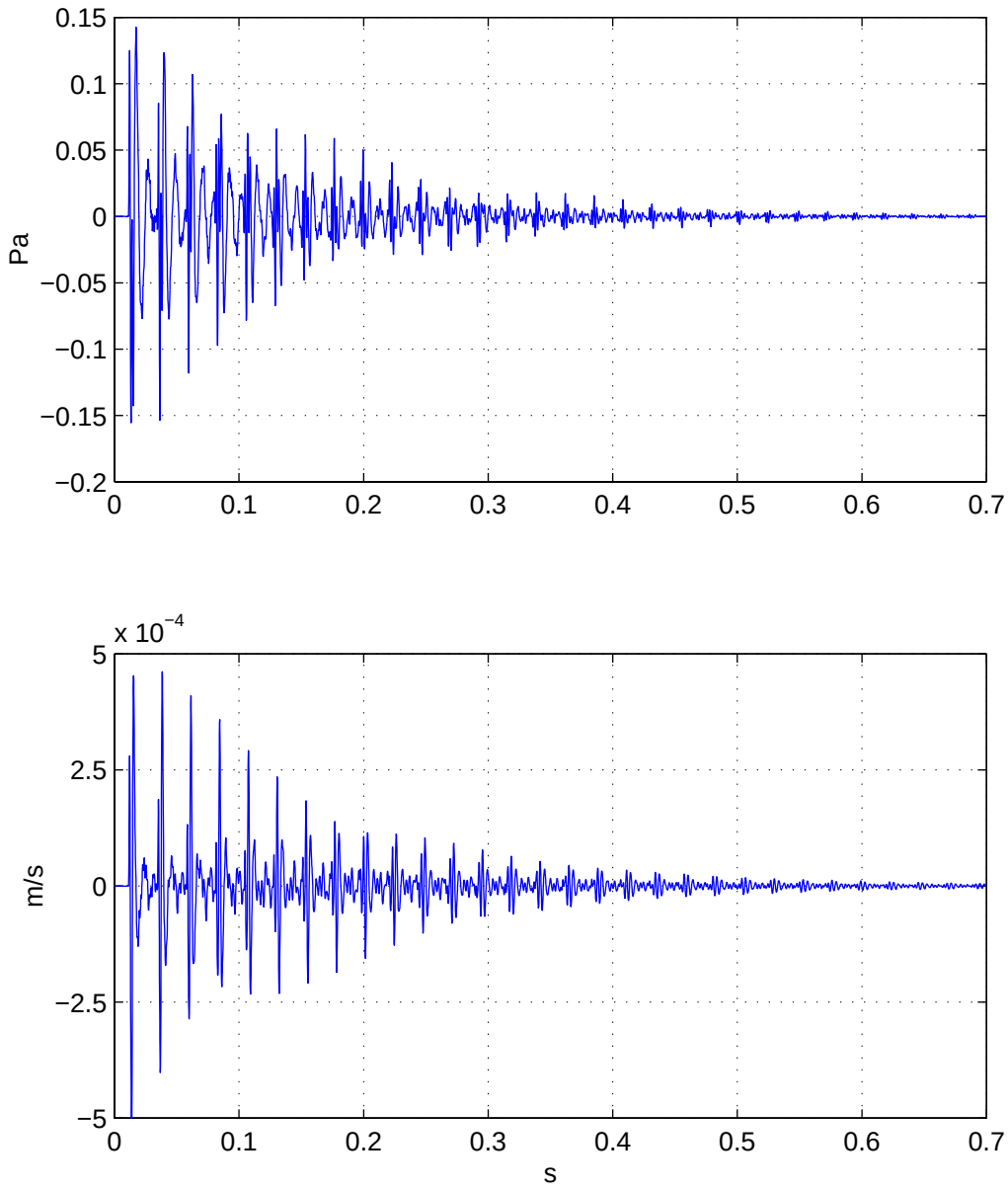

FIGURE 24. 1D field impulse responses in the duct closed by the aluminum panel. **Top**: pressure; **Bottom**: velocity.

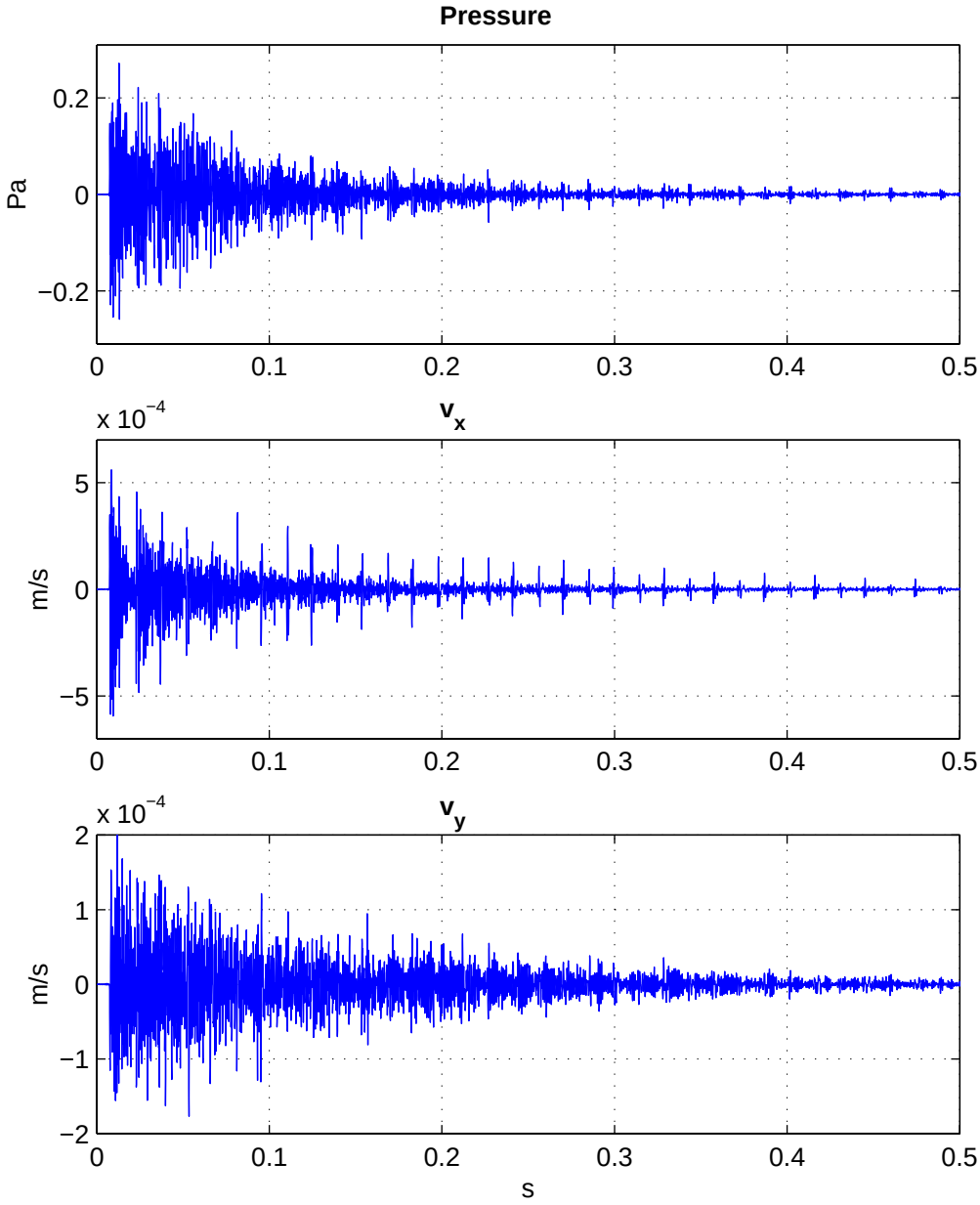

FIGURE 25. 3D field impulse responses in the duct closed by the aluminum panel. **Top**: p; **Middle**: v_x; **Bottom**: v_y.

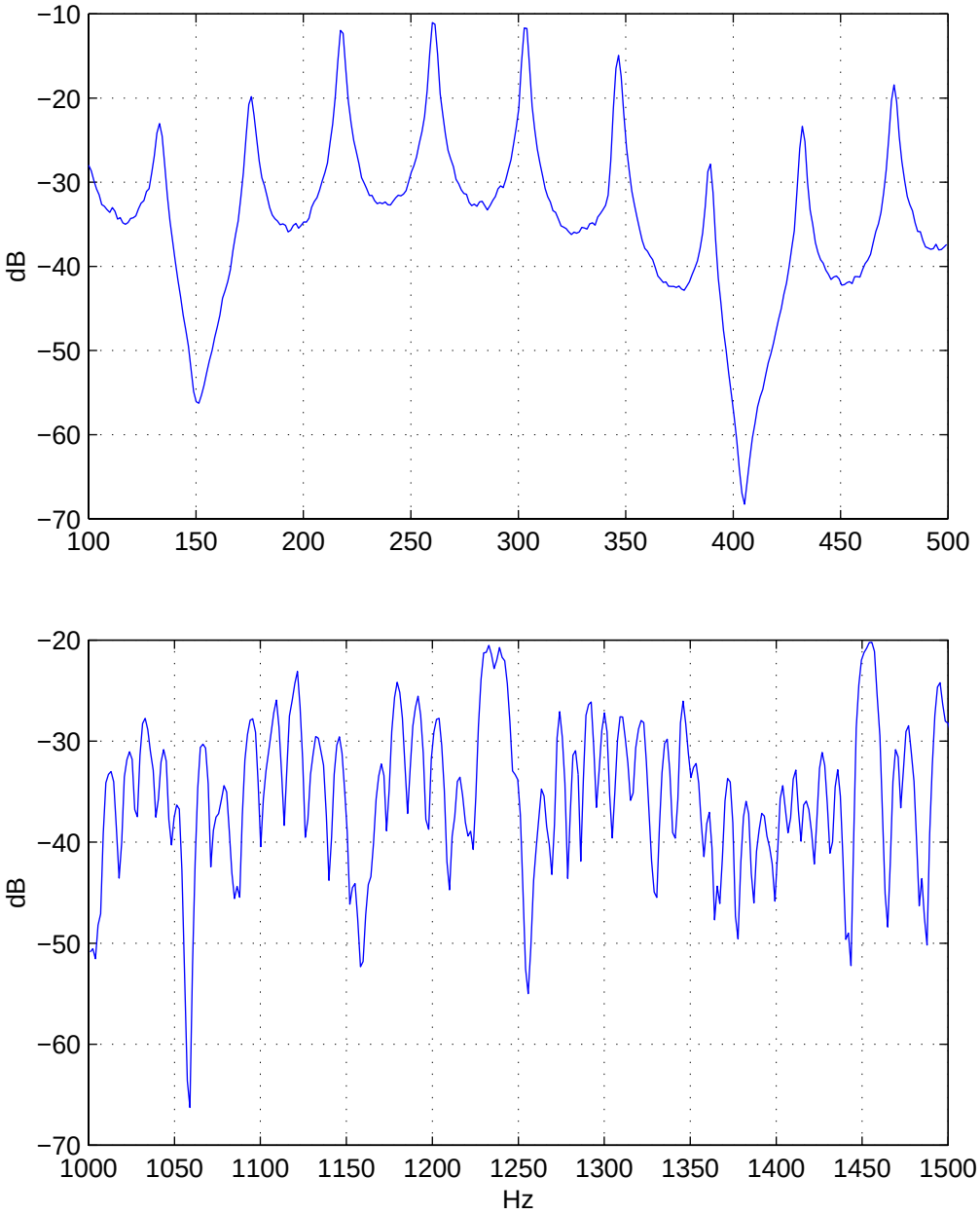

FIGURE 26. Examples of pressure power spectra in the aluminum termination case. **Top**: 1D field; **Bottom**: 3D field.

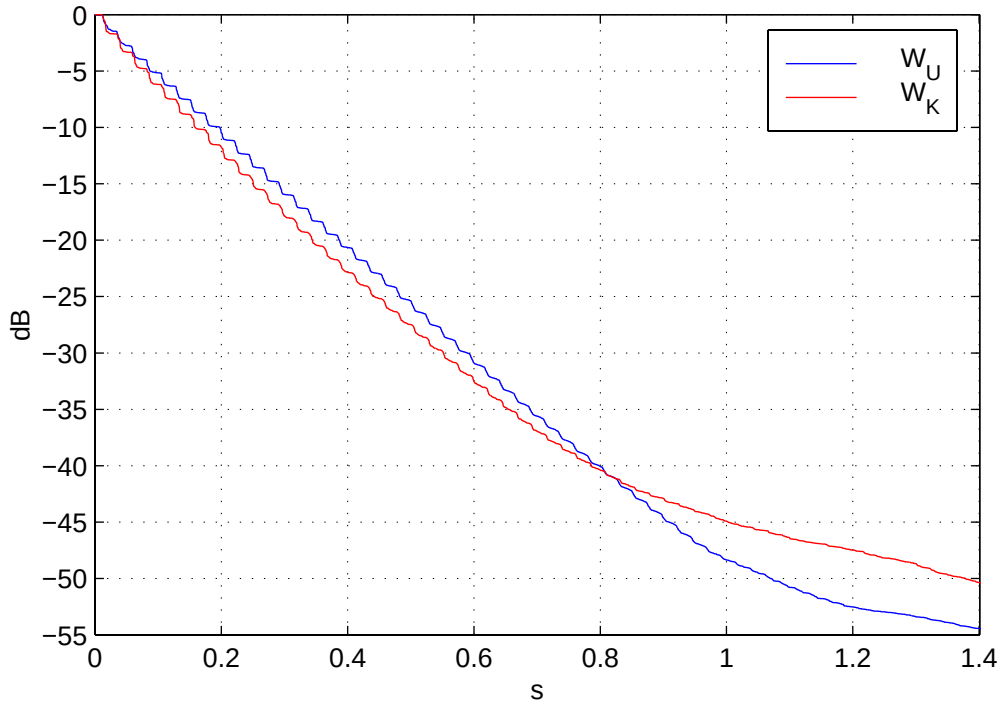

FIGURE 27. Potential and kinetic energy decays in the 1D field (aluminum panel).

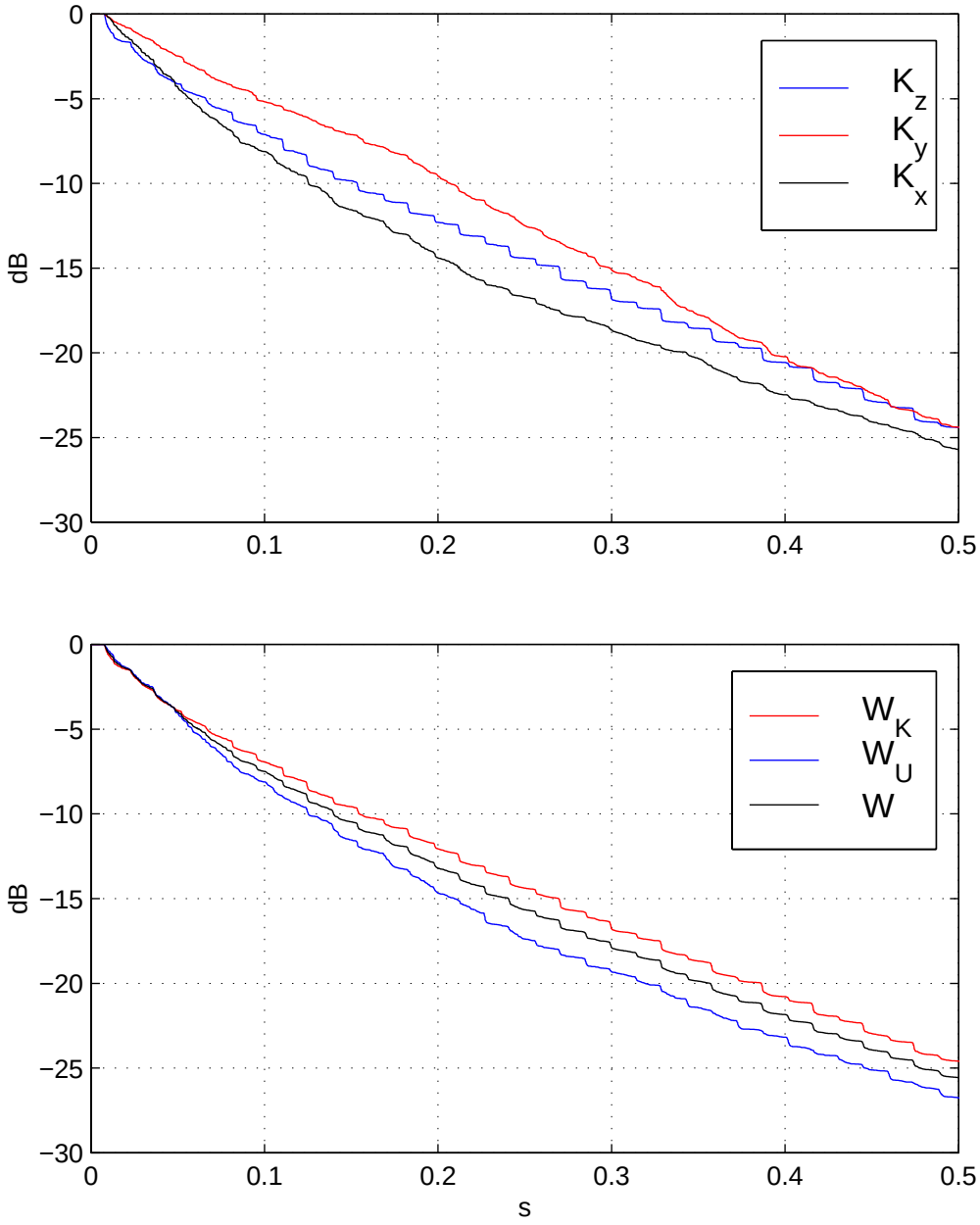

FIGURE 28. 3D field energy decays (aluminum panel). **Top**: x, y, z components of W_K; **Bottom**: W_K total, W_U and W.

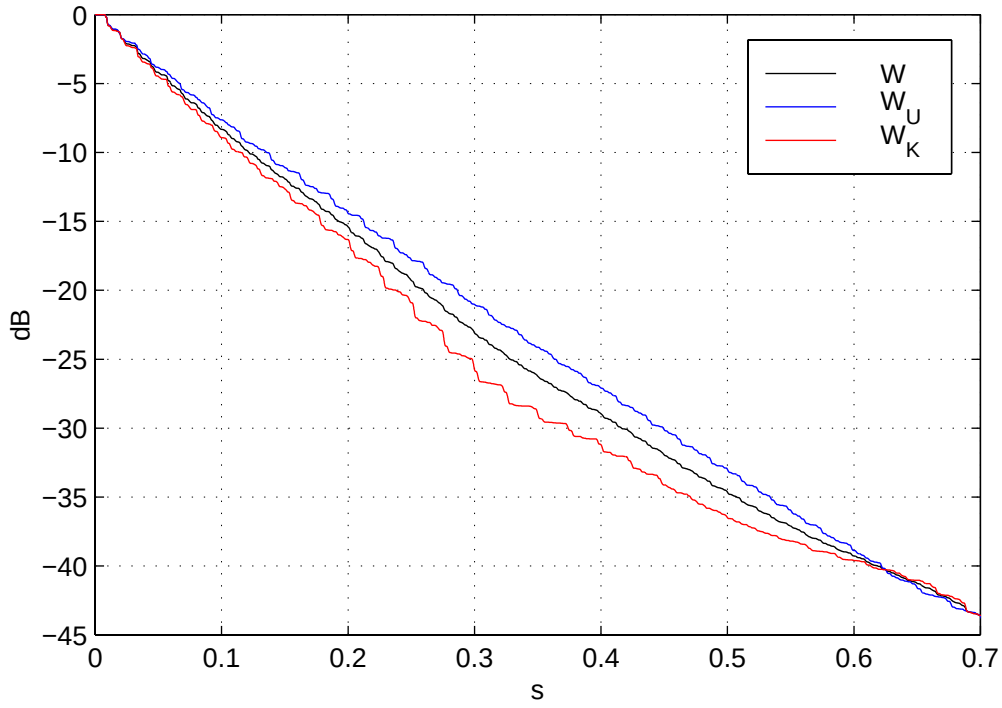

FIGURE 29. Energy decays in the 1D field (open duct).

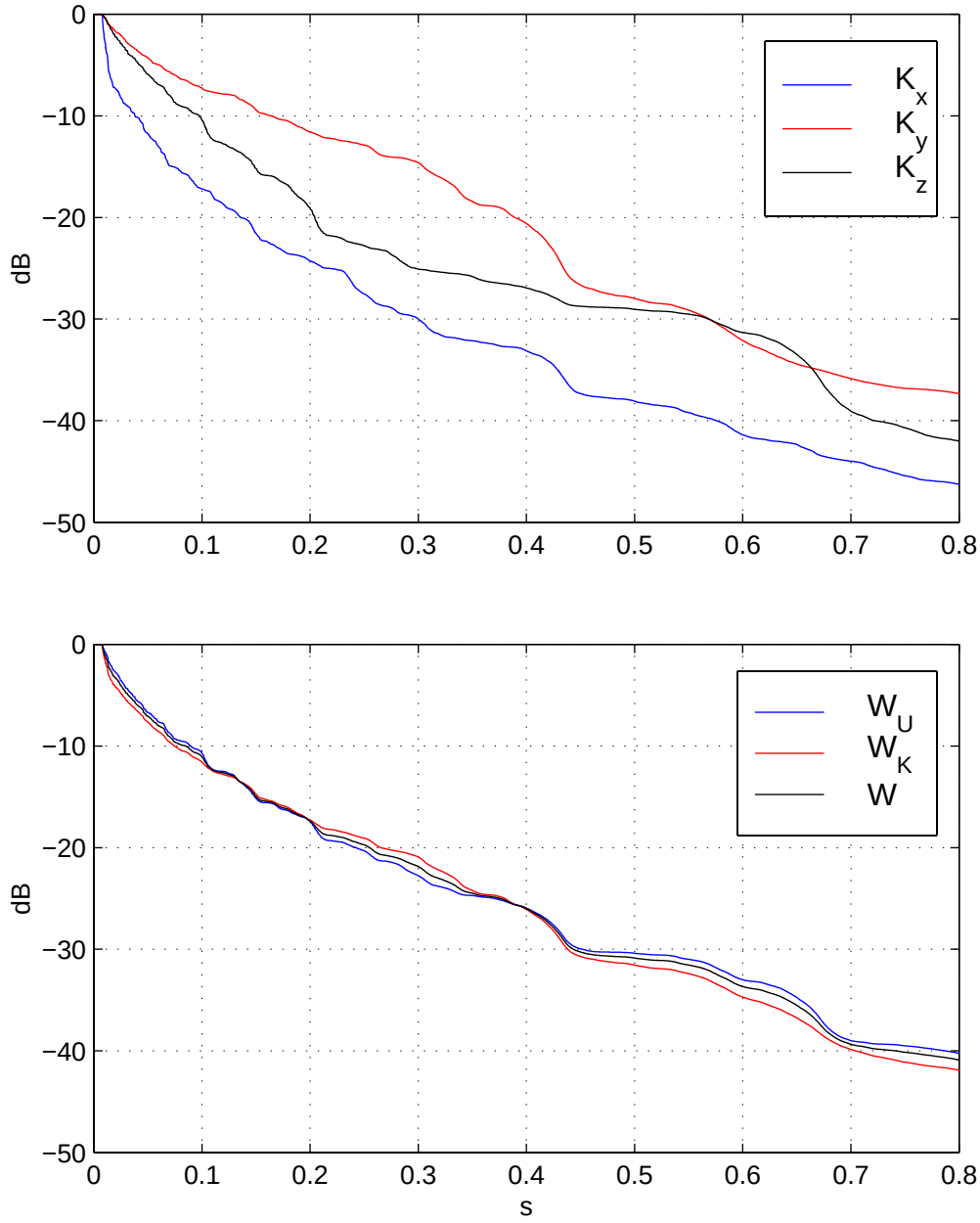

FIGURE 30. 3D field energy decays (open duct). **Top**: x, y, z components of W_K; **Bottom**: W_K total, W_U and W.

Intensity impulse responses and decays

We now want to analyze the transient behavior from the intensity viewpoint. First of all, we have to calculate the "intensity impulse response" $\mathbf{g_j} = g_p \mathbf{g_v}$, which may be interpreted as the intensity behavior observed due to an impulsive pressure. Its importance is due to Eq. (132) , stating the validity of the back integration method for finding the ensemble average of a broad band intensity signal during the decay.

It is interesting to take into account some examples of intensity impulses. From Fig. 31 in particular (1D field with probe at $x_0 = 2.3$ m from the loudspeaker), one realizes that the reflective patterns already noticed for g_p, appear in a much more evident way, meaning that the wavefronts behavior, which follow an impulsive excitation, is best represented by the flux time-history contained in $\mathbf{g_j}$. In fact, the energy oscillation mechanism is here highlighted due to the presence of a clear sequence of progressive and regressive energy streams. Fig. 32 (first $70\,\mathrm{ms}$) better shows this phenomenon: measuring the time intervals between two consecutive positive peaks and between a positive and a subsequent negative peak, one finds $\Delta t_1 \simeq 0.023\,\mathrm{s}$ and $\Delta t_2 \simeq 0.01\,\mathrm{s}$, respectively. The interpretation of these peaks as energy fronts traveling from side to side is supported by the values $c\Delta t_1 \simeq 8\,\mathrm{m} = 2L$ (twice the duct length) and $c\Delta t_2 \simeq 3.4\,\mathrm{m} = 2(L - x_0)$. From this point of view 3D fields behave in a quite different way. Look for instance at Fig. 33, which reports the components g_{j_x} related to the three boundary conditions: owing to the large amount of modes present in the duct, the energy flux now appears completely smeared. Anyway, it is worth noting the difference between the aspect of the first two plots and the last one (duct with aluminum termination), for this shows a greater negative regressive component due to the higher reflection property of the boundary. A more evident oscillating behavior is then encountered when comparing the x component with the two transversal directions (Fig. 34). The typical decaying statistical average $\overline{j(t)}$ in the 1D field is shown in Fig. 35. Its most outstanding characteristic is the non-monotonic nature, which is a direct consequence of the positive and negative peaks of $g_j(t)$. Actually, the behavior of j is oscillating: this appears to be marked passing from the foam to the aluminum termination, the latter being characterized also by a slower decrease. In particular, the corresponding energy decays, which are here reported for comparison, almost perfectly follow the large time scale behavior of the intensities. The 3D case is summarized in Figs. 36 and 37: the first one reports the magnitude of intensity ($\overline{|\mathbf{A}|}$) next to the corresponding total energy, while in the second one the first ms of the three single components in linear scale (aluminum termination) are shown.

4.2.2 Part II: stationary fields' parameters

The first aim of this section is to discuss, as quantitatively as possible, the phenomenological relationship between the energy decay time and the field parameters observed when exciting the environment in a steady manner.

Ergodicity

The first subject we want to treat is the check of the relation expressed by Eq. (135) , whose physical meaning is that the statistical average of an energetic quantity at the beginning of the decay, calculated from the impulse response integration, coincides with the time average of the same quantity when the excitation signal is stationary. For achieving this, we performed a set of measurements maintaining the MLS stimulus steady and using a *B&K 2133* analyzer to obtain the corresponding $\langle p^2 \rangle$, $\langle \mathbf{v}^2 \rangle$ and $\langle \mathbf{j} \rangle$. Since we decided to perform this test after having acquired

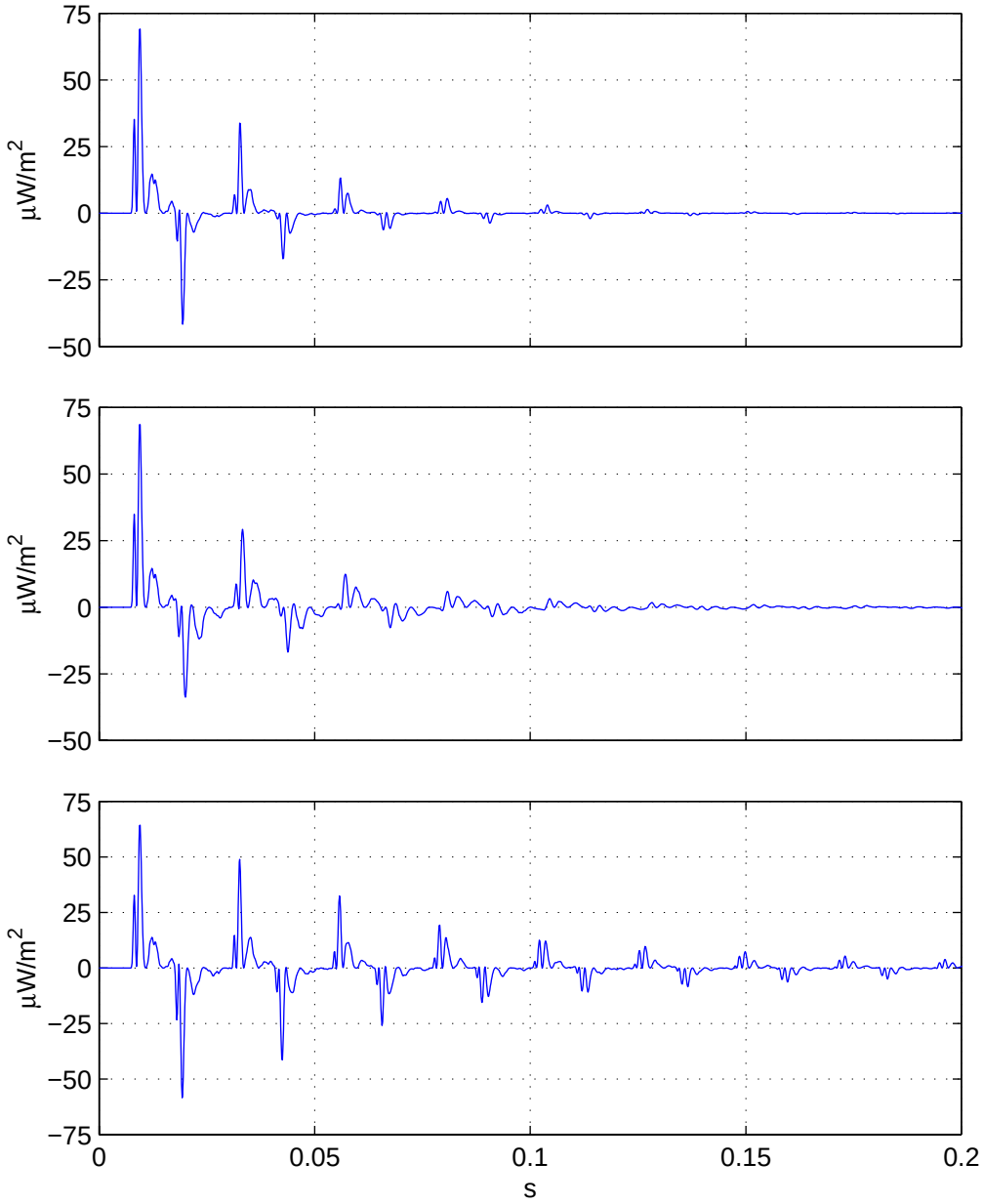

FIGURE 31. 1D intensity impulse responses in the three boundary conditions. **Top**: foam rubber; **Middle**: open duct; **Bottom**: aluminum.

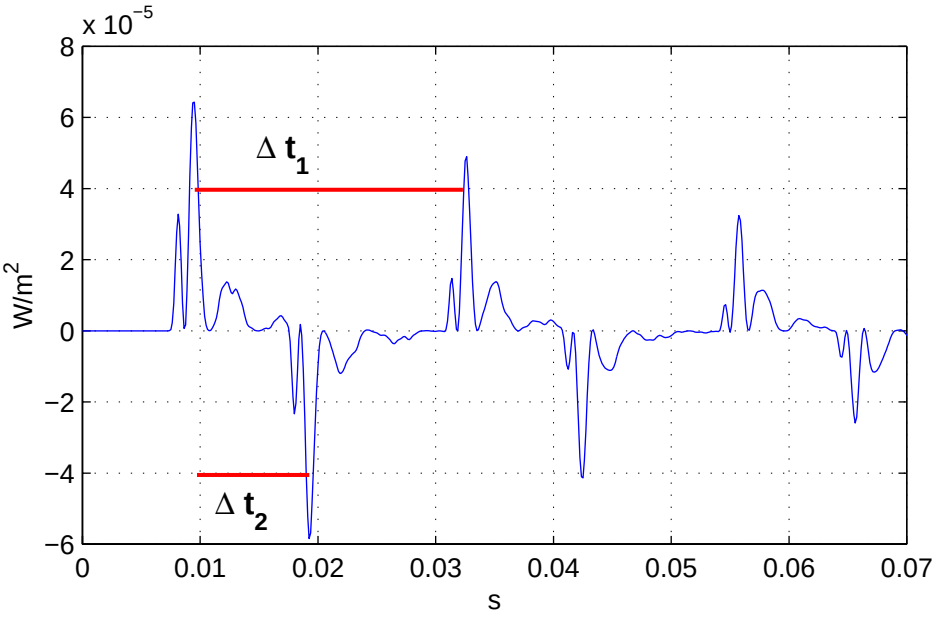

FIGURE 32. Time intervals between wavefronts in a 1D intensity impulse response.

the impulse responses and thus we couldn't recover the same excitation amplitude used at the beginning, we had to devise a trick in order to refer the signals obtained in the two cases to a common value. In practice, we decided to normalize the pressure and velocity impulse responses to the average values of the steady field, i.e. we imposed the ergodicity relation at $t = 0$ to g_p and $\mathbf{g_v}$, and then we checked wether the behavior of the intensity was the expected one. In short, the adopted procedure is was the following one (for simplicity we report the one relative to the 1D field, the 3D extension being obvious):

(1) calculation of:

$$\widetilde{g_p}(t) = \sqrt{\frac{\langle p_s^2 \rangle}{\int_0^\infty g_p^2(\tau)\, d\tau}}\, g_p(t) \qquad \widetilde{g_v}(t) = \sqrt{\frac{\langle v_s^2 \rangle}{\int_0^\infty g_v^2(\tau)\, d\tau}}\, g_v(t)$$

$g_p(t)$ and $g_v(t)$ being the previous impulse responses, $\langle p_s^2 \rangle$ and $\langle v_s^2 \rangle$ the stationary measurements;

(2) calculation of the impulsive intensity time integral:

$$\overline{j(0)} = \int_0^\infty \mathrm{d}\tau\, \widetilde{g_p}(\tau)\widetilde{g_v}(\tau)$$

(3) comparison of $\overline{j(0)}$ with $\langle j_s \rangle = \langle p_s v_s \rangle$.

Fig. 38 reports the superimposed plots of $\overline{j(0)}$ and $\langle j_s \rangle$ of five different points taken along the1D field, as usual in correspondence of the three boundary conditions. The top and middle ones, referred to the foam termination and the open duct respectively, show a good agreement of the two quantities; in fact, the discrepancy is never greater than $0.2\,\mathrm{dB}$ ($\Delta j / j_s \sim 1 \div 3\,\%$), which can be considered as the order of magnitude of the statistical and systematic errors affecting such a kind of measurements. The situation is quite different for the aluminum case (bottom plot):

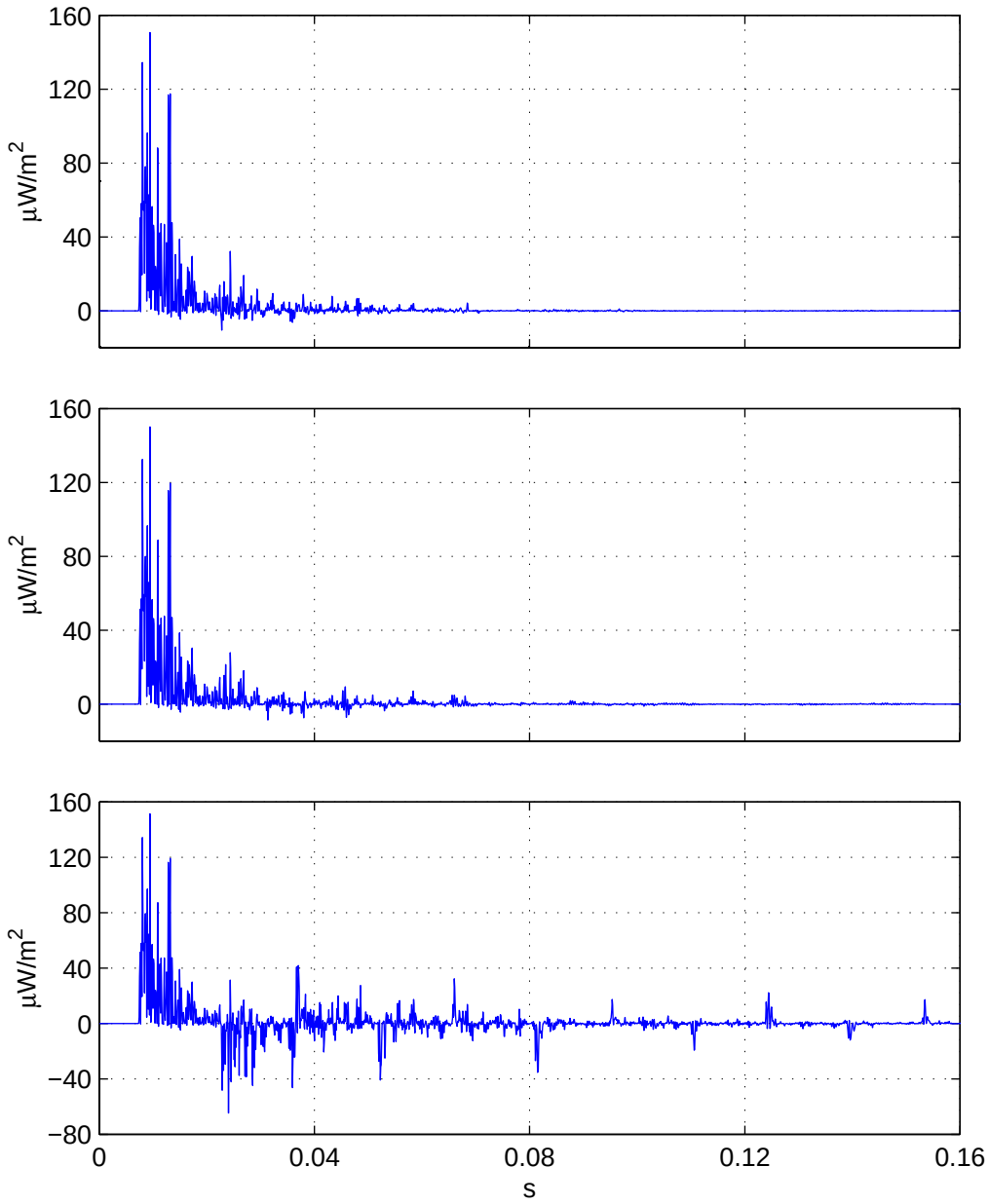

FIGURE 33. x component (duct axis) of 3D intensity impulse responses in the three boundary conditions. **Top**: foam rubber; **Middle**: open duct; **Bottom**: aluminum.

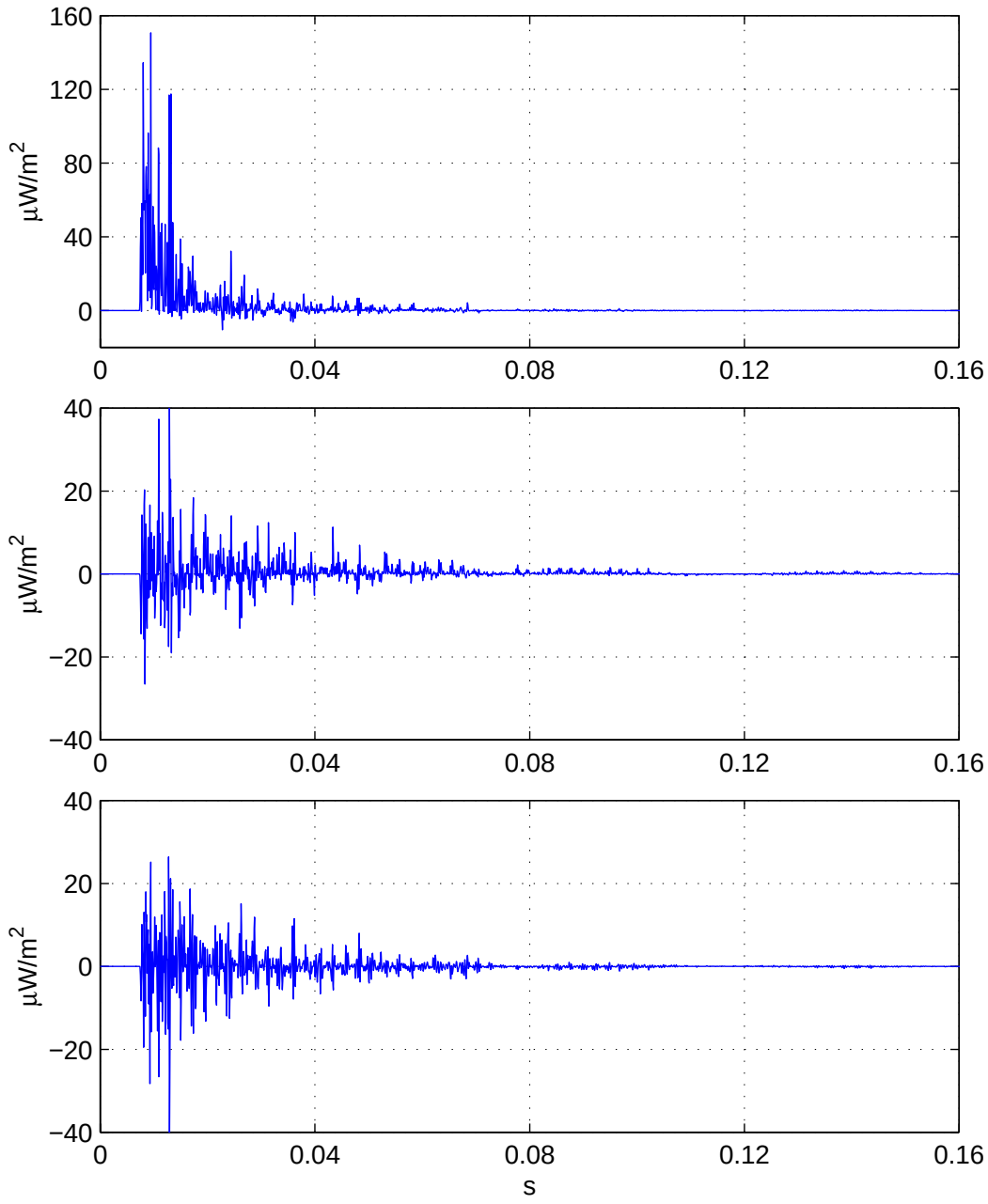

FIGURE 34. 3D intensity impulse responses with the foam rubber termination. **Top**: x component; **Middle**: y component; **Bottom**: z component.

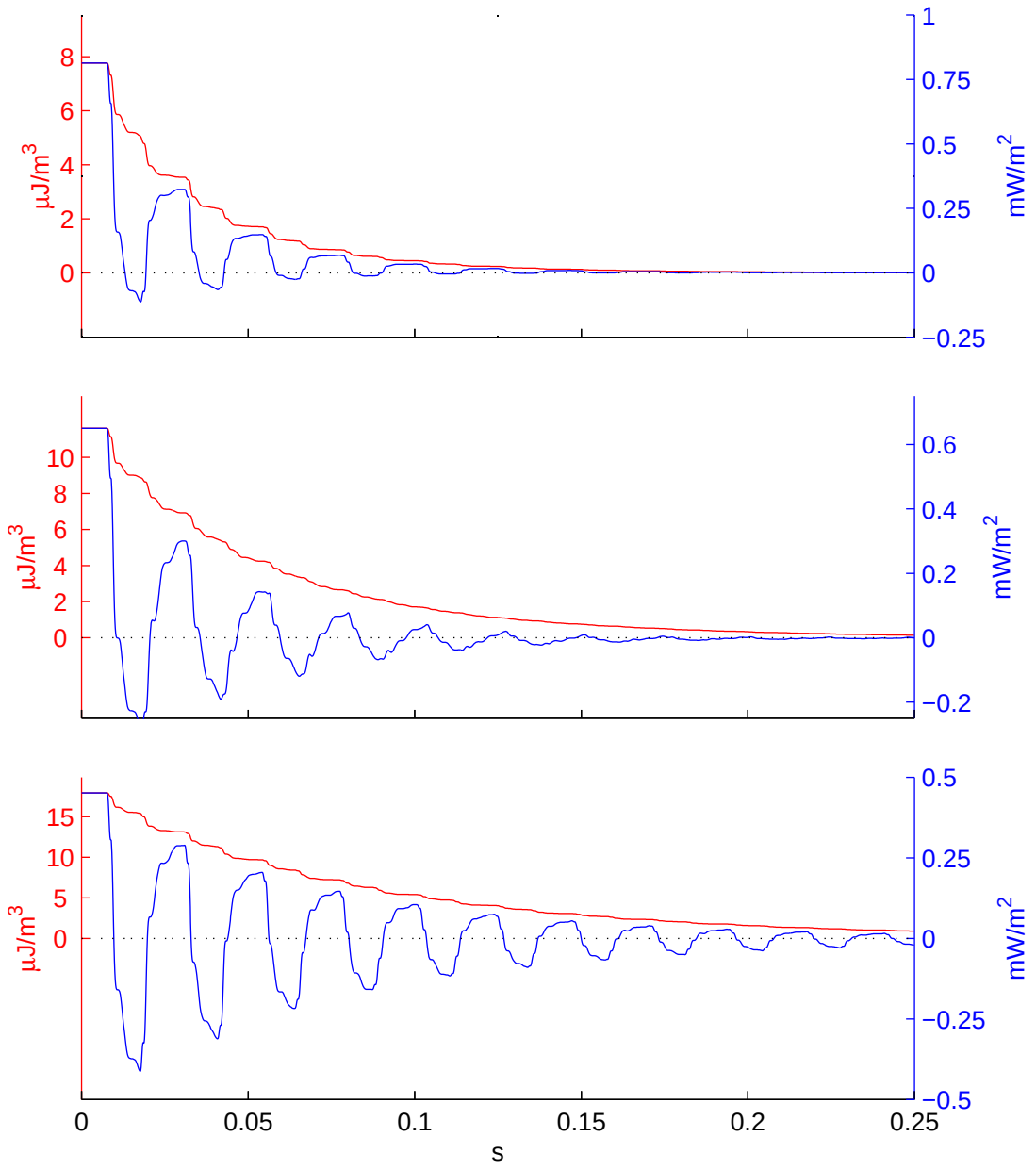

FIGURE 35. 1D field decays (lin. scale). Comparison between energy (red lines-left y axis) and intensity (blue lines-right y axis). **Top**: foam rubber; **Middle**: open duct; **Bottom**: aluminum panel.

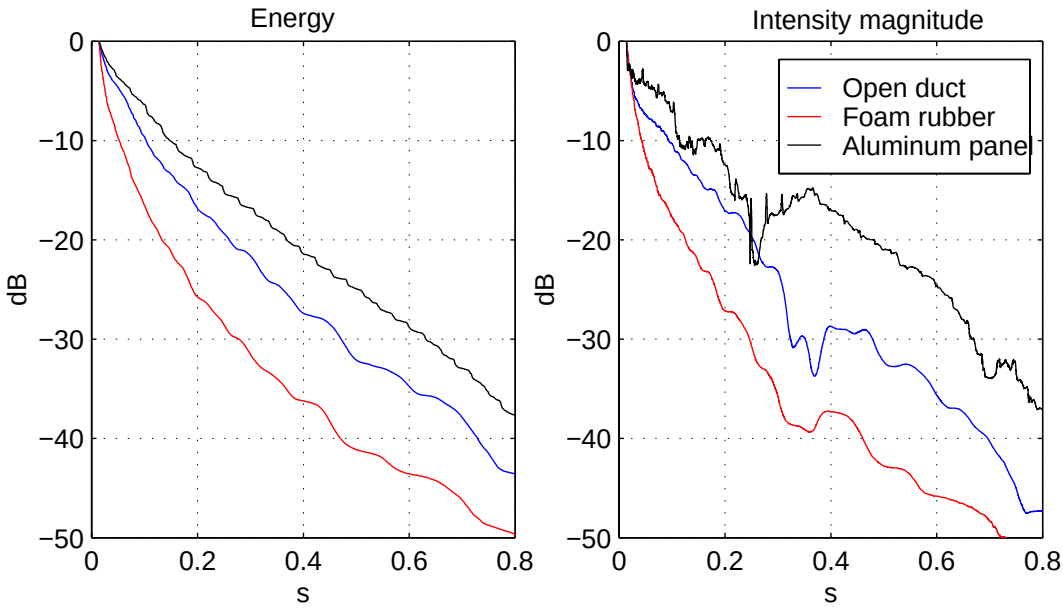

FIGURE 36. 3D field decays (log. scale). **Left**: energy; **Right**: intensity magnitude.

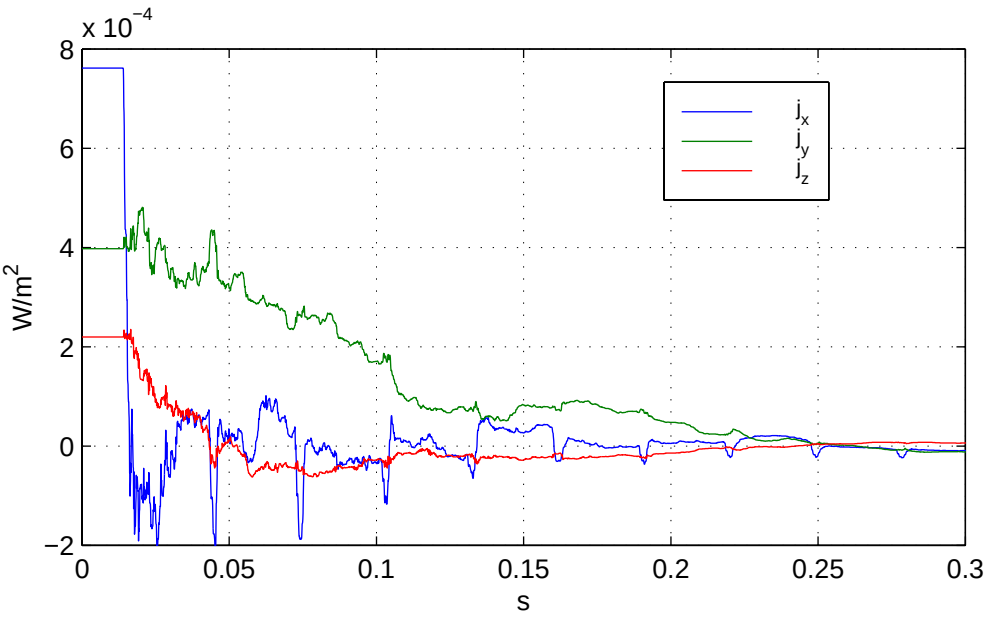

FIGURE 37. 3D field intensity decays (x, y, z components) with the aluminum panel. Lin. scale.

here the discrepancy between $\overline{j(0)}$ and $\langle j_s \rangle$ reaches $1.5\,\mathrm{dB}$ ($\Delta j / j_s \sim 20 \div 30\,\%$). Nevertheless, this does not suffice to establish that there exists a deviation from the ergodic behavior: one thing we can state is that, being the field more reverberating than in the first two cases, it is likely that the phase mismatch error is much more important, and that this may be of different entity in the two readout chains (this could have been somewhat expected, since the MLSSA system receives the signals from a single input, while the intensity analyzer elaborates two channels simultaneously).

In the 3D case the same behavior is found comparing the x component with the transversal ones; in fact, the latter here feel the effects of the strong confinement caused by the plexiglass walls. An example (open duct) is reported in Fig. 39: data along x differ by less than 0.2 dB, in contrast with the $1.5\,\mathrm{dB}$ observed in the y direction. In spite of this discrepancy, it is worth noting the astonishing similarity between the behaviors of $\overline{j(0)}$ and $\langle j_s \rangle$, which is probably the most convincing proof of the presence of a systematic error.

Effect of local energy transfer on reverberation

We now want to study the relationship between the decay rate and the energetic parameters in the stationary sound. In particular, we may follow the reasoning presented in Sect. 2.7, where we qualitatively explained how the η indicator may account for the energy absorption during the decay; this choice is supported also by the results of the measurements upon the organ pipe field, by which we were able to find an experimental evidence of the fact that η represents the local amount of energy transferred on average in the field. Since η is defined as the normalized ratio of the mean intensity and the mean energy, on the basis of the previous discussion about ergodicity, we may determine this quantity simply by the impulse response integration. The method may suffer from some inevitable limitations ascribed to systematic effects; nonetheless, it may be very useful for showing how one can obtain important information about transient and stationary fields, analyzing just a set of pressure impulse response measurements,.

As regards the characterization of the decay, first of all we assume for simplicity that, according to the diffuse field hypothesis, the curves behave in an exponential way. Even if in our case the property is not always well satisfied, this gives us the opportunity of expressing in an approximate way the decay rapidity, for instance by means of a simple parameter like the reverberation time (see Sect. 2.6.3). Actually, in our application we prefer to calculate the initial slope given by the first $10\,\mathrm{dB}$, in order to reduce the error done interpolating the level curve with a straight line: in practice, we will calculate T_{10} instead of T_{60},.

We report in Fig. 40 some different examples of early decays in the 1D case; note that, in order to extend the data sample, one more boundary conditions was added (double layer of foam rubber). Furthermore, from the same figure one clearly realizes the importance of a careful choice of the time interval to be fitted; in particular, it is evident that the real starting point of the decay does not coincide with $t = 0$ (the instant at which the excitation stops) but it comes after a little delay dependent on the probe-speaker distance. We performed this measurement on five points along the duct, $0.7\,\mathrm{m}$ apart (from $x = 3.7\,\mathrm{m}$ to $x = 0.9\,\mathrm{m}$), and for each of them we calculated both T_{10} and the η indicator. The average values of these parameters in the four field conditions are reported in Fig. 41. We estimate an experimental uncertainty of the order of $5 \div 7\,\%$ in both T_{10} and η: in the first case due to the variation with respect to the measurement point and to the fitting accuracy, and in the second case due to the systematic phase error. In spite of that, a clear inverse relation between the two quantities is evident: the decay time increases with decreasing η. Actually, this could have been expected even from the previous considerations about the physical meaning of η; nonetheless, this result is important

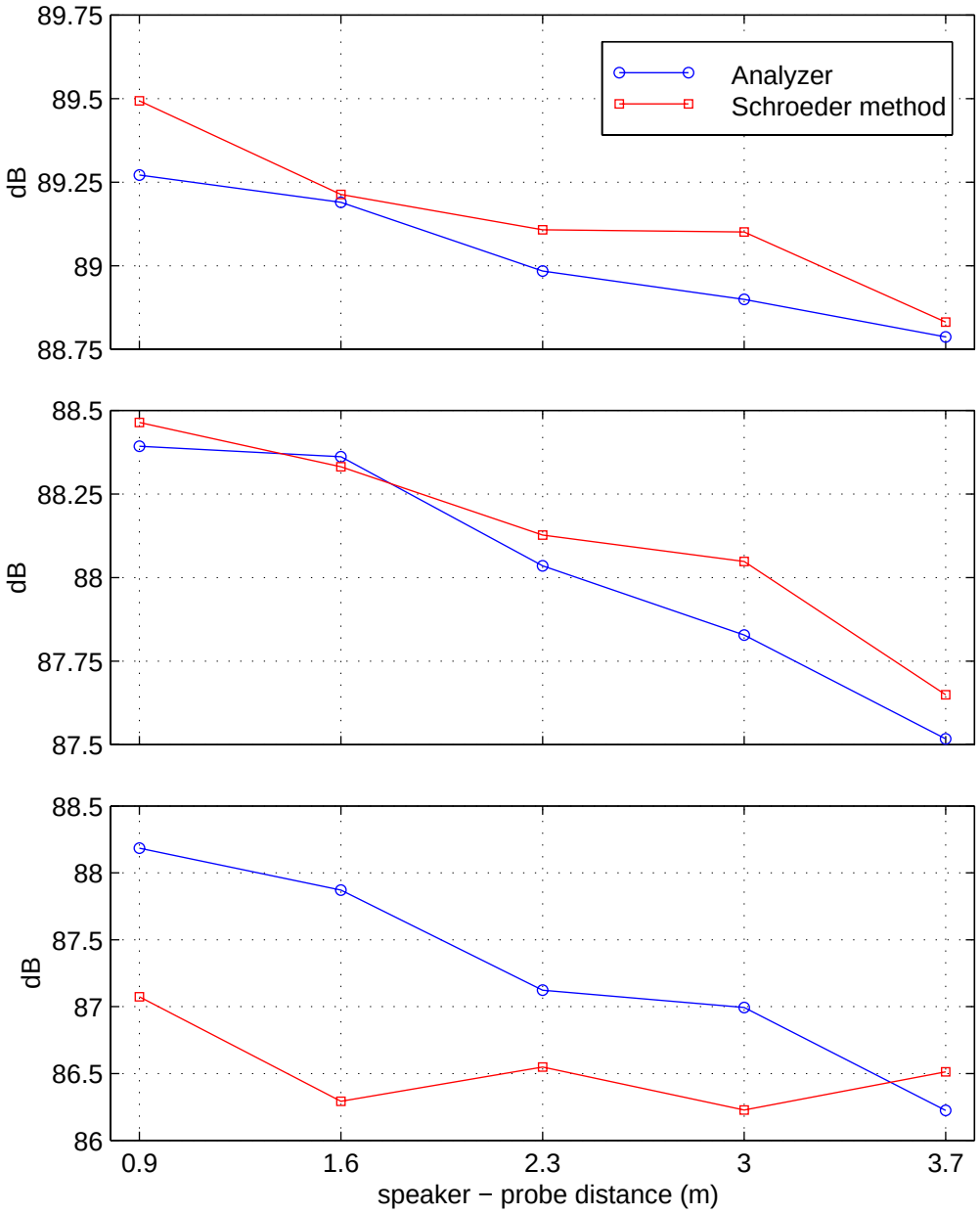

FIGURE 38. Ergodicity check in the 1D field: comparison between mean intensities on a steady signal (blue lines) and ensemble averages at the decay start (red lines). **Top**: foam rubber; **Middle**: open duct; **Bottom**: aluminum panel.

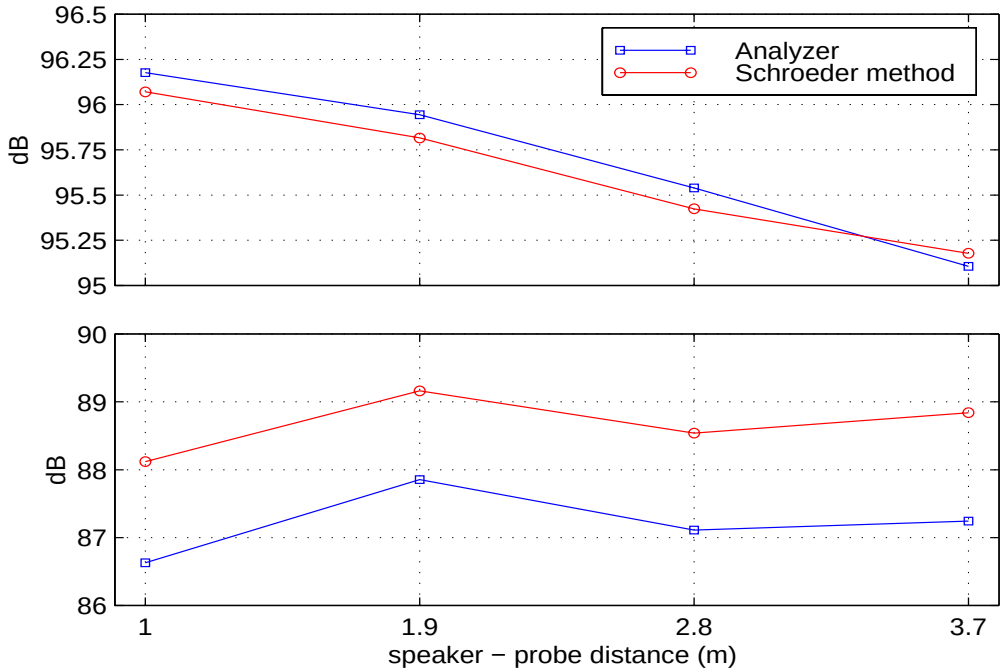

FIGURE 39. Ergodicity check in the 3D field (open duct). **Top**: x component; **Bottom:** y component.

by itself, for it highlights how a property characterizing the stationary state closely affects the transient behavior. Data related to the 3D fields are reported in the following table: they refer to three boundary conditions and to four measurement points $0.9\,\mathrm{m}$ apart (from $x = 3.7\,\mathrm{m}$ to $x = 1\,\mathrm{m}$).

	Foam	**Open**	**Aluminum**
T_{10} (s)	0.05	0.09	0.15
η	0.52	0.46	0.15

As explained above, the error on η is much bigger here ($\sim 10 \div 15\,\%$); moreover, also the uncertainties related to the evaluation of T_{10} are more relevant than the 1D case, being the behavior of the decay curves not perfectly exponential. Anyway, a certain inverse relationship between the two quantities can be observed in this case too.

Measurements of oscillating intensity

Of course, for the study of stationary parameters to be complete we have to include the oscillating intensity calculation: in particular, we may be interested into the effective value R. Yet, this cannot be directly obtained from the intensity impulse responses, as it had previously been done for the mean radiating intensity, this because the equivalence between statistical averages at the transient start and the time averages during the stationary sound holds just when dealing with second order quantities (e.g. w and $\mathbf{j}$). In short, for achieving our goal we then have to use the pressure and velocity signals of the steady field itself. Actually, this gives us the opportunity to reconstruct the sound field by implementing the convolution procedure. In particular, for finding the stationary signals corresponding to the same spectral composition of the impulse responses, we have just to transform them back by the inverse Hadamard algorithm.

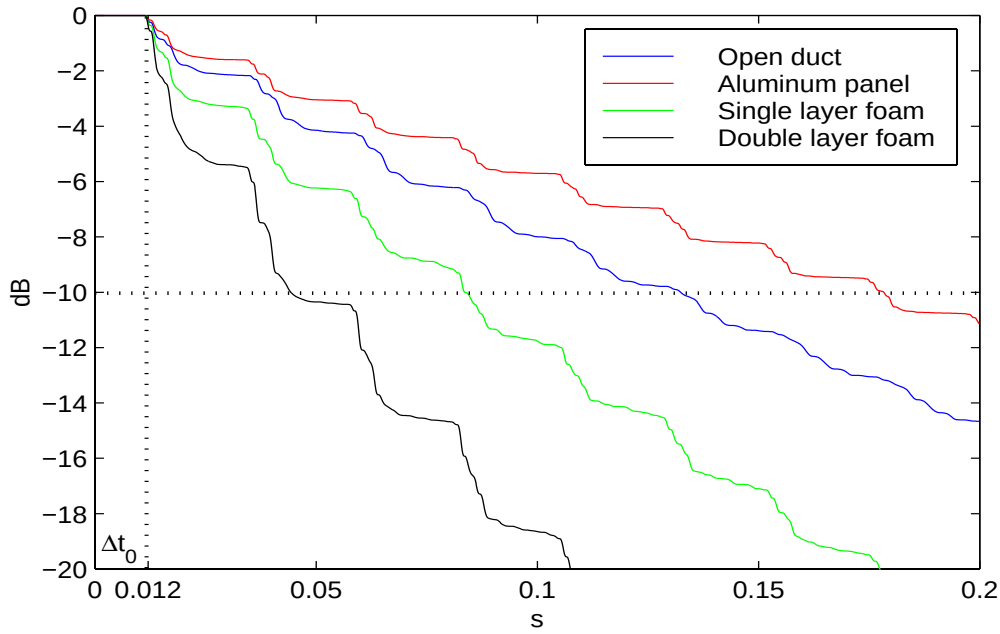

FIGURE 40. Early energy decays in four 1D fields. The $-10\,\mathrm{dB}$ level and the "initial time lag" (Δt_0) are shown.

The results we are going to present are referred to acquisitions taken at rates higher than the previous ones ($10\,\mathrm{kHz}$ for 1D fields and $50\,\mathrm{kHz}$ for 3D fields): this was done in order to have a set of signals more densely sampled and thus more suited to our purposes. Data relative to the1D field are shown in Fig. 42: we calculated both R and A, (even though, the latter corresponds to that obtained by the impulse response integration). We here can realize what happens to the oscillating intensity when drastically varying the boundary conditions: when the field becomes more confined (due to a less absorbing boundary surface), the oscillating part of the intensity increases while the radiating part decreases. Obviously, this somewhat agrees with the results of the previous section, where we have compared η with the reverberation time. Moreover, a glance at the vertical scales indicates that the two rates of change are not equal to each other; for better seeing this, we define the dimensionless ratio $\psi := R/A$: this is found to be $\psi \simeq 2.5, 5.7, 16.9, 42.8$. A similar behavior is observed in the 3D case (though in three conditions instead of four): in particular, $\psi \simeq 1.9$ (one foam layer), 2.7 (open duct), 8.6 (aluminum panel). Here the increment is less marked than before: actually, this is probably due to the fact that now the physical surface bounding the sound field is larger, since it comprises the transversal walls too, and the fraction which is changed (as usual the duct termination) is just a small part of the entire structure.

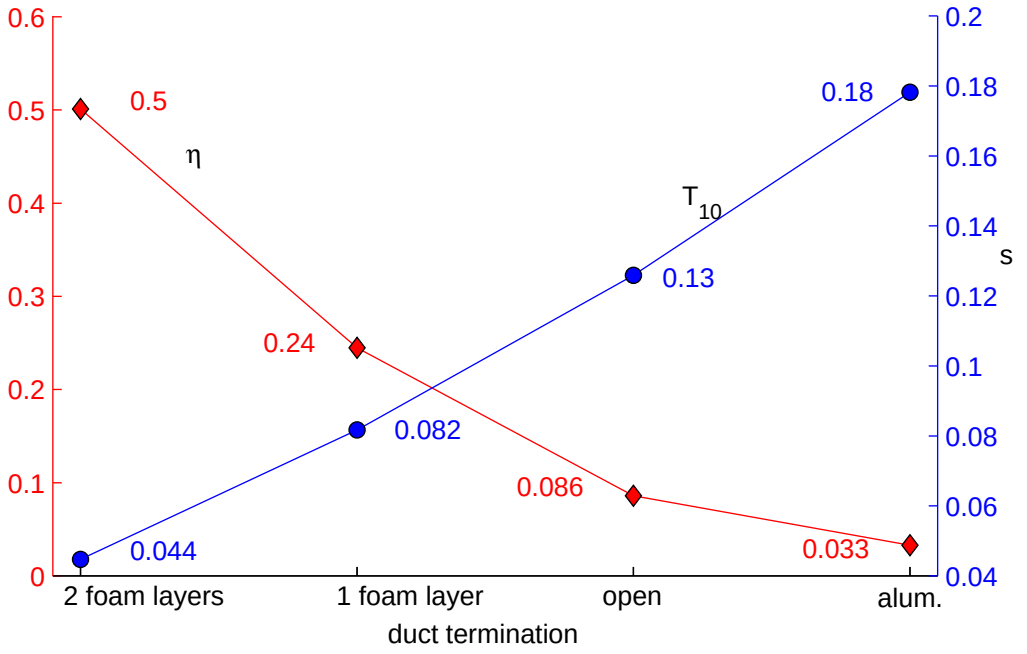

FIGURE 41. η indicator and early energy decay time (T_{10}) relative to the four field conditions shown in Fig. 25.

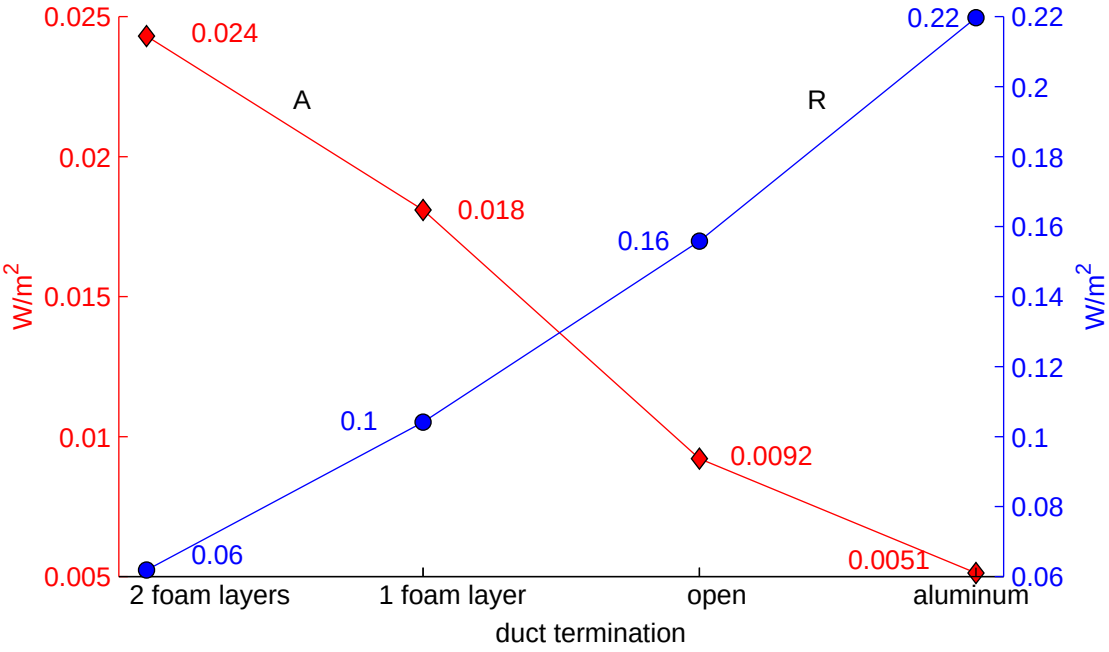

FIGURE 42. Oscillating intensity (blu line, right ordinate) and radiating intensity (red line, left ordinate) in the 1D field.

4.3 Measurements in an opera house

Since our efforts were mainly directed to the application of the intensimetric methods into ordinary room acoustics environments, we decided to perform the kind of analysis presented in Sect. 4.2 in one of these situations: to this aim we chose a historical opera house (the "Teatro Comunale" in Ferrara, built in 1798).

As a source we adopted the *Norsonic* dodecahedral speaker system (Fig. 43), capable of providing a good omnidirectional excitation; according to a common situation encountered during the performance, this was placed in the middle of the stage. Three locations were investigated: the mouths of two first order opposite boxes (17 and 7) and the central stall between them (row 13). Fig. 44 sketches the way how the vectorial probe reference frames (*B&K 4181* with a $5\,\mathrm{cm}$ long spacer) were set in the three measurement points: note that the x axis was always directed along the probe-source line. The analysis upon the acquired data was then performed in the band: $180\,\mathrm{Hz} \div 1400\,\mathrm{Hz}$ (3 octaves).

The energy decays measured in the three points are practically identical (Fig. 45 shows the one obtained in the stalls), furthermore, their behavior is almost perfectly exponential: this means that the environment behaves quite in accordance with the diffuse field properties. In particular, we get $T_{10} \simeq 0.13\,\mathrm{s}$ and $T_{60} \simeq 1.2\,\mathrm{s}$. Besides, the ratio of the two energy terms remains constant during the decay; in particular, these are very well balanced, being $\sigma \simeq 0.97$. Some important differences are found when comparing the intensity decays: look for instance at Fig. 46, which shows the single components of $\overline{\mathbf{j}(t)}$ in the stalls and in box 7. In the former case the initial j_x (component along the sight-line) and j_z (vertical component) are of the same order; subsequently, the decay of the first one occurs in a non monotonic way, starting at $t_{0,x} \simeq 0.05\,\mathrm{s}$: actually, this could mean that at the beginning the largest energy contribution comes from the source itself but thereafter, once this is passed, the positive front caused by the rear wall reflection prevails. On the other hand, the decay of the vertical component starts a little later, (roughly at $t_{0,z} \simeq 0.08\,\mathrm{s}$) and continues monotonically towards zero. The distances corresponding to these time lags are $ct_{0,x} \simeq 17\,\mathrm{m}$ and $ct_{0,z} \simeq 27\,\mathrm{m}$ respectively: since the first is the probe-speaker distance, the second could be interpreted as a sort of minimum path required for energy to reach the measurement point from the vertical direction. Note also that the lateral component (j_y) is quite small, both at the beginning (stationary value) and during the transient, as it can be expected looking the configuration of the probe-source system with respect to the symmetry of the environment.

As regards the decays in the box (bottom plots in Fig. 46), some meaningful characteristics may be noticed: first, differently from the previous case the x component behavior is monotonic. Moreover, the z component is much low, probably because the reduced vertical space suppresses the lowest frequencies. Let us now examine the stationary indicators η and ψ; we remind that the former is given simply by the impulse response integration, while the latter requires the calculation of R from the field obtained by the inverse Hadamard transform. The results are reported in the table below (the error on η is of the order of $5\,\%$).

	Stall 13	**Box 17**	**Box 7**
η	.28	.42	.42
ψ	4.6	2.9	3.0

We can clearly distinguish two distinct ranges; in fact, the stall differs from the boxes for having a smaller energy transfer coefficient and a larger ψ. In practice, this indicates that at the mouth of the lateral boxes there it occurs an increase of the amount of energy flowing away on aver-

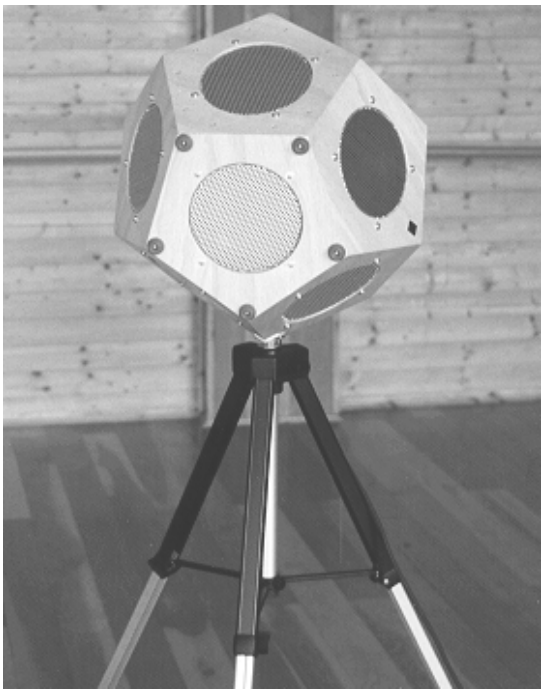

FIGURE 43. The dodecahedral speaker system used in the opera house.

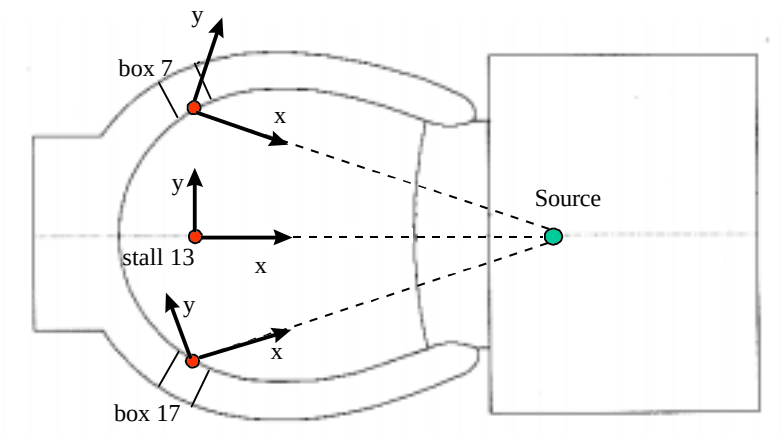

FIGURE 44. The three measurement points and their reference frames.

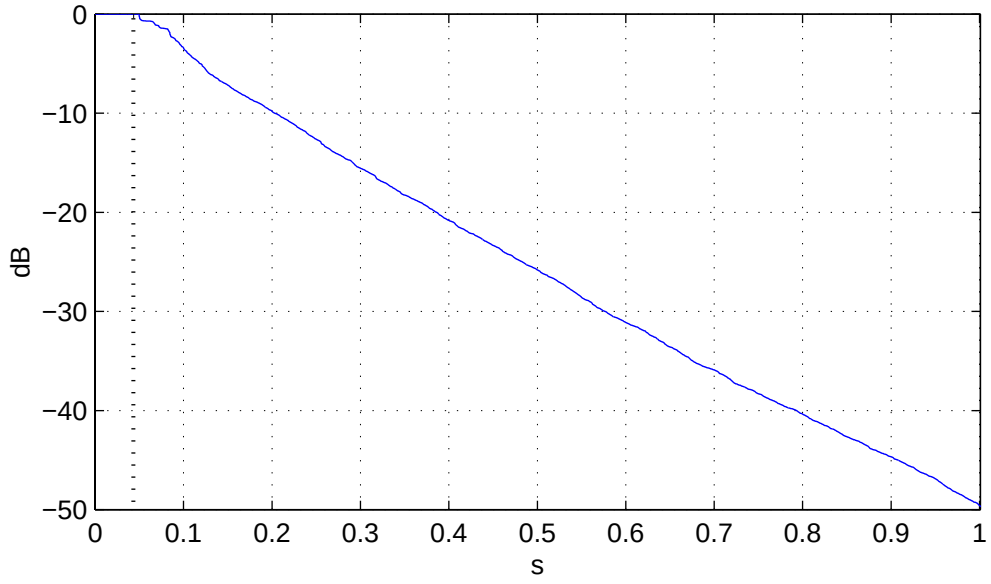

FIGURE 45. Example of energy decay in the opera house (the initial time lag is about $0.04\,\mathrm{s}$).

age. Therefore, we are in presence of a sort of symmetrical behavior with respect to the one discovered when studying the field in the duct: here, we find equal energy decays and different stationary parameters, while in the duct each decay curve corresponded to a specific parameter. This phenomenon is certainly worth of consideration; in fact, we must consider that in the present case data are taken moving the measurement point in a complex environment, formed by several communicating enclosures, which are completely different from each other (the large central hall and the small box). On the contrary, the previous measurements were done inside a simple environment, where just a small portion of the boundary conditions was changed. In summary, by this distinction we have found a direct evidence of the fact that both the environment dimension and the characteristics of the walls affect the local energy transfer inside the acoustic field.

The item we want to treat for completing the study of the stationary field conditions regards the visualization of the polarization ellipsoids; in practice, this is achieved by building the indicatrix quadric from the vectors $\mathbf{r}(t)$, obtained from the reconstruction of the field. We remind that the computational procedure consists of calculating the tensor $\mathfrak{N} = 2\langle \mathbf{r} \otimes \mathbf{r} \rangle$ and then plotting the quadric $\mathbf{q}\cdot\mathfrak{N}_+^{-1}\mathbf{q} = 1$ (see Sect. 1.7.3 and A.3.1); nevertheless, we here prefer to take the normalized tensor $\mathfrak{N}_n := \mathfrak{N}/|\mathbf{A}|^2$, which is related to the coefficient ψ through the relation $\psi = \sqrt{\mathrm{Tr}\,\mathfrak{N}_n}$. In Figs. 47 and 48 we report the ellipsoids of the stall and box 7, respectively. By means of them we may find the average oscillation properties in our two typical configurations. It may be noted that the first ellipsoid is strongly affected by the particular symmetric structure of the hall, since its axes are directed along the reference coordinates: in particular, the oscillation is maximum along x and minimum along y. The situation in the box is quite different; here a marked polarization is still present but this is roughly oriented along the bisecting line of x and y (thus roughly parallel to the previous polarization direction). In order to give a more quantitative evaluation of the asymmetries in the three cases, we also report in the table below the ellipsoids intrinsic semiaxes, that is the elements of the tensor $\mathfrak{N}_n$ in diagonal form. Any-

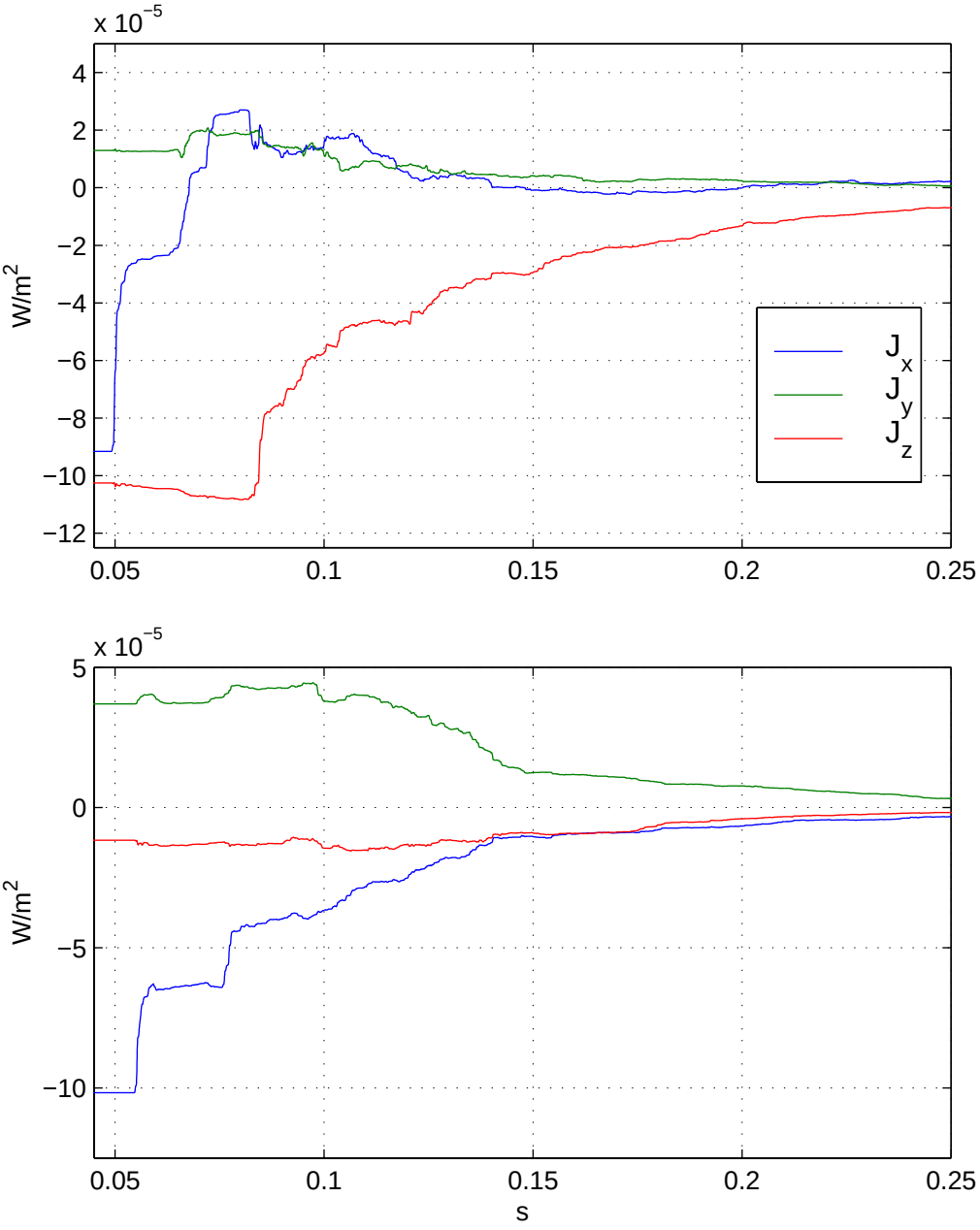

FIGURE 46. Single components of intensity decays in the opera house. **Top**: stalls; **Bottom**: box 7.

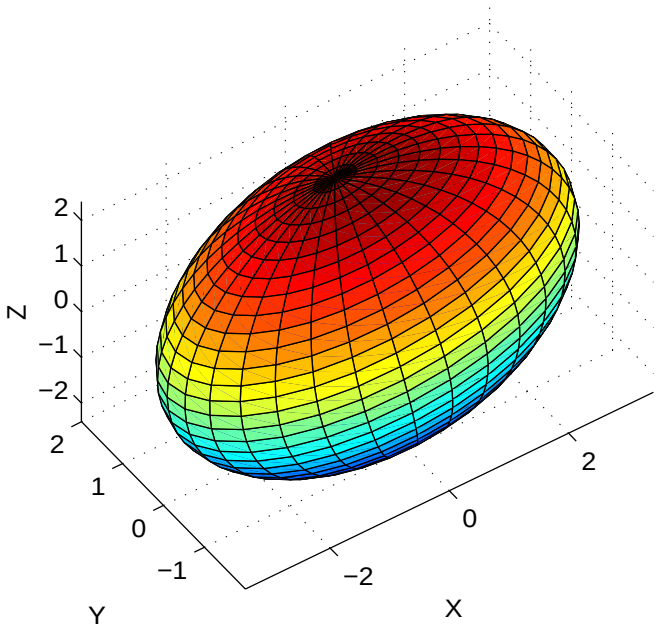

FIGURE 47. Polarization ellipsoid in the stall (dimensionless units).

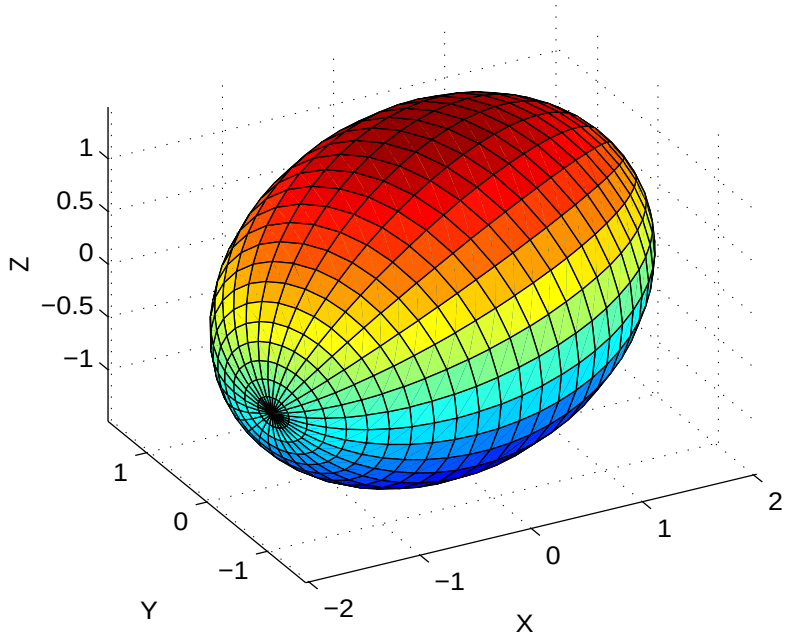

FIGURE 48. Polarization ellipsoid in box 7.

way, we must stress the fact that these data, as well as their graphical representations, have to be taken with a certain caution, since no precise evaluation of the systematic errors involved in the measurement procedure is actually available.

	Stall 13	**Box 17**	**Box 7**
x'	3.5	2.0	1.5
y'	2.0	1.4	1.5
z'	2.4	1.6	2.1

4.4 Pure tones analysis by convolutions

The last issue we want to deal with regards the stationary analysis of simple sound fields through the FFT-based convolution procedure described in Sect. A.7. We applied this method in some of the environments considered above: the duct at low frequency (1D field) and the stalls of the opera house. In particular, these served us for investigating the energy fluxes ratios in the monochromatic case: therefore, we completely disregarded the absolute evaluation of the quantities and just calculated the dimensionless parameters $\sigma = 2\sqrt{W_K W_U}/(W_K + W_U)$ (energies partition) and $\eta = |\mathbf{A}|/cW$ (energy transfer). We then introduced $\gamma = R/cW$, for evaluating the normalized amount of oscillating flux.

The procedure was implemented in specific frequency ranges, repeating the convolution at constant intervals. Each cycle may be summarized as follows:

(1) set the size of the measured impulse responses g (pressure and velocity) to a power-of-two number ($M = 2^m$), by appending, if needed, a series of zeros to its end;
(2) define a segment of a discrete harmonic excitation signal:

$$s(n) = A\cos(2\pi f n \Delta t) \qquad n = 0, 1 \ldots 2L$$

where $L = M + 1$. Being $f_s = 1/\Delta t$ the sampling rate (the same of the impulse response), the frequency f of the signal must be such that: $f \ll f_s, T \ll L\Delta t$.
(3) implement a two step overlap-add convolution between s and g, i.e. by executing two $2M$ points FFT in correspondence of the first and last L points of s respectively (note that $2M = L + M - 1$);
(4) extract the central part of the whole obtained signal (of length $2L + M - 1 = 3M + 1$) rejecting the first and the last M points.

In the table below we report the parameters used; note that in each case the frequency interval Δf is smaller than the frequency resolution $\Delta f_s = f_s/M$.

	M	f_s	**Signal freq.**	Δf	**Num. of points**
Duct	16384	10 kHz	$100 \div 550$ Hz	5 Hz	91
Op. house	32768	30 kHz	$200 \div 350$ Hz	2 Hz	76

The behavior of η in the duct field is shown in Fig. 49. We used two plots for distinguishing two corresponding patterns observed for the closed duct (top plot) and the open duct (bottom plot) respectively: in the first case the three reported behaviors are quite similar to each other, apart from the offset, which turns out to be strongly dependent on the absorption properties of the boundaries. The single frequency investigation thus confirms the property found by means

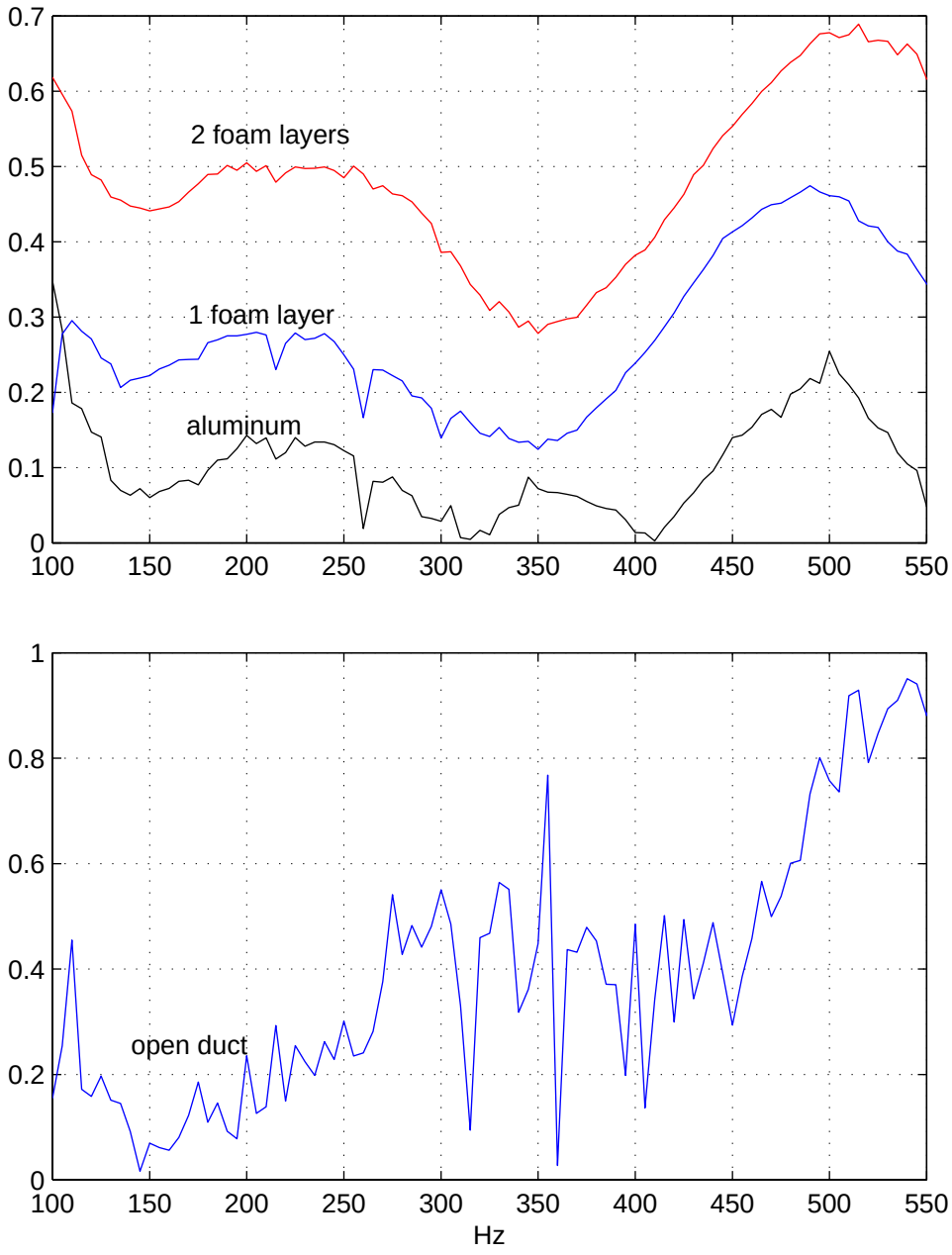

FIGURE 49. Dependence of η parameter on frequency in the 1D field.

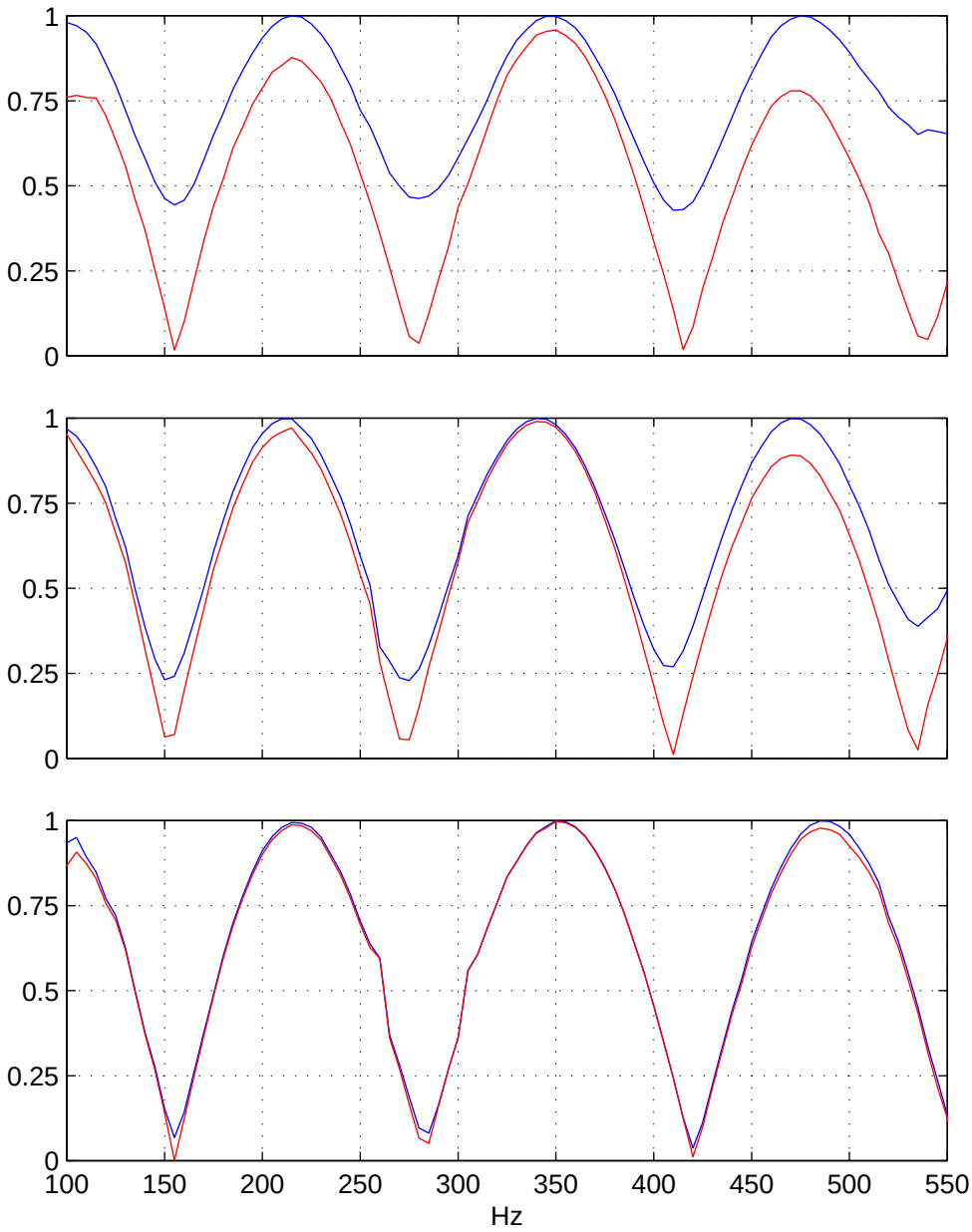

FIGURE 50. Behavior of σ (red lines) and γ (blu lines) in three 1D duct fields. **Top**: double foam layer; **Middle**: one foam layer; **Bottom**: aluminum panel.

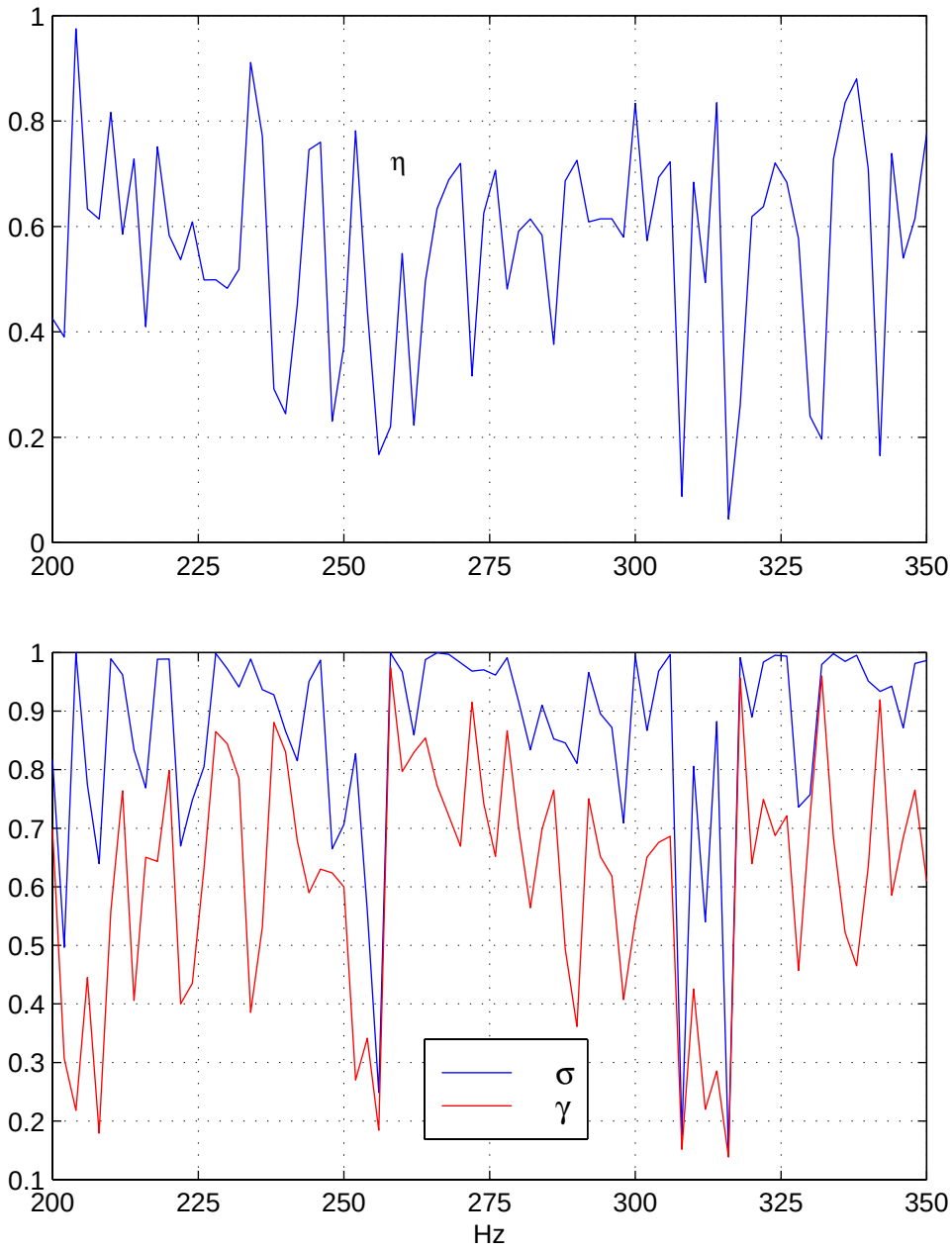

FIGURE 51. Behavior of stationary energetic parameters in the opera house field (stall 13). **Top**: η; **Bottom**: σ and γ.

of the broad band analysis performed with the MLS technique. On the contrary, it is interesting to note that the open duct gives rise to a different frequency dependence: in particular, this is much more irregular than the previous ones. Moreover, here the relationship with respect to the other three conditions does not identically reflect the overall behavior (remember that we found $\eta_{alum} < \eta_{open} < \eta_{foam}$), meaning that broad band value is mostly affected by the different spectral composition of the two filed types.

By Fig. 50 we can gain a deeper insight into the relation between σ and the behavior of the oscillating intensity, which it has already been mentioned in Chapter 1 (Sect. 1.8.1) and when studying the inner field of the organ pipe (Sect. 4.1.2). The first characteristic standing out is the clear similarity of the two quantities, furthermore, it may be also seen that from top to bottom they gradually tend to be identical. If we then contemporarily take into account the behavior of η reported in the top part of Fig. 51, we note that the smaller this is, the more the overlap between σ and γ is pronounced. This is evident also when dealing with a single behavior: for instance, in the single foam layer case (middle plot of Fig. 50) the two lines are distinct in the frequency range $400 \div 550\,\mathrm{Hz}$, where a remarkable increase of η occurs. In fact, this phenomenon is the experimental evidence of the relation: $\mathbf{A}^2 + R^2 = \langle p^2 \rangle \left\langle \mathbf{v}_p^2 \right\rangle + 2 \langle p^2 \rangle \left\langle \mathbf{v}_q^2 \right\rangle$ (Eq. (63)). In practice, the condition $\mathbf{A} \simeq \mathbf{0}$ is equivalent to $\mathbf{v}_p \simeq \mathbf{0}$ and $R^2 \simeq 2 \langle p^2 \rangle \left\langle \mathbf{v}_q^2 \right\rangle$, from which it follows $\sigma \simeq \gamma$.

In the 3D field of the opera house the behavior of η does not show any regular behavior: we realized it performing the analysis both in a small scale (like the one shown in Fig. 51) and in a large scale (i.e. increasing the interval Δf and extending the total frequency range). Actually, this seems quite a general property of complex fields (it has been observed in the 3D field of the duct as well). On the other hand, the comparison of γ and σ indicates the same property observed in the previous case.

Conclusions

The ultimate meaning of the experiments presented in the last chapter is that of highlighting the effectiveness of intensimetric techniques for understanding ordinary room acoustics phenomena. First of all, several physical quantities, rigorously defined when discussing the general laws of linear acoustics, were measured in the inner and outer steady field of an open organ pipe: this preliminary test confirmed the possibility of quantifying the sound radiation level through the ratio of the mean intensity to the total energy density (η indicator).

Subsequently, according to the interpretation of the sound reverberation processes on a local basis, we studied the way how the same field indicator can be employed for describing the variations of energy absorption when changing small portions of boundary conditions into simple test environments (e.g. the plexiglass duct in 1D and 3D sound propagation conditions). This was accomplished by a deep study of the various quantities taking part in the sound decay, with the aid of an original improvement of the cross-correlation technique, by which we could measure both the pressure and velocity impulse responses. The main result was the inverse relationship holding between the decay time and the η indicator: this means that, for a given environment, a high local energy transfer present during the steady sound preceding the transient state corresponds to a short time required for energy to extinguish. In particular, measurements related to the steady state were performed by the back integration of the corresponding impulsive quantities: the method was supported by a sort of ergodicity check, which confirmed the equivalence of stationary and ensemble averages in correspondence of transition from the steady to the transient state.

By executing the same kind of analysis in an ordinary environment (an opera house), we then realized the effect of room structure in the neighborhood of the measuring point; in practice, in a complex field two or more locations may be characterized by the same energy decay but a different local energy transfer, owing to a different energy balance.

In order to include into the analysis the oscillating intensity evaluation, which cannot be directly obtained by the impulse responses, we devised a procedure for recovering the stationary fields by implementing convolution techniques: in particular, for the broad band analysis we made use of the Inverse Fast Hadamard Transform while the reconstruction of monochromatic excitations was achieved through the FFT method. In this way, we could measure some additional field indicators, called γ and ψ, expressing in dimensionless units the amount of oscillating intensity with regard to the radiating intensity and to the total energy density, respectively.

The current aim is to follow the guidelines presented in this introductory study for understanding the role played in the traditional phenomenological laws of room acoustics (e.g. the reverberation time formulas) by the quantities we have introduced. Furthermore, another fundamental issue to be considered concerns the investigation of the way how the energy transfer affects the perception of sounds.

Notions of signal processing

In this short section we will present the theoretical fundamentals of signal processing, often adopted in the study of linear systems. The treatment of the matter will be limited to those particular aspects which can be of interest in our work; therefore, several formal details will be omitted.

A.1 Linear dynamic systems

The study of many physical phenomena is carried out by investigating the relationship between causes and effects [33] . This approach is the foundation of *dynamic systems theory*, mostly adopted in engineering, but often extremely helpful in many other contexts. Considering for instance the single variable case (e.g. time), the physical system may be depicted as a sort of transducer transforming a certain function $s(t)$ (*input*) into the effect $f(t)$ (*output*). The system is then completely characterized once the specifications from obtaining the output from a given input are known:

$$T\left[s(t)\right] = f(t)$$

where T is the operator which indicates a particular transformation law acting on s. A fundamental subclass of systems plays an important role: it is that one of *linear systems*. A system L is said to be linear if any linear combination of inputs gives an output which is the same linear combinations of the outputs obtained from the single inputs. This property is extremely important for deducing an explicit relationship between s and f: we can think to s as being composed of several infinitesimal unitary excitations (impulses), so that we may consider their corresponding elementary output and add them together in order to get the complete signal. Formally, we have

$$s(t) = \int_{-\infty}^{\infty} \mathrm{d}\tau \, s(\tau)\delta(t-\tau)$$

which transformed by L gives

$$f(t) = L\left[s(t)\right] = \int_{-\infty}^{\infty} \mathrm{d}\tau\, s(\tau) L\left[\delta(t-\tau)\right] = \int_{-\infty}^{\infty} \mathrm{d}\tau\, s(\tau) g(t;\tau) \tag{163}$$

where we have defined

$$g(t;t_0) = L\left[\delta(t-t_0)\right]$$

that is the response to an impulse. g is the called the *impulse response* of the system. This method is particularly useful when dealing with systems described by linear differential equations. Let us for example define the relation

$$H\, f(t) = s(t) \tag{164}$$

where H is a generic linear differential operator of order n acting on the function f and s is a known function. To the above equation may be possibly associated particular initial conditions, taking the form of numerical values imposed at $t = 0$ to the function itself and its derivatives up to $n-1$: for example, if Eq. (164) is of second order, these are of the kind: $f(0) = a$ and $f_t(0) = b$. It is well known that the most general solution of Eq. (164) can be expressed as a sum of the general solution of the *homogeneous* equation

$$H\, f(t) = 0 \tag{165}$$

satisfying the initial conditions, and a particular solution of the non-homogeneous equation. Eqs. (164) and (165) may be interpreted from the systems theory viewpoint: the first one is the representation of a linear dynamic system (for instance an electric circuit) with no external excitation, while the second one represents the same linear system when a certain source f is applied (for example an external voltage sent to the circuit). If then we call $g(t, t_0)$ the solution of the equation

$$Hg(t, t_0) = \delta(t - t_0) \tag{166}$$

we may express the particular f of Eq. (164) by a time integral analogous to Eq. (163) . g is here called the *Green function* of Eq. (164) .

Eq. (163) can be simplified when the system is said to be *time invariant*, which means that if $f(t)$ is the response to $s(t)$, $f(t-t_0)$ is the response to $s(t-t_0)$ (for differential equations this occurs when the coefficients are constants). In this case, the Green function doesn't depend on the parameter t_0 but just on the variable t. The integral takes the following form

$$f(t) = \int_{-\infty}^{\infty} \mathrm{d}\tau\, s(\tau) g(t-\tau) = \int_{-\infty}^{\infty} \mathrm{d}\tau\, g(\tau) s(t-\tau) = (s * g)\,(t) \tag{167}$$

which is called *convolution*.

Real systems must satisfy the *causality principle*, for which any physical agent cannot produce effects at times preceding its appearance. This means that if the input is zero for $t < t_0$ also the output must be zero for $t < t_0$. It can be seen that the conditions is satisfied if $g(t \leq 0) = 0$, so that the convolution expression becomes

$$f(t) = \int_{-\infty}^{t} \mathrm{d}\tau\, s(\tau) g(t-\tau) \tag{168}$$

A.2 The transfer function

If we pass from the time to the frequency domain applying the Fourier transform to Eq. (167) we obtain

$$F(\omega) = S(\omega)G(\omega) \tag{169}$$

where F, G, S are the Fourier transforms of f, g, s; in particular, G is the so-called *transfer function*: it's meaning is fundamental in the understanding of linear systems from the frequency viewpoint. Let's suppose that the system under consideration be excited by a harmonic function of angular frequency Ω: i.e. $s(t) = e^{i\Omega t}$. Therefore, we have $S(\omega) = 2\pi\delta(\omega - \Omega)$, which inserted into Eq. (169) gives $F(\omega) = 2\pi\delta(\omega - \Omega)G(\omega)$. Transforming back in the time domain

$$f(t) = G(\Omega)e^{i\Omega t} \tag{170}$$

which is still a harmonic function. This means that any harmonic signal is an eigenfunction of a linear time invariant operator: the corresponding complex eigenvalue is just given by the value of the transfer function at that particular frequency. It's important to underline that one sufficient condition for Eq. (169) to make sense is that the functions are absolutely integrable: in particular, when this is true for g, that is

$$\int_{-\infty}^{\infty} \mathrm{d}t\, |g(t)| < \infty \tag{171}$$

the system is said to be *stable*: i.e. its response to any finite input is also finite. This is the most frequent situation occurring in real systems and has an interesting consequence: for instance, let's suppose that an excitation, started at $t \ll 0$, be switched off at a $t = 0$, so that we can write

$$s(t) = \begin{cases} e^{i\Omega t} & t < 0 \\ 0 & t \geq 0 \end{cases}$$

Thus, a particular solution for $t \geq 0$ is expressed by

$$f(t) = \int_{-\infty}^{0} \mathrm{d}\tau \mathrm{e}^{\mathrm{i}\Omega\tau} g(t - \tau)$$

and it must be equal to the solution of the homogenous equation with appropriate conditions for $t = 0$. The asymptotic behavior of $f(t)$ is given by

$$\lim_{t\to\infty} |f(t)| \leq \lim_{t\to\infty} \int_{-\infty}^{0} \mathrm{d}\tau \left|\mathrm{e}^{\mathrm{i}\Omega\tau} g(t - \tau)\right| = \int_{-\infty}^{0} \mathrm{d}\tau \left[\lim_{t\to\infty} \left|\mathrm{e}^{\mathrm{i}\Omega\tau} g(t - \tau)\right|\right] = 0$$

where we have used the property $\lim_{t\to\infty} |g(t)| = 0$, which is a direct consequence of Eq. (171) . This reasoning shows that a generic solution for a homogeneous stable system (*transient state*) is limited in time.

A.3 Signals averaging

There are various procedures for computing the averages of signals: the most important distinction is related to the kind of mathematical function which describes the process under consideration.

A.3.1 Deterministic signals

A *deterministic signal* is formally expressed by a mathematical relationship, so that measuring the corresponding physical quantity several times one obtains always the same value. Deterministic signals may be classified as being periodic (sinusoidal or complex periodic) or non periodic (transient or almost periodic) [34] . The average of a generic deterministic stationary quantity $g(t)$ may be defined as

$$G = \langle g \rangle := \lim_{T\to\infty} \frac{1}{2T} \int_{t_0-T}^{t_0+T} \mathrm{d}t\, g(t) \tag{172}$$

The limit in the integration interval is introduced in order to make the definition suitable also for non periodic signals, in practice it is taken long enough to include every frequency of interest.

It often happens that the simple average doesn't suffice for describing the mean behavior of the quantity. For this reason it's useful to introduce the *central moments* $G^{(p)}$ ($p = 2, 3, \ldots$) [3] :

$$G^{(p)} := \langle (g - G)^p \rangle \tag{173}$$

If $p = 2$ we obtain the usual *variance*, which gives the *root mean square* $\sqrt{G^{(2)}}$. This concept is extendable also to vectors, whose central moments are tensors of order p. In particular, for a 3D vector $\mathbf{g}(t)$ and $p = 2$ one obtains the dyadic

$$\mathfrak{F}^{(2)} = g_{ij}\mathbf{e}^i \otimes \mathbf{e}^j \qquad g_{ij} = \langle (g_i - G_i)\,(g_j - G_j) \rangle \tag{174}$$

The tensor $\mathfrak{F}$ (from now on we will drop the superscript for brevity) is symmetric and semi-definite positive; this comes out if we interpret the average as a scalar product in a Hilbert space so that $\{g_{ij}\}$ is the Gram matrix of the vectors $g_i - G_i$, whose determinant is positive or null. Furthermore, the tensor is definite positive if and only if the three components are linearly independent. It is then possible to find an orthogonal operator $\mathbb{O}$ transforming the tensor in diagonal form and subsequently calculate the square root. In this way, after having performed the inverse transformation, one may define the root mean square tensor:

$$\mathfrak{R} := \mathbb{O}^T \sqrt{\mathfrak{F}_d}\, \mathbb{O} \equiv R_{ij}\mathbf{e}^i \otimes \mathbf{e}^j \qquad \mathfrak{F}_d = \mathbb{O}\mathfrak{F}\,\mathbb{O}^T \tag{175}$$

in fact $\mathfrak{R}\mathfrak{R} = \mathbb{O}^T\sqrt{\mathfrak{F}_d}\mathbb{O}\,\mathbb{O}^T\sqrt{\mathfrak{F}_d}\mathbb{O} = \mathbb{O}^T\mathfrak{F}_d\,\mathbb{O} = \mathfrak{F}$, so that it is possible to write $\mathfrak{R} := \sqrt{\mathfrak{F}} = \sqrt{\langle \mathbf{g} \otimes \mathbf{g} \rangle}$.

It is useful to represent graphically the tensor $\mathfrak{F}$ by means of the so-called indicatrix quadric:

$$\mathbf{x}\cdot\mathfrak{F}_+^{-1}\mathbf{x} = 1 \tag{176}$$

where $\mathbf{x}$ is a variable vector representing a physical quantity of the same kind as $\mathbf{g}$ and $\mathfrak{F}_+$ is the restriction of $\mathfrak{F}$ to the subspace of positive eigenvalues λ_i of $\mathfrak{R}$. If these are all positive (i.e. $\mathfrak{F}_+ = \mathfrak{F}$) the quadric is an ellipsoid having the principal axis along the eigenvectors $\mathbf{x}_i$ and length $2\lambda_i$, while it reduces to an ellipse, a segment or a point if it happens that one, two or all λ_i are zero respectively.

A particularly interesting case occurs when all components of $\mathbf{g}$ have the same time dependence, that is $\mathbf{g}(t) = g(t)\mathbf{h}$: then, the tensor $\mathfrak{R}$ becomes:

$$\mathfrak{R} = \sqrt{\langle (g - G)^2 \rangle}\, |\mathbf{h}| \left(\frac{\mathbf{h}}{|\mathbf{h}|} \otimes \frac{\mathbf{h}}{|\mathbf{h}|} \right) \tag{177}$$

Here the only non zero eigenvalue is $\lambda = \sqrt{\langle (g-G)^2 \rangle}\,|\mathbf{h}|$, corresponding to the eigenvector $\mathbf{h}$.

A.3.2 Random signals

We speak of random signals when the physical phenomenon gives data which cannot be described by an explicit relationship and each observation produces an unique result. Formally, it is represented by a *stochastic process*, consisting of a random variable ($x(t)$) with the time t as a parameter; this quantity has at any instant a definite *sample space (* the ensemble of values that the variable can take) and a probability density function $f(x,t)$, representing the rate of change of the probability when varying x itself and keeping the time fixed [34] . The main method for accomplishing a quantitative analysis of a random process is based on the *ensemble average*, that is an average executed on the overall ensemble at a certain time; it is defined for a generic function $h(x)$ of the random variable:

$$E(h) = \int_{-\infty}^{\infty} \mathrm{d}x\, h(x) f(x,t) \tag{178}$$

The most usual quantities derived by this general definition are the following ones:

- *average*: $\mu_x(t) = \overline{x(t)}$
- *quadratic average*: $\psi_x(t) = \overline{x(t)^2}$
- *variance*: $\sigma_x^2(t) = \overline{[x(t) - \mu_x(t)]^2} = \psi_x(t) - \mu_x^2(t)$
- *autocorrelation*: $\mathfrak{R}_x(t_1,t_2) = \overline{x(t_1)x(t_2)}$

In the last case the integration is carried out weighting with the probability density $f(x_1,t_1;x_2,t_2)$. In order to compare the relative behavior of two different stochastic processes it is necessary to define the following functions too

- *covariance*: $\sigma_{xy}(t) = \overline{[x(t) - \mu_x(t)][y(t) - \mu_y(t)]}$
- *cross-correlation*: $\mathfrak{R}_{xy}(t_1,t_2) = \overline{x(t_1)y(t_2)}$

Among the stochastic processes a fundamental role is played by those named *stationary*, which are defined by the following properties:

(1) $f(x,t) = f(x)$
(2) $f(x_1,t_1;x_2,t_2) = f(t_2 - t_1)$

the first one implies: $\mu_x(t) = \mu_x$, $\psi_x(t) = \psi_x$, $\sigma_x^2(t) = \sigma_x^2$ (mean values independent of time), while the second: $\mathfrak{R}_x(t_1,t_2) = \mathfrak{R}_x(t_2 - t_1)$ (cross-correlation dependent from the time shift only).

We have seen that the statistical analysis of random data requires the knowledge of the probability density function, this means that practical calculations have to be performed over a large number of samples. Nevertheless, one almost always has a single measurement, that is just one record, so the quantities mentioned above cannot be obtained. Fortunately in most cases one deals with a subclass of stochastic stationary processes, called *ergodic*, for which the ensemble average coincides with the time average over a single infinite record. This justifies the following relations:

- $\mu_x = \langle x \rangle = \lim_{T\to\infty} \frac{1}{2T} \int_{-T}^{T} \mathrm{d}t\, x(t)$

- $\psi_x = \langle x^2 \rangle = \lim_{T\to\infty} \frac{1}{2T} \int_{-T}^{T} \mathrm{d}t\, x^2(t)$
- $\sigma_x^2 = \langle (x-\mu_x)^2 \rangle = \lim_{T\to\infty} \frac{1}{2T} \int_{-T}^{T} \mathrm{d}t\, [x(t) - \langle x \rangle]^2$
- $\mathfrak{R}_x(\tau) = \langle x(t)x(t+\tau) \rangle = \lim_{T\to\infty} \frac{1}{2T} \int_{-T}^{T} \mathrm{d}t\, x(t)x(t+\tau)$

A.4 Continuous and discrete Fourier series

It's well known that a periodic distribution f of one real variable, let's say time, having period T ($f(t+T) = f(t)$) can be expressed as a sum of complex exponential [33] :

$$f(t) = \frac{1}{2\pi} \sum_{n=-\infty}^{\infty} \alpha_n \mathrm{e}^{\mathrm{i}n\Omega t} \qquad \Omega = \frac{2\pi}{T} \tag{179}$$

where

$$\alpha_n = \frac{1}{T} \int_{-T/2}^{T/2} \mathrm{d}t\, f(t) \mathrm{e}^{-\mathrm{i}n\Omega t} \tag{180}$$

If $\lim_{n\to\infty} \alpha_n = 0$ in some way, then f is an ordinary function. Otherwise, if $\lim_{n\to\infty} \alpha_n = const.$ or even diverges (at most as a power of n), then f is properly a distribution. In this case Eq. (179) converges in the sense of distribution theory. The Fourier transform of f ($F(\omega)$) is a singular distribution consisting of a sequence of equidistant pulses

$$F(\omega) = \sum_{n=-\infty}^{\infty} \alpha_n \delta(\omega - n\Omega) \tag{181}$$

so that it is thus customary to consider the sequence $\{\alpha_n\}$ itself as the Fourier transform of f. We also note that Eq. (179) , which is the usual *Fourier Series* expansion of a periodic function, can be thought of as a special case of the Fourier integral.

We now ask ourselves what happens when $f(t)$ is a singular distribution of the form

$$f(t) = \sum_{n=-\infty}^{\infty} x(n) \delta(t - n\Delta t) \tag{182}$$

where $\Delta t = T/N$ where N is an integer and $\{x(n)\}$ a periodic sequence, i.e. such that:

$$x(n) = x(n+N) \tag{183}$$

The situation is of great practical interest, because in such a way it is possible to represent a periodic signal properly sampled and discretized [25] .

It is still possible to write the function or, if we prefer, the sequence itself, in terms of a Fourier series, but now the frequencies involved are all multiplies of the fundamental frequency $2\pi/N$ of $\{x(n)\}$ and for this reason the sum consists of just those N distinct exponential functions with a period that is an integer submultiple of N. It follows:

$$x(n) = \frac{1}{N} \sum_{k=0}^{N-1} X(k) \mathrm{e}^{\mathrm{i}(2\pi/N)nk} \tag{184}$$

which is the *Discrete Fourier Series* representation of the sequence $x(n)$. $\{X(k)\}$ is a periodic sequence of period N representing the Fourier coefficients of $\{x(n)\}$: it is given by an inverse transformation analogous to Eq. (180) :

$$X(k) = \sum_{n=0}^{N-1} x(n) \mathrm{e}^{-\mathrm{i}(2\pi/N)nk} \tag{185}$$

We have so realized that the frequency content of our sequence is discrete and finite:

$$\omega_k = \frac{2\pi k}{T} = \frac{2\pi k}{N\Delta t} \qquad k = 0, 1, 2, \ldots N-1$$

A.5 Wiener-Khinchin relations

Spectral density functions for stationary random processes can be defined in a number of ways [34] ; among these, the one based on the Fourier transform of the correlation function is the most useful from a formal point of view. Let's consider a stationary random process $\{x_k(t)\}$ and calculate its autocorrelation function $\mathfrak{R}_x(t)$, furthermore let's assume this quantity be absolutely integrable, i.e.

$$\int_{-\infty}^{\infty} \mathrm{d}t \, |\mathfrak{R}_x(t)| < \infty$$

The *two-sided autospectral density function* of $\{x_k(t)\}$ is defined as

$$S_x(\omega) = \int_{-\infty}^{\infty} \mathrm{d}t \, \mathfrak{R}_x(t) \mathrm{e}^{-\mathrm{i}\omega t} \tag{186}$$

its inverse is of course

$$\mathfrak{R}_x(t) = \frac{1}{2\pi} \int_{-\infty}^{\infty} \mathrm{d}\omega \, S_x(\omega) \mathrm{e}^{-\mathrm{i}\omega t} \tag{187}$$

These relations, together with the analogous ones for the cross-spectral density, are referred to in literature as the *Wiener-Khinchin theorem*, from the name of the two mathematicians who proved them in the early Thirties.

In the mathematical context it is advantageous to deal with functions defined both for positive and negative frequencies, since calculations are often simplified by the use of complex exponentials. Yet, we know that just the positive part makes physical sense in practice, so it is customary to define also the *one-sided autospectral density function:*

$$G_x(\omega) = \begin{cases} 2S_x(\omega) & 0 \leq \omega \leq \infty \\ 0 & \text{otherwise} \end{cases}$$

Thanks to the symmetry properties of correlation function, $S_{xx}(\omega)$ is a real even function of ω, it follows:

$$G_x(\omega) = 4 \int_0^{\infty} \mathrm{d}t \mathfrak{R}_x(t) \cos \omega t$$

while

$$\mathfrak{R}_x(t) = \frac{1}{2\pi} \int_0^{\infty} \mathrm{d}\omega \, G_x(\omega) \cos \omega t$$

which at $t = 0$ becomes

$$\mathfrak{R}_x(0) = E\left[x^2(t)\right] = \frac{1}{2\pi}\int_0^\infty \mathrm{d}\omega\, G_x(\omega)$$

Among the various kinds of processes, we here want to mention two remarkable examples. One is the so-called *white noise* **,** defined as a stationary random process with a constant autospectral density and, consequently, $\mathfrak{R}_x(t) \propto \delta(t)$. The other one is the case of a harmonic function, for which $\mathfrak{R}_x(t) \propto \sin(\Omega t)$ and $S_x(\omega) \propto \delta(\omega - \Omega)$.

A.6 Spectrum of an MLS signal

Now let's take into consideration one interesting practical case, encountered in Chap. 3: the spectrum of the MLS signal. Let's start calculating the autocorrelation function which, being the signal periodic, is a periodic signal as well. It can be easily demonstrated [23] that for an MLS sequence M_N having period $N = 2^m - 1$

$$\mathfrak{R}_{M_N}(n) = \frac{1}{N}\sum_{l=0}^{N-1} s(l)s(l+n) = \begin{cases} 1 & \text{if } n = 0, N, 2N, \ldots \\ -\dfrac{1}{N} & \text{otherwise} \end{cases}$$

where the sum is performed over the N elements of the sequence. We obtain the spectrum using the discrete Fourier series:

$$G_{M_N}(k) = \sum_{n=0}^{N-1} \mathfrak{R}_{M_N}(n)\mathrm{e}^{-\mathrm{i}(2\pi/N)nk} = \begin{cases} 1 - \displaystyle\sum_{n=1}^{N-1} \frac{1}{N} = 1 - \frac{N-1}{N} = \frac{1}{N} & \text{if } k = 0 \\ 1 - \displaystyle\sum_{n=1}^{N-1} \frac{\mathrm{e}^{-\mathrm{i}(2\pi/N)nk}}{N} = \frac{N+1}{N} & \text{if } 0 < k \leq N-1 \end{cases}$$

where the bottom equality is due to the relation

$$\sum_{l=1}^{N-1} \mathrm{e}^{-\mathrm{i}(2\pi/N)lk} = \mathrm{e}^{-\mathrm{i}(2\pi/N)k}\frac{1 - \mathrm{e}^{\mathrm{i}(2\pi/N)(N-1)k}}{1 - \mathrm{e}^{-\mathrm{i}(2\pi/N)k}} = -1$$

For instance, in the case where $N = 7$, mentioned in Sect. 3.3.2, we have

$$\begin{aligned} \mathfrak{R}_{M_7} &\equiv [1, -1/7, -1/7, -1/7, -1/7, -1/7, -1/7] \\ G_{M_7} &\equiv [1/7, 8/7, 8/7, 8/7, 8/7, 8/7, 8/7] \end{aligned}$$

A.7 Discrete Fourier Transform and convolutions

We have treated the frequency representation of periodic sequences: we now want to expand the same formalism in order to include finite sequences [25] . In practice, a finite sequence $x(n)$ of length N ($0 \leq n \leq N-1$) is thought to be one period of the periodic sequence built by

extending $x(n)$ indefinitely. The expansion of $x(n)$ has a unique DFS representation, so that its period may be taken as the transform of the initial finite sequence: this is called the *Discrete Fourier Transform* (DFT) of $x(n)$ (see Eqs. (184) and (185)). Let's now see the way how to express convolutions between finite length sequences; for instance, consider a finite input signal $s(n)$ and a certain impulse response $g(n)$, both of length N. Their convolution is still a finite sequence, though of length $2N-1$: it is written like that

$$f(n) = \sum_{m=0}^{N-1} s(m)g(n-m) \tag{188}$$

According to the general relation defined by Eq. (169) , we can transform Eq. (188) in the frequency domain:

$$F(k) = S(k)G(k)$$

It is then straightforward to verify that the original signal f is given by the inverse transform (IDFT) of the sequence F, provided that the DFT S and G, as well as the IDFT itself, are computed on the basis of at least $2N-1$ points, that is extending the length of the original sequences with $N-1$ zero elements. In short:

$$\begin{aligned} S(k) &= \sum_{n=0}^{2N-2} s(n)\mathrm{e}^{-\mathrm{i}(2\pi/N)nk} \qquad G(k) = \sum_{n=0}^{2N-2} g(n)\mathrm{e}^{-\mathrm{i}(2\pi/N)nk} \\ f(n) &= \frac{1}{2N-1}\sum_{k=0}^{2N-2} [S(k)G(k)]\,\mathrm{e}^{\mathrm{i}(2\pi/N)nk} \qquad n = 0 \ldots 2N-1 \end{aligned} \tag{189}$$

Actually, the calculation of a N points DFT requires N^2 arithmetical operations, so that practically, when N increases, the time spent by a normal computer may be too long; fortunately, very efficient algorithms can be employed for reducing this number: the most common and effective one, discovered in the mid Sixties, allows us to obtain the DFT of a $N = 2^m$ sequence through just $N/2\log_2 N$ operations. These procedures, called *Fast Fourier Transforms* (FFT), are currently implemented in several digital signal processing programs. Nevertheless, when one has to convolve two sequences of unequal lengths, a further improvement of the procedure represented by Eq. (189) may be necessary: this mostly happens when one of the two sequences is of indefinite duration, like for example during the stationary acoustic excitation of an environment. One procedure for accomplishing the convolution consists of performing many FFTs on consecutive sections of the signal, rather than on the signal as whole, and then adding the single convolved parts together in an appropriate way (*overlap-add* method). In practice, one may divide the sequence $s(n)$ in many segments of length L:

$$s(n) = \sum_{h=1}^{\infty} s_h(n)$$

where $s_h(n) = s(n)$ for $hL \leq n < (h+1)L$ and zero otherwise. It follows

$$f = s * g = \sum_{h=1}^{\infty} s_h * g = \sum_{h=1}^{\infty} f_h$$

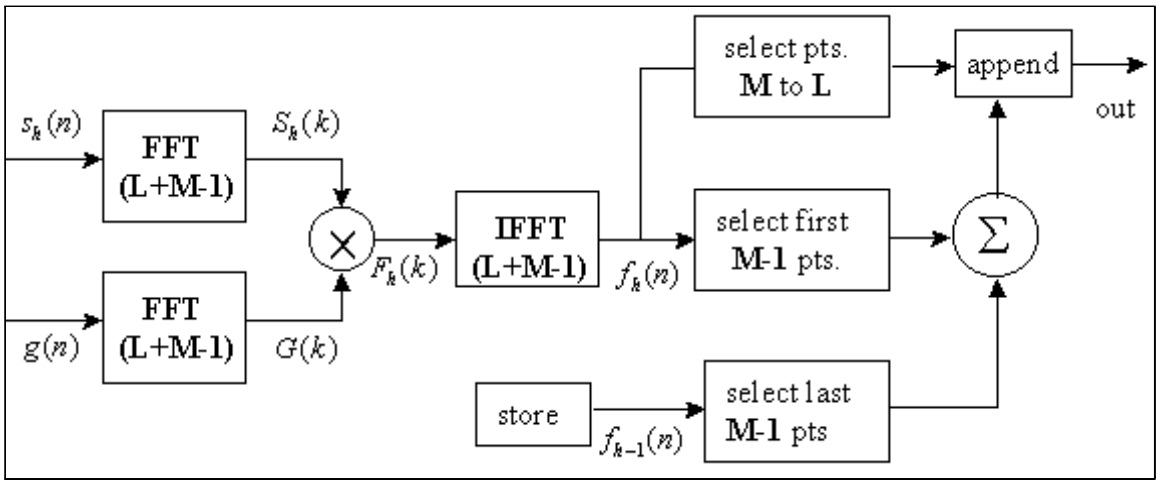

FIGURE 52. Flowgraph of the convolution procedure through the overlapp–add method.

Being g of length M and s_h of length L, each section f_h turns out to be of length $L+M-1$, thus it has to be computed by means of a $L+M-1$ points FFT. The sum must then be performed taking into account that the last $M-1$ points of each section have to be superimposed on the first $M-1$ points of the next one (f_{h+1}). The entire procedure is synthetically represented in Fig. 52.

Bibliography

[1] W.C. Sabine, *Collected papers on acoustics*, Harvard University Press, Cambridge-Mass. (1927).

[2] P.M. Morse, K.U. Ingard, *Theoretical Acoustics*, Princeton University Press, Princeton (1986).

[3] G. Schiffrer, *Lezioni di Acustica* (lecture notes), University of Ferrara, Ferrara (1998).

[4] A.D. Pierce, *Acoustics*, Acoustical Society of America, New York (1989).

[5] E. Meyer, E.G. Neumann, *Physical and Applied Acoustics*, Academic Press, New York (1972).

[6] D. Bonsi, N. Prodi, G. Schiffrer, D. Stanzial, *Note sulla pressione di radiazione sonora*, Proc. 25th AIA Conference, 175-182, Perugia (1997).

[7] F.J. Fahy, *Sound Intensity*, Elsevier, London (1987).

[8] R.V. Waterhouse et al., *Energy Streamlines of a Sound Source*, J. Acoust. Soc. Am. **78**, 758-762 (1985).

[9] J.A. Mann III, J. Tichy, *Acoustic intensity analysis: Distinguishing energy propagation and wave-front propagation*, J. Acoust. Soc. Am. **37**, 409-412 (1965).

[10] D. Stanzial, N. Prodi, G. Schiffrer, *Reactive acoustic intensity for general fields and energy polarization*, J. Acoust. Soc. Am. **99**, 1868-1876 (1996).

[11] J.F. Nye, *Physical properties of Crystals. Their Representation by Tensors and Matrices*, Clarendon Press, Oxford (1964).

[12] G. Schiffrer, D. Stanzial, *Energetic properties of acoustic fields*, J. Acoust. Soc. Am. **96**, 3645-3653 (1994).

[13] P.M. Morse, H. Feshbach, *Methods of theoretical physics*, McGraw-Hill, New York (1953).

[14] P.M. Morse, K.U. Ingard, *Linear acoustic theory*, in *Handbuch der Physik,* Vol. XI/1 (Akustik 1), Springer-Verlag, Berlin (1961).

[15] H. Kuttruff, *Room acoustics* (3rd edition), Elsevier, London (1991).

[16] M.R. Schroeder, *New method for measuring reverberation time*, J. Acoust. Soc. Am. **37**, 409-412 (1965).

[17] J.A. Mann III, J. Tichy, A.J. Romano, *Instantaneous and time-averaged energy transfer in acoustic fields*, J. Acoust. Soc. Am. **82**, 17-29 (1987).

[18] F. Jacobsen, *A note on instantaneous and time-averaged active and reactive sound intensity*, J. Sound Vib. **147**, 489-496 (1991).

[19] D. Stanzial, N. Prodi, *Measurements of newly defined intensimetric quantities and their physical interpretation*, J. Acoust. Soc. Am. **102**, 2033-2039 (1997).

[20] Brüel & Kjær, *Microphone Handbook*, Brüel & Kjær, Nærum, Denmark (1996).

[21] R.W. Guy, *Intensity assessment employing probe reversal*, Appl. Acoust. **40**, 57-68 (1993).

[22] Brüel & Kjær, *Users Manual of Real-time Frequency Analyzers Types 2123, 2133*, Brüel & Kjær, Nærum, Denmark (1989).

[23] M.R. Schroeder, *Integrated impulse method measuring sound decay without impulses*, J. Acoust. Soc. Am. **66**, 497-500 (1979).

[24] S.W. Golomb, *Shift Registers Sequences*, Aegean Park Press, Laguna Hills-CA (1982).

[25] A.V. Oppenheim, R.W. Schafer, *Digital Signal Processing*, Prentice-Hall, (1975).

[26] W.T. Chu, *Impulse-Response and Reverberation-Decay Measurements Made by Using a Periodic Pseudorandom Sequence*, Appl. Acoust. **29**, 193-205 (1990).

[27] M. Harwit, N.J.A. Sloane, *Hadamard Transform Optics*, Academic Press, New York (1979).

[28] J. Borish, J.B. Angell, *An efficient algorithm for measuring the impulse response using pseudorandom noise*, J. Audio Eng. Soc. **31**, 478-87 (1983).

[29] M. Cohn, A. Lempel, *On fast M-sequence transforms*, IEEE Trans. Inf. Theory **IT-23**, 135-137 (1977).

[30] N.H. Fletcher, T.D. Rossing, *The physics of musical instruments*, Springer-Verlag (1991).

[31] D. Stanzial, D. Bonsi, N. Prodi, *An Intensimetric Technique for Distinguishing the Radiative Characteristics of Sound Sources: a Case Application to an Organ Pipe*, Proc. ISMA '98 Conference, 279-282, Leavenworth, WA-U.S.A. (1998).

[32] D. Stanzial, N. Prodi, *A novel Intensimetric Technique for Monitoring the Radiative Properties of Sound Fields*, submitted do J. Audio. Eng. Soc (July 1998).

[33] A. Papoulis, *The Fourier integral and its applications*, McGraw-Hill, New York (1962).

[34] J.S. Bendat, A.G. Piersol, *Random Data* (2nd edition), Wiley (1986).